Quantitative Analysis of Cellular Processing of Antibody-Drug Conjugates

by

Katie F. Maass

B.S. Chemical Engineering
University of Texas at Austin, 2011

Submitted to the Department of Chemical Engineering in Partial Fulfillment of the Requirements for the degree of

DOCTOR OF PHILOSOPHY
in Chemical Engineering

at the

MAASSACHUSETTS INSTITUTE OF TECHNOLOGY

FEBRUARY 2016

Signature of Author: _____

Katie F. Maass
Department of Chemical Engineering
December 17, 2015

Certified by: _____

K. Dane Wittrup
Carbon P. Dubbs Professor of Chemical Engineering and Biological Engineering
Thesis Supervisor

Accepted by: _____

Richard D. Braatz
Edwin R. Gilliland Professor of Chemical Engineering
Chairman, Committee for Graduate Students

Quantitative Analysis of Cellular Processing of Antibody-Drug Conjugates

by

Katie F. Maass

Submitted to the Department of Chemical Engineering
on December 17th, 2015 in Partial Fulfillment of the
Requirements for the Degree of Doctor of Philosophy in Chemical Engineering

ABSTRACT

Antibody-Drug Conjugates (ADCs) are a promising therapeutic class which combines the potency of chemotherapeutic drugs with the specificity of a tumor targeting antibody. ADCs aim to reduce systemic toxicity and maintain or improve therapeutic efficacy. Once an ADC reaches a tumor and binds its target antigen, it is internalized via receptor-mediated endocytosis. The ADC is internalized into an endosomal/lysosomal compartment, where the ADC is degraded, releasing the drug component from the antibody. The drug component can then leave the endosomal/lysosomal compartment and bind its intracellular target; hopefully, resulting in tumor cell killing.

In this thesis, we focus on how ADCs get processed at a cellular level. First, we developed a flow cytometric clonogenic assay and used this assay to study the single-cell potency of the chemotherapeutic drug doxorubicin. Across a number of cancer cell lines, we found that a cell's ability to proliferate was only dependent on the amount of doxorubicin inside the cell and independent of varying drug media concentration, length of treatment time, or treatment with verapamil. We established a single-cell IC_{50} of 4 – 12 million doxorubicin molecules per cell.

Next, we developed a model for ADC cellular processing and parameterized this model using a clinically approved ADC, T-DM1. Sensitivity analysis suggests that the amount of drug that is delivered to cells is a function of the amount of drug that comes in via internalization and the amount the leaves via drug efflux. This work also demonstrates how it is important to consider ADC processing as a complete system rather than isolating individual steps when designing ADCs. We also incorporated this cellular level processing model into a larger pharmacokinetic/pharmacodynamic model.

Finally, we used fluorescence microscopy with a Trastuzumab-Doxorubicin ADC to track where within a cell the drug component traffics once released from the antibody. We find that the ADC does not deliver a significant number of doxorubicin molecules to the nucleus, suggesting that escape from the lysosome limits the amount of drug that can be delivered to its target via an ADC. The ability to escape the lysosome should be considered when designing an ADC.

Thesis Supervisor: K. Dane Wittrup
Title: Carbon P. Dubbs Professor of Chemical Engineering and Biological Engineering

Acknowledgements

First, I would like to thank my thesis advisor, Dane Wittrup, for his support throughout my graduate work. I've been consistently impressed by Dane's ability to be reasonable, patient, encouraging, and scientifically savvy. Dane has made the PhD process an opportunity for me to grow personally and professionally and for that I sincerely thank him.

In addition, thank you to Alison Betts, our main collaborator at Pfizer. Alison initiated this collaboration, which was the core focus of my thesis work. I appreciate her enthusiasm and interest in discussing our work, as well as her support for me personally. I enjoyed learning about her perspective from industry on ADC design and development. During the course of this project, Alison also recruited the help of a Chethana Kulkarni, a Post-doc at Pfizer. Chethana was an instrumental part of this project. She helped synthesize and purify the Trastuzumab-Doxorubicin ADC using the Doxorubicin-SMCC linker. In addition, Chethana was engaged in technical discussions - asking pertinent questions and sharing her experiences and perspective as it relates to the work. I appreciate her detailed comments on manuscript drafts to help make the work easier to follow and the language more precise and concise. Throughout the project, we also engaged in technical discussions with Lindsay King and Nahor Haddish-Berhane at Pfizer. Thank you to Pfizer for partial funding support of this project.

Thank you to Paula Hammond, a member of my thesis committee. Paula was enthusiastic and supportive throughout my graduate work. She helped connect me to Mohi Quadir, a Post-Doc in her lab who has strong chemical synthesis expertise and was able to help synthesize and purify the Doxorubicin-SMCC linker, which we used to make the Trastuzumab-Doxorubicin ADC. This was crucial for helping many parts of my project move forward.

Thank you to Joe Balthasar, a member of my thesis committee. I am grateful to Professor Balathasar for asking probing questions and sharing alternative perspectives to consider when evaluating my results. He also helped me connect with the PK/PD community.

After we developed the model for ADC cellular processing, we wanted to incorporate these results into a larger PK/PD model, similar to the Bench to Bedside work done previously by Dhaval Shah, Nahor Haddish-Berhane, and Alison Betts. Alison helped connect us with Professor Dhaval Shah at the University of Buffalo and Aman Singh, a graduate student working in the Shah Lab. The implementation of the work described in Chapter 4 was spearheaded by Aman and Dhaval. I appreciate their collaboration on this work and efforts for multiple rounds of modification and revisions of the PK/PD model. The incorporation of the cellular level processing into a larger PK/PD model has brought more meaning to these results. Dhaval was also involved with my work early on during his time at Pfizer. He provided useful insight and discussions.

I appreciate all of the support I have gotten from my Wittrup Lab labmates throughout my time in the lab. I appreciate my labmates' willingness to teach me techniques, discuss data with me, brainstorm experimental approaches, and friendly faces to connect with in the office. Thank you to Annie Gai, John Rhoden, Xiaosai Yao, Jordi Mata-Fink, Tiffany Chen, Seymour de Picciotto, Cary Opel, Nicole Yang, Byron Kwan, Alice Tzeng, Eric Zhu, Ryan Kelly, Monique Kauke, Naveen Mehta, Adrienne Rothschilds, and Alison Tisdale. Thank you to the Post-Docs who have overlapped time with me in the lab: Alessandro Angelini, Michael Traxlmayr, and Jim Van Deventer.

Thank you to the Hertz Foundation for honoring me with a Hertz Foundation Fellowship. My graduate school experience would not have been the same without the support of the Hertz

Fellowship and the Hertz Community. I have enjoyed expanding my scientific breadth via interactions with other In-school Hertz Fellows and other members of the Hertz community. When experiments weren't going well, I got a boost of confidence knowing that the Hertz Foundation believed in my success.

I have especially enjoyed being a part of the MIT Koch Institute for Integrative Cancer Research. I've appreciated the enthusiasm to bring together scientist and engineers from a range of backgrounds to learn from and collaborate with one another. It has been a fantastic place to work. In addition, during my graduate work, I have used a number of the core facilities in the Koch Institute Swanson Biotechnology Center, which I would like to thank for technical support, specifically the Flow Cytometry facility (Glenn Paradis and Michael Jennings), the Microscopy facility (Eliza Vasile), and the Biopolymers and Proteomics facility (Richard Cook, Alla Leshinsky, and Heather Amoroso). This work was supported in part by the Koch Institute Support (core) Grant P30-CA14051 from the National Cancer Institute.

In addition, I appreciate the funding support from a National Science Foundation (NSF) Graduate Research Fellowship.

There are a number of other MIT communities that have shaped my MIT experience and made MIT feel more like a home to me. Thank you to my ChemE classmates for being a supportive group as we all travel through the PhD process together. In addition, during my first few years at MIT, I lived in Sidney-Pacific Graduate Housing. The Sid-Pac community was a welcoming family that made me feel part of the graduate community at MIT. During my time at MIT, I also had the privilege to ride and race with the MIT Cycling team. Thank you for the friendship and for teaching me about road bikes, racing, bike maintenance, and cyclocross. I look forward to joining the ranks of MIT Cycling West!

I would also like to thank my family – my parents, my brother Nick, my grandparents, aunts, uncles, and cousins – for their endless love and support. They never fail to remind me how proud of me they are.

Finally, I would like to thank my boyfriend Raymond Smith for his unwavering support and kindness. His willingness to lend an ear and patience to help talk me through a problem – whether it is about science, data presentation, or a personal issue – brings me strength and courage to tackle whatever the world brings me. His scientific curiosity is inspiring to me and pushes me to think about the world around me and continuously learn. He has contributed in so many ways directly and indirectly to this thesis. Thank you, Ray!

In loving memory of Faye Maass

TABLE OF CONTENTS

List of Figures

List of Tables

List of Abbreviations

ADC	Antibody-Drug Conjugate
ADCC	Antibody-Dependent Cellular Cytotoxicity
ATCC	American Type Culture Collection
DAR	Drug-to-Antibody Ratio
FDA	(United States) Food and Drug Administration
HER2	Human Epidermal Growth Factor Receptor 2
IC_{50}	half maximal Inhibitory Concentration
MDR1	Multi-Drug Resistance Pump 1
PD	Pharmacodynamics
Pgp	P-GlycoProtein 1
PK	Pharmacokinetics
SMCC	Succinimidyl 4-[N-Maleimidomethyl] Cyclohexane-1-Carboxylate
T-DM1	Trastuzumab-DM1, also known as Trastuzumab Emtansine or Kadcyla
TM-ADC	Trastuzumab Maytansinoid Antibody-Drug Conjugate
TM-ADC-647	Alexa Fluor 647 labeled Trastuzumab Maytansinoid Antibody-Drug Conjguate
Tras-Dox	Trastuzumab-Doxorubicin Antibody-Drug Conjugate
Tras-647	Alexa Fluor 647 labeled Trastuzumab

Chapter 1: Introduction

1.1 Background

Cancer is the second most common cause of death in the United States, behind heart disease, resulting in approximately 585,000 deaths per year in the United States[1]. Standard treatments include a mix of surgery, radiation, and chemotherapy depending on the tumor type, location, and severity. Current cancer chemotherapy treatments are limited in dose by systemic toxicity.[2] The standard of care for cancer patients involves combination therapies to maximize the cytotoxic effect of multiple drugs while limiting the organ specific toxicity.[3] One promising cancer therapy, antibody-drug conjugates (ADCs), uses the combination of potent chemotherapeutic drugs with an antibody to target cancer cells in order to reduce toxicity while maintaining efficacy. ADCs consist of three components: (1) an antibody targeting an antigen overexpressed on cancer cells, (2) a small-molecule cytotoxic drug, and (3) a chemical moiety to link the antibody and drug. Design considerations for each of these components are described below.

The basic proposed mechanism of action for ADCs follows that depicted in Fig. 1.1[4]. Once the ADC reaches an antigen-expressing tumor cell, the ADC binds its target antigen. Then, the ADC is internalized via receptor-mediated endocytosis into endosomal/lysosomal compartments. In the endosomal/lysosomal compartment, the ADC is degraded, in a mechanism dependent on the linker design, and the drug component is released from the antibody. The free drug or drug metabolite is released from endosomal/lysosomal compartments into the cytosol. Then, the drug either binds to its intracellular target, such as microtubules or DNA in the nucleus, or is pumped or diffuses out of the cytosol into the extracellular space. The drug released into the cytosol may also be pumped back into endosomal/lysosomal compartments by p-glycoprotein 1 (pgp), also known as multi-drug resistance pump 1 (MDR1). These drug pumps have been shown to be overexpressed in drug resistant cell lines and are correlated with sequestration of drugs in the acidic compartments in the endosomal/lysosomal pathway.[5]

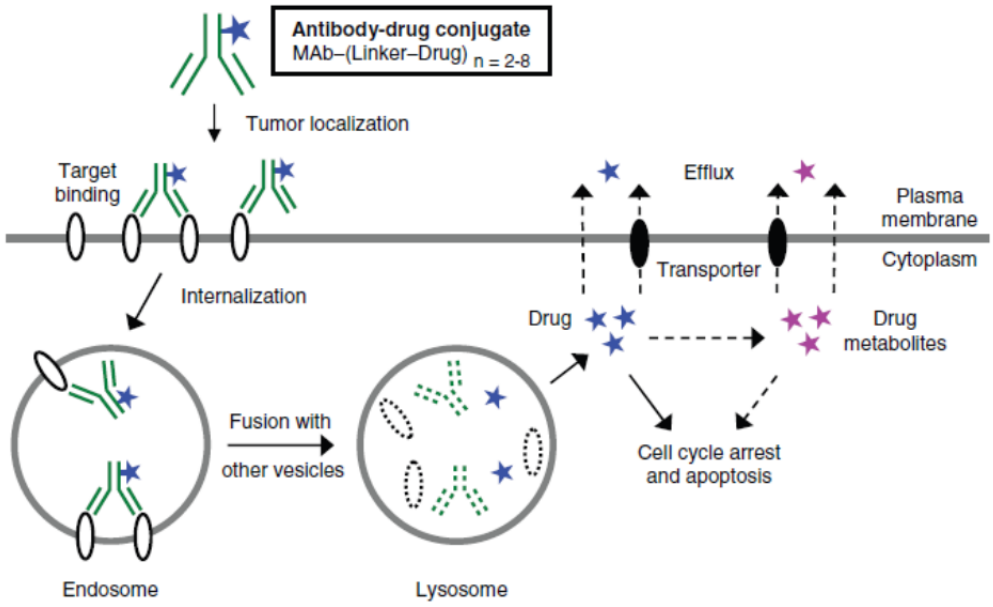

Figure 1.1 Proposed mechanism of action for antibody-drug conjugates[4]

1.1.1 Antibody Design Considerations for ADCs

A wide range of antigen targets have been considered in ADC development. Targets on B, T, endothelial, stromal, vascular, myeloid, hematopoietic, and carcinoma cells have been tested.[6] The parameters to consider for antigen selection include overexpression on target cells versus healthy normal cells, absolute expression level, internalization rate, and surface expression versus shed antigen.

Having a low antigen expression level on healthy normal cells is critical to limiting toxicity of ADCs. A few ADCs in development have been removed from clinical trials due to toxicity related to expression of the target antigen in normal tissues.[7,8] The absolute expression level of antigen may or may not be critical as there have been successful results with ADCs targeting CD33 in acute myeloid leukemia, which is expressed at a level of 5,000-10,000 per cell.[4] More typically, the target antigen is expressed at a level of 10^5-10^6 per cell.[9]

Typically, it is assumed that the ADC must be internalized for the drug to be delivered to tumor cells. Thus, the rate of internalization is important for dictating how much drug is delivered to the tumor. However, it has also been demonstrated that non-internalizing ADCs can also be efficacious.[10] The antibody binding to tumor antigens helps concentrate the drug in the tumor vicinity and provides a drug sink for the tumor. Expression of the target antigen on all tumor cells may also not be critical based on the phenomenon known as the bystander effect. The

bystander effect is the killing of cells nearby a cell targeted by an ADC caused by the drug component which has been cleaved from the ADC, released from the cell, and then taken up by nearby cells.[11,12] Antigen which is shed from the surface can be problematic since it reduces the number of ADCs that reach a tumor cell and get internalized.

The conjugation site on an antibody is also an important ADC design choice. The two most common sites for conjugation are the free amines of lysine residues and free thiols from cysteine residues. The use of non-natural amino acids has also been explored.[13] Fig. 1.2 shows the different typical conjugation sites that have been used. There are on average 40 lysine residues distributed across an antibody available for conjugation; however, most ADCs using conjugation via the lysine residues will have a drug to antibody ratio (DAR) of only four.[4,14] Contrary to the initial hypothesis that ADCs with the highest DAR would be most effective, ADCs with 2-4 drug molecules are more effective than those with 8.[4,15] ADCs with 8 drug molecules loaded tend to have a much shorter half-life and are cleared more rapidly than ADCs with fewer drug molecules.[15] The pharmacokinetics of an ADC with only 2 drug molecules is very similar to that of the parent antibody.[15]

Conjugation via the hinge region cysteine in an antibody has been another approach used. IgG1 antibodies are used most commonly for therapeutic antibodies and they have four disulfide bonds between cysteine residues in the hinge region.[4,16] The hinge region is the region between the antigen binding fragment, F_{Ab}, and the constant fragment, F_C, of the antibody. With various reducing agents, these disulfide bonds can be broken and conjugated to a drug. As depicted in Fig. 1.2 B-D, the average DAR using these cysteine conjugation sites is four. However, heterogeneous mixtures of ADCs with two, four, six, or eight drug molecules are produced with this approach.[15]

Another type of conjugation site is the site-specific conjugation to engineered cysteine sites.[17,18] Rather than conjugate to the hinge region cysteine residues, selected amino acids are mutated to cysteine residues and used as the conjugation site. Specific conjugation to the engineered sites is achieved by complete reduction of all exposed cysteine residues and then re-oxidation of the hinge region cysteine residues via $CuSO_4$ or dhAA.[17] This type of conjugation has been pioneered by Genentech and the resulting antibody-drug conjugates are known was THIOMABs.[17] Using site-specific conjugation can be advantageous from a regulatory

perspective because the ADC is much more homogenous and results in fewer degradation products to characterize.

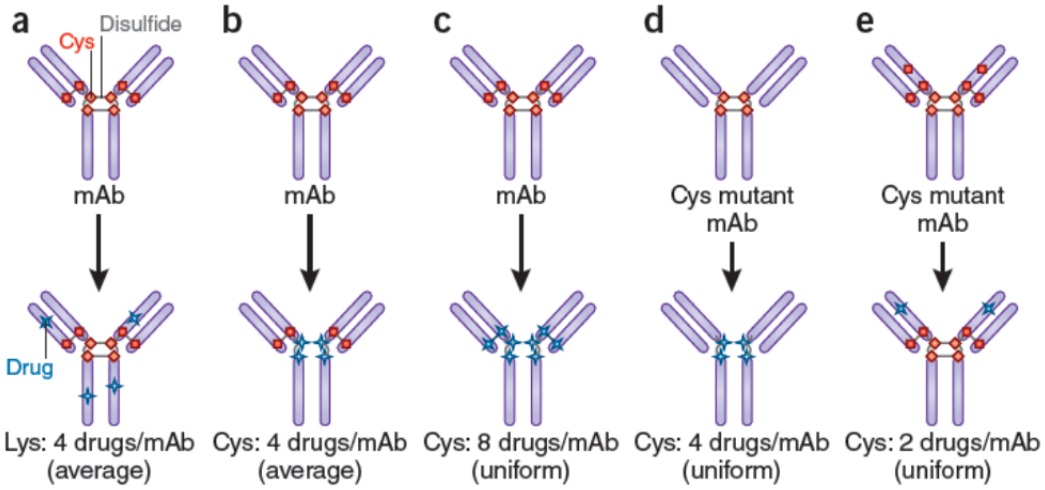

Figure 1.2 Different types of conjugation sites used to create ADCs. (A) Conjugation using lysine residues, (B) heterogeneous conjugation of hinge cysteine residues, (C) and (D) homogeneous conjugation of hinge cysteine residues with 4 or 8 drugs per antibody, and (E) homogeneous conjugation of engineering cysteine residues to produce THIOMABs.[19]

One final consideration for antibody selection is the activity of the antibody itself. Antibodies have been used on their own as cancer therapeutics in multiple ways including as receptor antagonists or agonists, to cause signal disruption, and immune-dependent cell killing such as antibody-dependent cellular cytotoxicity (ADCC).[20] The antibody component of an ADC may have a therapeutic effect itself independent of its drug payload. Advances in the technological development of antibodies as therapies including the advent of humanized monoclonal antibodies has eliminated many of the immunological problems with early generation ADCs.[21] It is still unclear whether the binding of Fcγ receptor and FcRn are advantageous for ADCs and how drug conjugation affects binding to these receptors. It has been shown that antibody binding to Fcγ receptors is important for ADCC[22] and is diminished by mutations in the hinge region.[23] Binding to FcRn is important for the long half-life observed for antibody therapies. Upon antibody internalization, binding to FcRn causes the antibody to be rescued from degradation and recycled to the cell surface.[24] While rescue of antibodies via FcRn binding is desired for ADCs taken up by pinocytosis in normal tissues, FcRn recycling of ADCs

is undesired in the tumor cell because it may prevent the drug from being released from the ADC or cause antigen binding sites for new ADC molecules to be blocked by naked antibody.

1.1.2 Drug Design Considerations for ADCs

The key characteristics in drug selection include potency, toxicity, and a functional group for conjugation. Most of the drugs used in ADCs target either DNA or microtubules, as demonstrated by the list of drug classes that have been used in ADCs shown in Fig. 1.3[11]. The early generation ADCs used drugs that are much less potent than the ADCs currently being developed.[25] One rule of thumb for drug selection is that the IC_{50} should 0.01-0.1 nM.[25] With most drugs, increased potency is associated with increased toxicity. Thus, with higher potency drugs, the importance of the stability of the linker while the ADC is in circulation is increased.

Cytotoxic compounds that have been used in antibody–drug conjugates

Name	Target	Mode of action
Anthracycline drugs (e.g. doxorubicin)	Topoisomerase II–DNA complexes	Inhibit DNA re-ligation, leading to double-strand breaks in DNA
Maytansinoids and dolastatin derivatives (auristatins)	β-Subunit on tubulin dimers and microtubules	Suppress microtubule dynamics at low concentrations; depolymerize microtubules at high concentrations
Taxol derivatives (taxoids)	The interior surface of microtubules	Stabilize microtubules excessively, altering microtubule dynamics
Calicheamicin derivatives	TCCT sequences on the minor groove of DNA	Cause sequence-specific double-strand DNA cleavage
CC-1065 and duocarmycin analogs	AT-rich regions of the minor groove of DNA	Induce adenine alkylation

Figure 1.3 Drug classes which have been used in ADCs[11]

1.1.3 Linker Design Considerations for ADCs

Key parameters affecting linker choice include stability, two chemical functional groups to react with the antibody and the drug, and ability to release drug upon arrival to the tumor. An ideal linker would release no drug during circulation in the blood; however, would rapidly release the drug at the site of the tumor. There are three classes of linkers that have been used in ADC development: (1) chemically-labile, (2) enzymatically-labile, and (3) non-cleavable linkers.[26]

Chemically-labile linkers cleave due to chemical differences within the cancer cell or tumor environment versus the environment outside the cell and circulating in the blood. One chemically-labile linker is hydrazone linkers which cleave due to the higher pH of endosomal/lysosomal compartments inside the cell. Another chemically-labile linker is disulfide bonds, which cleave inside cells due to the higher reduced glutathione concentration within cells. Examples of both of these linkers are illustrated in Fig. 1.4A and 1.4B.[4,26]

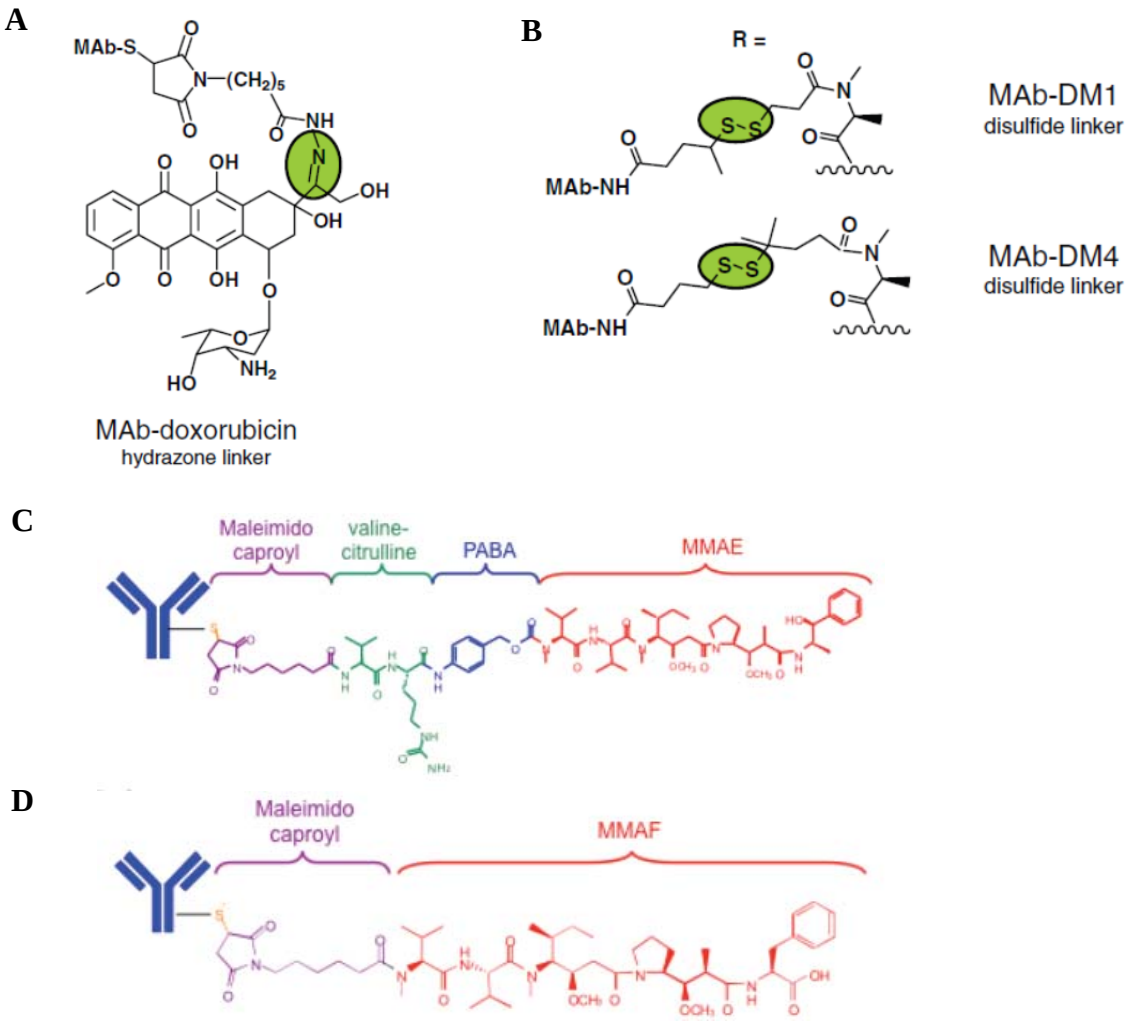

Figure 1.4 Examples of ADC linkers. (A) Hydrazone linker; the cleavage point is highlighted in green[4]. (B) Disulfide linker with and without steric hindrance[4]. (C) Enzymatically-labile linker with valine-citrulline amino acids[18] and (D) Non-cleavable linker[18].

Enzymatically-labile linkers consist of peptide bonds which are cleaved by enzymes found within cells, such as lysosomal proteases. A common enzymatically-labile linker is valine-

citrulline (vc), which is cleaved by cathepsin. An example of the vc linker in an ADC is shown in Fig. 1.4C. Enzymatically-labile linkers have been shown to have more stability when circulating in plasma than chemically labile-linkers.[27]

Non-cleavable linkers are designed to remain intact rather than be cleaved. The initial active drug component is then the drug, linker, and a residual amino acid from the degraded antibody. An example of a non-cleavable linker is shown in Fig. 1.4D. Non-cleavable linkers tend to include thioethers such as those introduced via maleimide groups.

The active drug component released from an ADC depends on the linker used. Fig. 1.5[28] illustrates an example of the difference in degradation products for a non-cleavable linker (SMCC) and a chemically-labile disulfide linker (SPDB). The degradation products lysine-linker-drug are considered highly potent within the cell since they act like the potent drug component but have low potency outside the cell because the charged lysine residue prevents this component from re-entering the cell and reaching its intracellular target, microtubules.

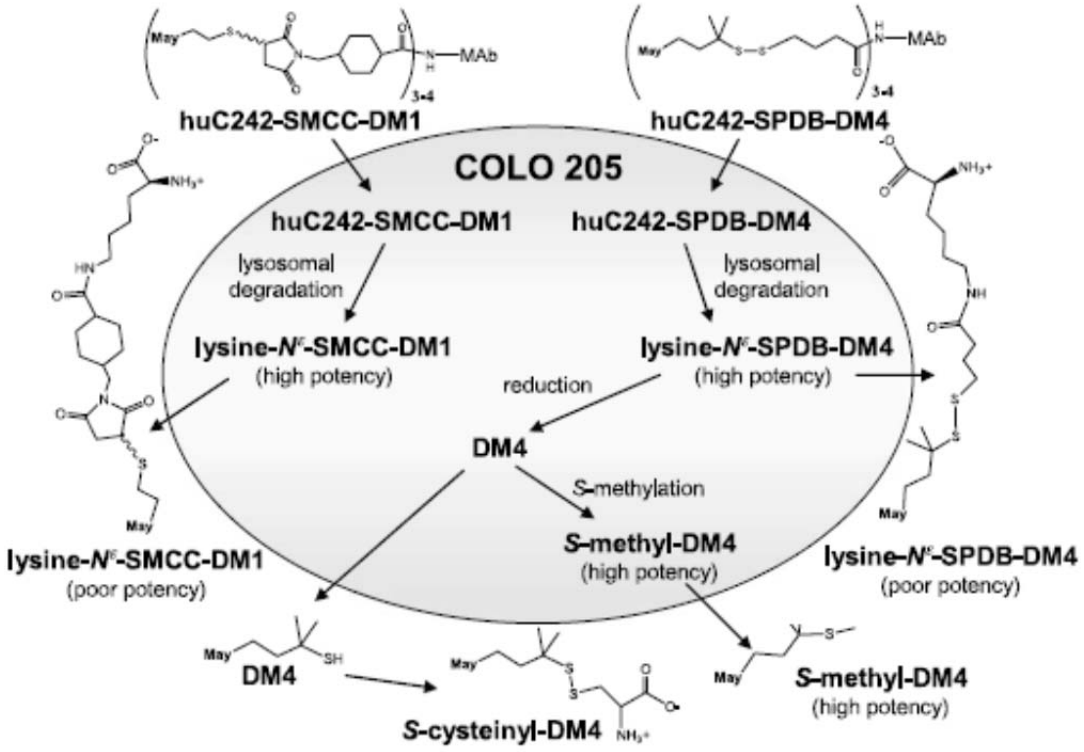

Figure 1.5 Demonstration of ADC degradation depending on linker type. The left-hand side pathways are for degradation of the ADC with the linker SMCC which is non-cleavable. The right-hand side pathways are for degradation of the ADC with the SPDB linker which includes a disulfide bond and is chemically labile.[28]

1.1.4 Clinically Approved ADCs

Although more than 40 ADCs are currently in clinical trials[29], only two ADCs are currently approved by the U.S. Food and Drug Administration (FDA). These approved ADCs will be described in the following and are illustrated in Fig. 1.6.

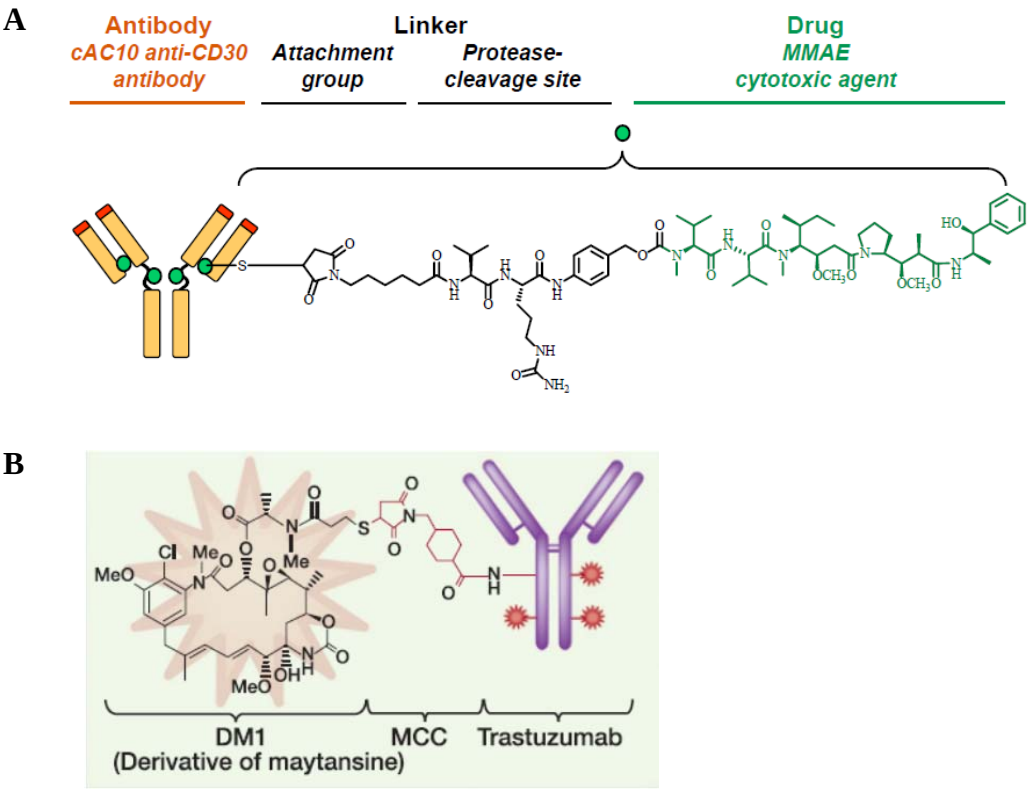

Figure 1.6 Illustrations of the two FDA approved ADCs. (A) brentuximab vedotin[30] and (B) Trastuzumab-DM1[31].

The first approved ADC in the US was approved in 2000. The FDA granted accelerated approval for gemtuzumab ozogamicin, Mylotarg®. Mylotarg consists of a humanized antibody (IgG4) targeting CD33, an acid cleavable hydrazone linker, and a calicheamicin derivative drug conjugated to lysine residues.[20] It was approved for patients with acute myeloid leukemia (AML); however, it was removed from US markets in 2010 after safety concerns and failure to prove efficacy in further clinical trials.[32]

More than 10 years after Mylotarg was approved, brentuximab vedotin, Adcetris™, was approved in 2011 for treatment of Hodgkin lymphoma and systemic anaplastic large cell

lymphoma after failure of other standard therapies.[30] It consists of a chimeric anti-CD30 antibody, an enzymatically labile valine-citruline linker, and the auristatin drug MMAE conjugated to hinge region cysteine residues with an average DAR of 4.[19] Brentuximab vedotin has shown much success as a therapy and is a landmark for the field of ADCs.[19] Note that both Mylotarg and Adcetris are for haematological cancers, which eliminates some of the tumor penetration concerns and obstacles that may be encountered with solid tumors.

The other ADC that is currently approved in the United States is Trastuzumab-DM1 (T-DM1).[31,32] T-DM1 consists of a humanized antibody, Trastuzumab or Herceptin®, that is also FDA-approved on its own in combination therapy for HER2-positive breast cancer. The potent tubulin targeting maytansinoid drug DM1 is conjugated to Trastuzumab via the non-cleavable linker MCC and lysine residues on the antibody.

As is apparent from the previous description of design considerations, there are many parameters to consider for each of the three components in an ADC. However, it is unclear which parameters are most important for ADC optimization and how changes in multiple parameters affect the overall ADC efficacy. Experiments have shown for individual ADCs how parameters such as linker type[28] or conjugation site[18] affect ADC potency, but it is unclear how generalizable these results are.

1.2 Thesis Overview

The focus of this thesis is on the cellular level processing of antibody-drug conjugates (ADCs). With a better understanding of how ADCs get processed, ADCs can be designed more rationally hopefully resulting in more effective ADCs.

- In **Chapter 2**, we developed a flow cytometric clonogenic assay to answer the question "How many drug molecules do you need to deliver to an individual cell to cause it to stop proliferating?" We then applied this assay to determine the single-cell potency of the chemotherapeutic drug, doxorubicin.
- In **Chapter 3**, we developed a basic model for the cellular processing of T-DM1, one of the two approved ADCs, and experimentally measured each of the relevant model parameters. These results illustrate how the various processing steps interact with one another.
- In **Chapter 4**, we incorporated the cellular level ADC processing model into a larger pharmacokinetic/pharmacodynamic model. This work has been done in close collaboration with Aman Singh and Professor Dhaval Shah at the University of Buffalo.
- In **Chapter 5**, we study how ADCs spatially traffic through a cell as they are processed. We use a Trastuzumab-Doxorubicin ADC with fluorescence microscopy to compare how much drug is delivered to its target with an ADC versus the free drug.
- In **Chapter 6**, we provide an overall conclusion and outlook for antibody-drug conjugate development.

Chapter 2: Flow Cytometric Clonogenic Assay Development and Application with Doxorubicin

The contents of this chapter have been published previously in the Journal of Pharmaceutical Sciences.[33]

2.1 Abstract

Standard cell proliferation assays use bulk media drug concentration to ascertain the potency of chemotherapeutic drugs; however, the relevant quantity is clearly the amount of drug actually taken up by the cell. To address this discrepancy, we have developed a flow cytometric clonogenic assay to correlate the amount of drug in a single cell with the cell's ability to proliferate using a cell tracing dye and doxorubicin, a naturally fluorescent chemotherapeutic drug. By varying doxorubicin concentration in the media, length of treatment time, and treatment with verapamil, an efflux pump inhibitor, we introduced 10^5 – 10^{10} doxorubicin molecules per cell; then used a dye-dilution assay to simultaneously assess the number of cell divisions. We find that a cell's ability to proliferate is a surprisingly conserved function of the number of intracellular doxorubicin molecules, resulting in single-cell IC_{50} values of 4 – 12 million intracellular doxorubicin molecules. The developed assay is a straightforward method for understanding a drug's single-cell potency and can be used for any fluorescent or fluorescently-labeled drug, including nanoparticles or antibody-drug conjugates.

2.2 Introduction

Routinely used *in vitro* proliferation assays provide a high throughput method for evaluating the potency of chemotherapeutic drugs.[34,35] Typical proliferation assays use the bulk media concentration to determine the drug potency (i.e. IC_{50} or IC_{90}). However, the drug concentration on a media volumetric basis would need to be freely in equilibrium with the drug's intracellular target for this to truly represent the drug's intrinsic potency. This is not true in almost any case since drugs encounter membranous diffusion barriers and may be substrates for active uptake or efflux transporters.[36] The amount of drug internalized into the cell is a more physiologically relevant basis for comparison than the bulk media concentration[37,38] especially when considering drug delivery systems that involve endosomal transport and processing steps, such as antibody-drug conjugates or liposome drug delivery systems.[39] It is now within the purview and capability of the drug designer to attempt to alter a drug's interaction with these transport and processing machineries, in order to attain more efficient delivery on target. However, a key piece of information in such cases is the number of drug molecules on target necessary for the desired effect (e.g. how many doxorubicin molecules does it take to kill a cell?). This information is not directly available from potencies determined on a media-volume basis. The assay described herein uses the amount of drug in an individual cell as the basis for cellular response rather than the drug concentration in the cell growth media.

Standard chemotherapy potency assays include non-clonogenic assays that are based on changes in cell membrane permeability (Lactate Dehydrogenase or Trypan Blue), mitochondrial function (MTT (3-(4,5-dimethylthiazol-2-yl)-2,5- diphenyltetrazolium bromide) or WST-1 Assay), or markers for early (Annexin V) or late apoptosis (Terminal deoxynucleotidyl transferase dUTP nick end labeling (TUNEL) or cytochrome c).[40] In contrast, clonogenic assays measure a cell's ability to proliferate after treatment. Traditionally, proliferation is measured by counting clones that have grown out after cells have been plated at low density.[41] Clonogenic assays capture all types of cell death and include cell growth after reversible damage, whereas non-clonogenic assays measure acute cellular toxicity, often specific to one type of cell death. Since clonogenic assays capture the integrated effect of many different types of cellular response to drug treatment, we focused on this assay type.

Here, we develop a flow cytometric dye-dilution clonogenic assay to determine the relationship between the amount of drug in a single cell and the cell's ability to proliferate. Flow cytometry enables high-throughput screening of thousands of individual cells, resulting in analysis on a single-cell level rather than a bulk population level. The assay uses a cell tracing dye and a fluorescent drug. A cell tracing dye is used to track cell proliferation via dye dilution. All cells are initially stained with dye and the dye is diluted in half with each cell division. A fluorescent drug is used in order to measure the amount of drug taken up by each cell.

In this work, we used doxorubicin, a standard chemotherapeutic drug[42], which is also naturally fluorescent[43], as a model drug to demonstrate application of the assay. Doxorobucin is known to bind DNA and inhibit topoisomerase II[42] and is widely used as a front-line therapy for a number of different types of cancer.[44]

2.3 Materials and Methods

2.3.1 *Cell Lines and Materials*

Eight different cell lines were used in this work: BT-474, HCT-15, HT-29, IGROV-1[45], MDA-MB-231, NCI-N87, SK-BR-3, and T-47D. Cell Lines were purchased from American Type Culture Collection (ATCC). All cell lines except HT-29 and SK-BR-3 were grown in RPMI (Corning) supplemented with 10 % fetal bovine serum (FBS) and 5 % penicillin-streptomycin. HT-29 and SK-BR-3 cells were grown in Dulbecco's Modified Eagle Medium (DMEM, Corning) and McCoy's 5A Medium Modified (Lonza), respectively, supplemented in the same way. Doxorubicin hydrochloride and verapamil were purchased from Sigma.

2.3.2 *Assay Set-up*

Cells were stained using CellTrace™ Violet Cell Proliferation Kit (Life Technologies) following the "Standard Method for Labeling Cells in Suspension" as described in the product manual. Then, 10^5 cells were plated per well in 6-well tissue culture plates (BD). The cells were treated with doxorubicin hydrochloride at concentrations ranging from 10 nM to 5 μM in standard growth media. Control cells that were either stained with CellTrace Violet only or unstained were plated at the same time. After 24 h, the cells were washed with PBS and the media was replaced with fresh growth media. After an additional 3 days, the cells were trypsinized and prepared for flow cytometry. Flow cytometry was performed using a BD FACSCanto II. The doxorubicin signal was measured using excitation with a 488 nm laser and detection with a 585 nm ± 42 nm filter. The CellTrace Violet signal was measured using excitation with a 405 nm laser and detection with a 450 nm ± 50 nm filter. We collected data for 10,000 cells (gated based on forward and side scatter) per condition, unless there were an insufficient number of cells remaining. See also Appendix B.4.

2.3.3 *Treatment Length Study*

For the dosing time study, MDA-MB-231 cells were plated as described above in the Assay Set-up section. Initially, the media either had a medium (0.3 μM) or high (5 μM) dose of doxorubicin. The cells were washed at various time points (12, 24, 48, 72, and 96 h) and the

media was replaced with fresh growth media. All cells were read on the flow cytometer at the same time after a total of 4 days after plating.

2.3.4 *Verapamil Treatment*

Using HCT-15 cells, the study with verapamil treatment was set up as described above in the Assay Set-up section with 20 μM verapamil in the growth media. The replacement media after 24 h also contained 20 μM verapamil.

2.3.5 *Data Analysis*

The raw flow cytometry data were processed in the following manner in order to draw together the results from numerous single-cell measurements from different treatment conditions. FlowJo software and MATLAB (Mathworks) were used for data processing. First, the doxorubicin signal was calibrated as described in the "Calibration of Doxorubicin Signal" section. Next, we normalized the CellTrace signal with respect to the median CellTrace Signal for untreated cells as described in equation 2.1.

$$\text{Proliferation factor} = \frac{\text{Median CellTrace Fluorescence Signal of Untreated Cells}}{\text{CellTrace Fluorescence Signal of Sample}} \qquad (2.1)$$

Note that the fluorescence signal from untreated cells is in the numerator of the expression in equation 2.1. Cells that did not proliferate at all have a high CellTrace signal because the CellTrace has not been diluted by growth. Thus, the proliferation factor is low for cells which had fewer cell divisions and is equal to one if cells were unaffected by treatment. The theoretical minimum for the proliferation factor with complete inhibition of growth is 2^{-n}, where n is the number of doublings for untreated cells.

With both fluorescence signals converted, the cells were binned based on amount of intracellular doxorubicin. 100 bins were used with even logarithmic spacing from 10^4 to 10^{10} intracellular doxorubicin molecules. Any bin with fewer than 100 cells was omitted. For each bin of cells, median proliferation factor was plotted versus the median number of intracellular doxorubicin molecules resulting in a cellular response curve to doxorubicin treatment. The included plots show cellular response curves for either individual treatment conditions or for data

from all treatment conditions concatenated into one response curve. When processing the fluorescence signal from control cells, half of the untreated cells appear as if they have doxorubicin signal despite never being treated with doxorubicin since the median doxorubicin signal for untreated cells was used to subtract out background fluorescence signal. In addition, the lower half of the control cells appear to have a negative number of doxorubicin cells based on the calibration of the doxorubicin signal and thus do not appear in the analysis plots since the plots are log-based.

2.3.6 *Calculation of Standard and Single-Cell* IC_{50}

The standard IC_{50} is the media doxorubicin concentration required for 50 % of maximum reduction in proliferation factor. The single-cell IC_{50} is the number of intracellular doxorubicin molecules required for a 50% of maximum reduction in proliferation factor. The IC_{50} values were calculated from a nonlinear regression with the "log(inhibitor) vs. response (three parameter)" equation in GraphPad Prism software. Median proliferation factor for each treatment condition was used for standard IC_{50} and the median values from bins for the concatenated data for each cell line was used for single-cell IC_{50}. Confidence intervals were also calculated in the GraphPad Prism software.

2.3.7 *Calibration of Doxorubicin Signal*

In order to convert the fluorescence signal from doxorubicin to numbers of intracellular doxorubicin molecules, we used calibration beads (Quantum™ Simply Cellular® anti-Human IgG, Bangs Laboratories, Inc.) and a Trastuzumab-Doxorubicin conjugate (Tras-Dox). In future work, we will characterize the pharmacodynamics of Tras-Dox; however, for the purposes of the present discussion, it serves only as a useful calibration standard. BT-474, NCI-N87, and SK-BR-3 cells were used since they have a high expression of HER2, the antigen target for Trastuzumab. These cells were fixed using BD Cytofix™ Fixation Buffer following the recommended protocol. For each cell line, 1.25×10^5 cells were stained with 60 nM Alexa Fluor-647 labeled Trastuzumab (Tras-647) in staining buffer (PBS with 0.2 % bovine serum albumin and 0.09 % sodium azide). Another 1.25×10^5 cells were stained with 50 nM Tras-Dox in staining buffer. Cells were stained overnight at 37 °C. After staining, cells were washed twice with cold stain buffer before being read on the flow cytometer.

Calibration beads were stained with 100 nM Tras-647 following the manufacturer's recommended protocol. The calibration beads and Tras-647 labeled cells were read on a BD Accuri C6 Flow Cytometer. Using the linear fit from calibration, the HER2 receptor expression level on each of the cell lines was determined from the fixed cells stained with Tras-647. Cells stained with Tras-Dox were read on a BD FACS Canto II. From the HER2 expression level, Tras-Dox drug-to-antibody ratio, and doxorubicin fluorescence intensity of cells saturated with Tras-Dox, the number of doxorubicin molecules per fluorescence signal unit was determined. This was used as a scaling factor to convert fluorescence signal from cells to number of intracellular doxorubicin molecules. The fluorescence signal above background (median fluorescence signal of untreated cells) was considered signal from doxorubicin.

2.3.8 *Synthesis of Doxorubicin-SMCC*

Doxorubicin-SMCC was prepared using a modification of a previously published procedure[46] as illustrated in Fig. 2.1. Doxorubicin HCl salt (1, 0.050 g, 0.086 mmol, 1.0 equiv.), succinimidyl 4-[N-maleimidomethyl] cyclohexane-1-carboxylate (SMCC, 2, 0.035 g, 0.104 mmol, 1.2 equiv.), and diisoprpylethylamine (Hünig's base, 0.065 mmol, 1.5 equiv.) were added to anhydrous DMF (3.0 mL) in a 100 mL round-bottomed flask. The reaction was allowed to run in the dark at room temperature under inert conditions overnight.

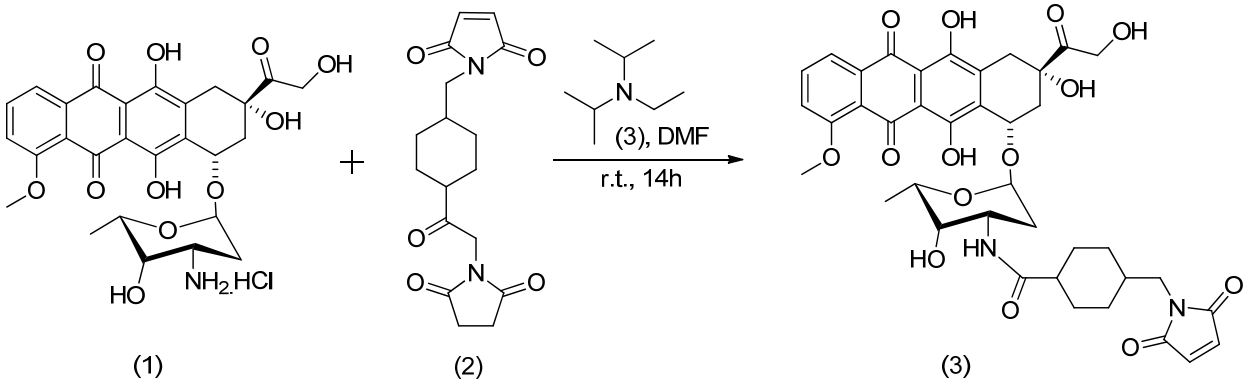

Figure 2.1 Synthesis of Doxorubicin-SMCC

After evaporation of the solvent under vacuum at 35 – 40 ºC, the residue was dissolved in 15 mL dichloromethane and washed with brine three times (3 x 5 mL). The organic phases were pooled together and dried over anhydrous magnesium sulfate. After filtration and washing of the

solid filter cake with additional dichloromethane (2 x 5 mL), the filtrate and washings were combined and concentrated *in vacuo* to viscous oil. Silica gel column chromatography of the residue (eluted with 0 – 5 % methanol/dichloromethane) yielded a red solid product at 89 % yield: MALDI-TOF MS m/z 785.559 [with Na^+, the K^+ adduct also observed at 801.528]; R_f 0.31 (95/5 CH_2Cl_2/MeOH); UV λ_{max} 204, 251, 479, 490 nm. Major ^1H NMR signals were found to be identical with previously reported[46] compound (3): ^1H NMR (400 MHz, DMSO-d_6) δ = 0.91 (m), 1.19 (m), 1.62 (m, 4H), 1.84 (m, 1H), 2.20 (m), 3.21 (d, 2H), 3.81 (m, 1H), 4.21 (m, 4H), 4.62 (s, 2H), 4.80 (d, 1H), 4.94, 5.24 (s, 1H), 5.80 (s, 1H), 7.40 (d, 1H), 7.67 (d, 1H), 7.96 (m, 2H), 12.43 (s, 1H), 13.21 (s) ppm.

2.3.9 *Preparation of Trastuzumab-Doxorubicin Conjugate (Tras-Dox)*

A Trastuzumab antibody mutant with an engineered cysteine site for conjugation, Trastuzumab A114C, was prepared according to literature procedure.[17] Trastuzumab A114C antibody (7 mg/mL final concentration) was reacted with 6 equivalents of doxorubicin-SMCC in PBS with 15 % dimethylacetamide. The reaction tube was incubated in a Thermomixer (Eppendorf) at 25 °C and 700 rpm for 2 h. Initial clean-up and concentration of the reaction mixture were completed using a PD-10 desalting column (GE Healthcare) and an Amicon centrifugal filter unit (EMD Millipore), respectively. An AKTA size exclusion chromatography system (GE Healthcare) was employed for purification. The final conjugate had a drug-to-antibody ratio (DAR) of 2, based on LC-MS characterization results.

2.3.10 *Preparation of Trastuzumab-Alexa Fluor 647 Conjugate (Tras-647)*

A Trastuzumab antibody mutant with an engineered cysteine site for conjugation, Trastuzumab A114C, was prepared according to literature procedure.[17] Trastuzumab A114C antibody (1 mg/mL final concentration) was reacted with 5 equivalents of NHS-Alexa Fluor 647 (Life Technologies) in PBS with 10 % 1 M borate buffer (pH 9). The reaction tube was affixed to a rotator at room temperature for 2.5 h. Initial clean-up and concentration of the reaction mixture were completed using a PD-10 desalting column (GE Healthcare) and an Amicon centrifugal filter unit (EMD Millipore), respectively. An AKTA size exclusion chromatography system (GE Healthcare) was employed for purification. The final conjugate had a fluorophore-to-antibody ratio of 1.4, based on LC-MS characterization results.

2.4 Results

2.4.1 *Data Processing for Flow Cytometric Clonogenic Assay*

For meaningful comparisons, the raw flow cytometry data were processed as illustrated in Fig. 2.2. The doxorubicin signal was converted to number of intracellular doxorubicin molecules using the calibration method as described in the methods section. The doxorubicin signal from calibration beads (10^5 antibody binding sites) saturated with Tras-Dox was too dim to use for calibration (data not shown). Instead, we measured the signal for saturated, fixed cells (10^6 antibody binding sites) stained with Tras-Dox and correlated this signal with the known number of doxorubicin molecules per antibody and number of HER2 receptors per cell, which was measured using calibration beads and Alexa Fluor 647 labeled Trastuzumab (Tras-647). This calibration yielded a scaling factor for the doxorubicin signal observed and number of intracellular doxorubicin molecules. With our flow cytometry settings, 100,000 ± 19,000 (standard error of the mean) doxorubicin molecules result in one flow cytometric fluorescence unit. See Table 2.1 for the flow cytometry data used to reach this conversion factor.

Table 2.1 Conversion of Fluorescence Signal to Number of Intracellular Doxorubicin Molecules

Cell Line	**Tras-647 Cell Signal** (Treated MFU – untreated MFU)	**HER2 Expression Level** (# of HER2 receptors per cell)	**Tras-Dox Cell Signal** (Treated MFU – untreated MFU)	**Number of Intracellular Doxorubicin Molecules per MFU**
BT-474	1.2×10^6	2.34×10^6	70.0	6.7×10^4
N87	1.4×10^6	2.67×10^6	40.2	13.3×10^4
SK-BR-3	1.1×10^6	2.23×10^6	45.0	9.9×10^4
			Average	$10.0 \times 10^4 \pm 1.9 \times 10^4$

Fig. 2.2A and 2.2B illustrate the data processing for untreated control cells and cells treated with the highest doxorubicin treatment (5 μM doxorubicin in media). As expected, the cells treated with doxorubicin did not proliferate at the rate of control cells, and consequently did not dilute the tracer dye to as great an extent. The control cells are included as a reference for background signal and variability.

Fig. 2.2C and 2.2D illustrate results for a typical experiment when cells were treated with a range (10 nM to 5 μM) of media doxorubicin concentrations. The data from all treatment

conditions were combined and processed together, resulting in one cellular response curve, as illustrated in Fig. 2.2D (black line). For reference, the response curves for individual doxorubicin treatment conditions are also shown in Fig. 2.2D (each color represents one media doxorubicin concentration). The horizontal dashed lines shown in Fig. 2.2B and 2.2D indicate where the proliferation factor is equal to 1, when cells are proliferating as if they were untreated, as well as the theoretical lower limit (maximum inhibition) for the proliferation factor with an assumed cell doubling time of 24 h.

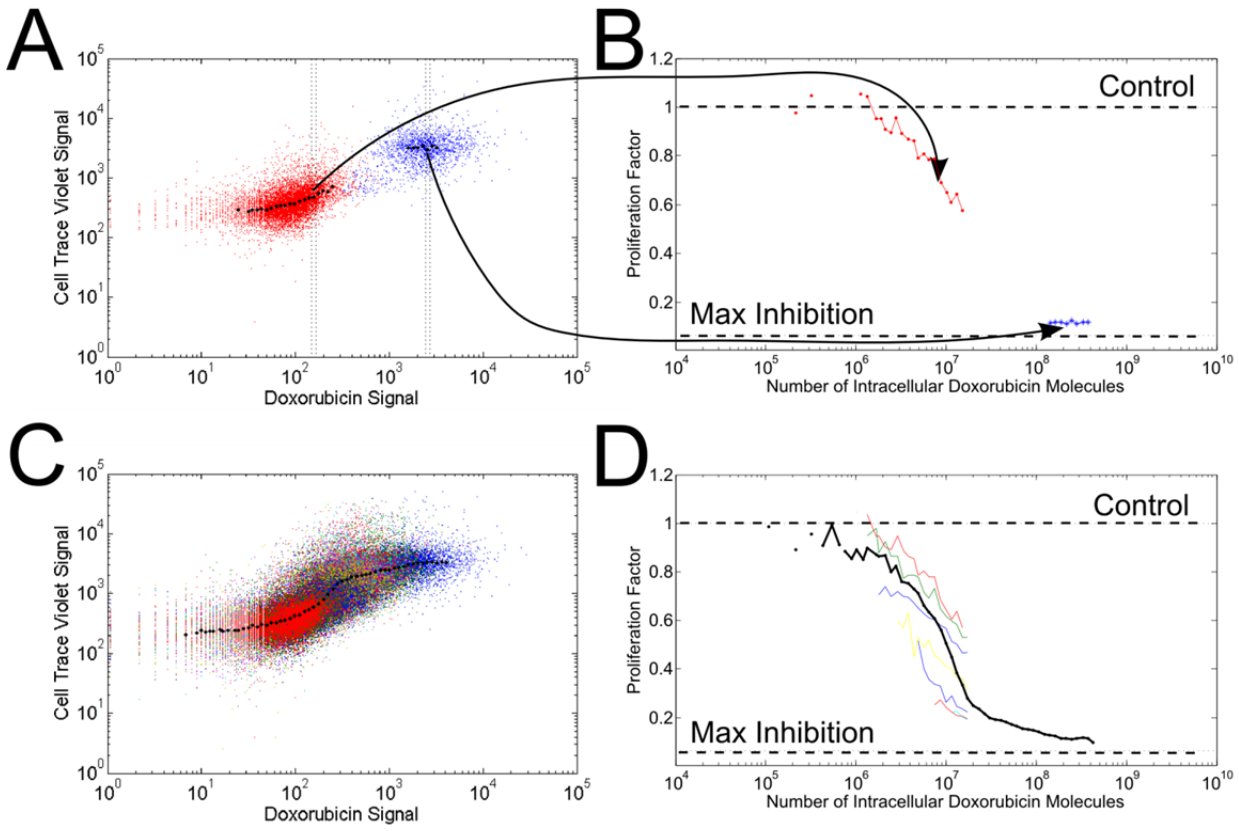

Figure 2.2 Data processing steps for flow cytometric clonogenic assay. (A) The raw flow cytometry results for the control population (stained with CellTrace, no doxorubicin treatment) are shown in red and the highest doxorubicin treatment population (5 μM doxorubicin in media) are shown in blue. (B) Conversion of fluorescence signals to number of intracellular doxorubicin molecules and the proliferation factor are shown for cell populations shown in A. The horizontal lines illustrate growth equivalent to untreated cells and maximum inhibition with a cell doubling rate of 24 h for untreated cells. (C) and (D) demonstrate the same transformation as in (A) and (B) with the full range (10 nM – 5 μM) of media doxorubicin treatment concentrations. In (D), each color represents an individual doxorubicin media concentration. The solid black line is the resulting response curve from the concatenation of all cell treatment data.

2.4.2 *Proliferation Response with a Range of Doxorubicin Treatment*

The growth response of six cell lines (BT-474, HCT-15, HT-29, IGROV-1, MDA-MB-231, and T-47D) to varying concentrations of doxorubicin was determined on the most commonly used culture volumetric basis for the drug (Fig. 2.3A). There appears to be substantial variation in potency of doxorubicin across these cell lines, ranging from 0.8 nM to 1.1 μM IC_{50} as listed in Table 2.2. This variation may be due to differences in transport efficiency of the drug to the nucleus amongst cell lines, or instead because there are differential responses to a given quantity of doxorubicin in the nucleus. From the information available in this plot, it is not possible to discriminate between these two fundamentally different possibilities.

We used our flow cytometric clonogenic assay to determine cell proliferation response to a particular number of intracellular doxorubicin molecules for the same six cell lines, as illustrated in Fig. 2.3B. Note that the response data points shown in Fig. 2.3B are the product of data concatenated from all treatment conditions from replicate experiments. Response curves for each individual treatment condition are shown in Figure 2.4. More variability was seen in the BT-474 cell response to doxorubicin treatment than in the responses of other cell lines. The BT-474 cell line is known to have a variable response to chemotherapy,[47] which may be due to protein fluctuations.[48]

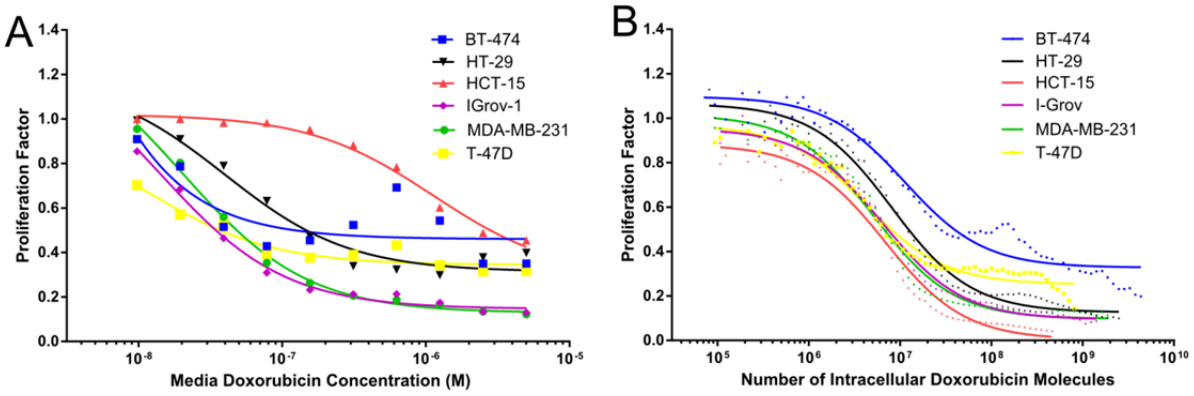

Figure 2.3 Cell proliferation response to doxorubicin treatment. Flow cytometric clonogenic assay results are shown with (A) media doxorubicin concentration as the basis and (B) intracellular doxorubicin concentration as the basis. Data were processed in same manner described in Fig. 2.2. Lines represent the curves for IC_{50} value fits. In (A), the data points represent the median proliferation factor for a given media doxorubicin treatment, whereas in (B), the data points represent bins from the concatenation of all treatment conditions and replicates.

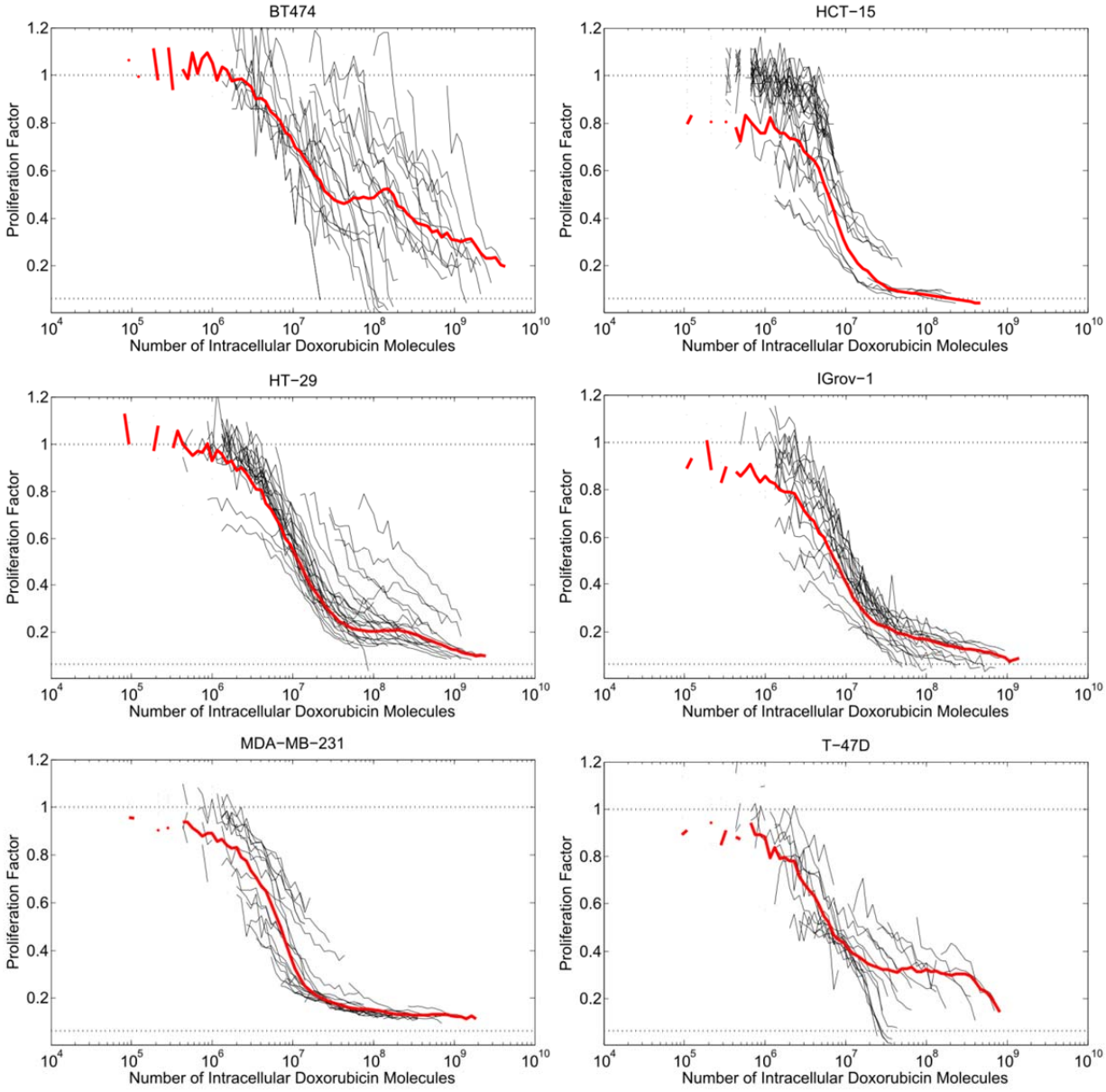

Figure 2.4 Assay results for six different cell lines with individual treatment responses. Data processed in same manner as described in Fig. 2.2. Red line represents concatenation of all cell treatment data and is the line plotted for each cell line in Fig. 2.3B. Black lines represent response to individual treatment conditions.

Table 2.2 Doxorubicin IC_{50} Values (on a media concentration basis)

Cell Line	**IC_{50}** (Media Doxorobucin Concentration, M)	**95% Confidence Interval on IC_{50}** (M)
BT-474	1.8×10^{-8}	$1.3 \times 10^{-10} – 2.7 \times 10^{-6}$
HCT-15	1.3×10^{-6}	$7.4 \times 10^{-7} – 2.3 \times 10^{-6}$
HT-29	7.1×10^{-8}	$2.2 \times 10^{-8} – 2.3 \times 10^{-7}$
IGrov-1	2.9×10^{-8}	$1.3 \times 10^{-8} – 6.7 \times 10^{-8}$
MDA-MB-231	4.5×10^{-8}	$1.78 \times 10^{-8} – 1.2 \times 10^{-7}$
T-47D	1.1×10^{-8}	$1.8 \times 10^{-9} – 7.2 \times 10^{-8}$

Table 2.3 lists the single-cell IC_{50} for each cell line. Thus, cellular uptake of 4 – 12 million molecules of doxorubicin results in 50 % of maximum reduction in proliferation. It is noteworthy how similar the IC_{50} is on a per-cell basis, as opposed to a culture-volumetric basis, indicating that differential subcellular trafficking rather than differential drug responsiveness accounts for the apparent variation in sensitivity in Fig. 2.3A.

Table 2.3 Doxorubicin Single-cell IC_{50} Values

Cell Line	**Single-Cell IC_{50}** (# of Intracellular Doxorubicin molecules)	**95% Confidence Interval on Single-Cell IC_{50}**
BT-474	11.3×10^6	8.6×10^6 to 14.8×10^6
HCT-15	6.9×10^6	5.6×10^6 to 8.4×10^6
HT-29	8.2×10^6	7.3×10^6 to 9.1×10^6
IGrov-1	6.5×10^6	5.9×10^6 to 7.3×10^6
MDA-MB-231	5.2×10^6	4.5×10^6 to 6.0×10^6
T-47D	4.2×10^6	3.5×10^6 to 5.1×10^6

2.4.3 *Proliferation Response as a Function of Length of Treatment*

Next, we considered doxorubicin dose rate effects on cell proliferation. All experiments described up to this point involved a one-day treatment period followed by a three-day growth period. Fig. 2.5 illustrates how cells respond to varying treatment period length. At the high dose (5 μM doxorubicin), cells take up sufficient drug to stop proliferation within the first 12 h. Additional treatment time resulted in increased uptake of doxorubicin, but no change in

proliferation. However, at the moderate dose (0.3 μM doxorubicin), cell proliferation decreased in response to increased doxorubicin treatment time in a manner dependent on the amount of doxorubicin in the cell. The cellular response to doxorubicin is one continuous function of the amount of doxorubicin in the cell, independent of the rate at which that level of doxorubicin was obtained. This effect is not observed when the length of treatment was used as the metric to evaluate cell proliferation instead of the amount of doxorubicin in the cells, as in Fig. 2.5B.

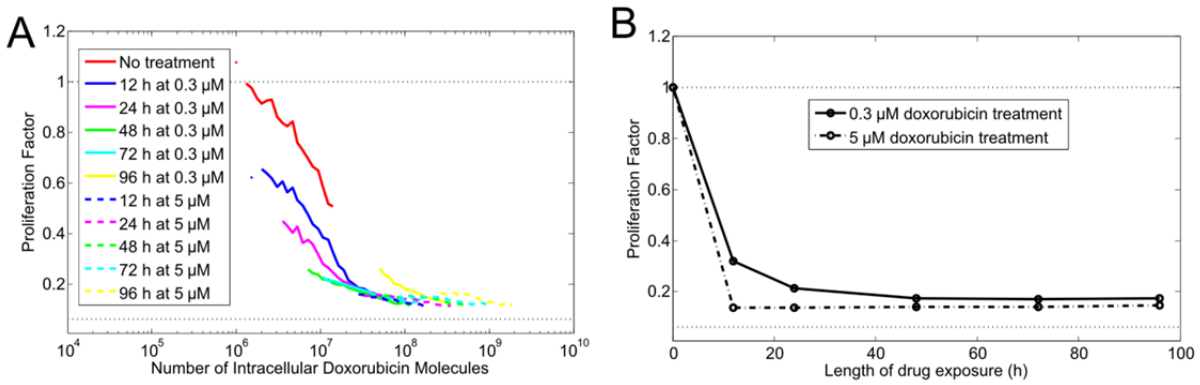

Figure 2.5 Effect of length of drug exposure on cell proliferation. MDA-MB-231 cells were treated with a moderate drug concentration (0.3 μM, solid lines) or high drug concentration (5 μM, dashed lines). (A) Flow cytometric clonogenic assay with cell proliferation as a function of amount of doxorubicin in cells. Length of doxorubicin exposure is given by different colors as described in legend. (B) Proliferation as a function of the length of doxorubicin exposure with either 0.3 μM media doxorubicin concentration (solid line) or 5 μM media doxorubicin concentration (dashed line).

2.4.4 *Doxorubicin Uptake and Cell Proliferation in Pgp Expressing Cells*

Doxorubicin treatment is known to induce multidrug resistance via expression of the drug efflux pump P-glycoprotein (Pgp).[49–51] In Fig. 2.6, we observed how treatment with a Pgp inhibitor, verapamil, affected doxorubicin uptake and cell proliferation in Pgp-expressing cells. Of the cell lines that we tested, only HCT-15 cells expresses Pgp without any pre-treatment with doxorubicin.[51] Again, the cell proliferation response to intracellular doxorubicin is one continuous response curve, rather than different response curves in the presence or absence of verapamil treatment. In contrast, the cell proliferation response curves with respect to the media doxorubicin concentration are two distinct curves in the presence or absence of verapamil treatment, as shown in Fig. 2.6B. Thus, the key factor for HCT-15 cell proliferation is the amount of doxorubicin in the cell. It is irrelevant in terms of cell proliferation whether the

amount of doxorubicin in the cell resulted from a higher media doxorubicin concentration or from a lower media doxorubicin concentration with verapamil treatment.

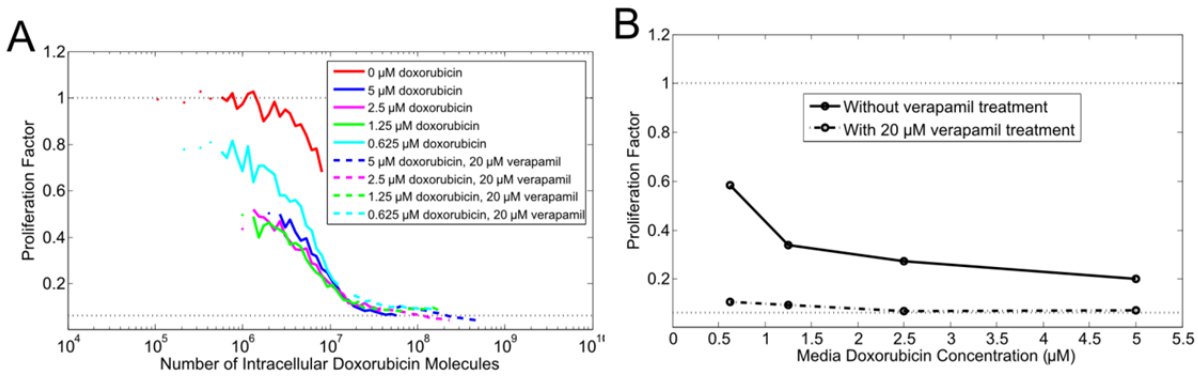

Figure 2.6 Effect of verapamil treatment on cell proliferation. HCT-15 cells, which express the drug efflux pump P-glycoprotein (Pgp), were treated with doxorubicin in the presence (dashed lines) and absence (solid lines) of 20 μM verapamil, a Pgp inhibitor. (A) Flow cytometric clonogenic assay with cell proliferation as a function of amount of intracellular doxorubicin in cells. Doxorubicin media concentration is given by different colors as described in legend. (B) Proliferation as a function of the media doxorubicin concentration with (dashed line) or without (solid line) 20 μM verapamil.

2.5 Discussion

In this work, a flow cytometric clonogenic assay was developed and the application of this assay was demonstrated with the model drug doxorubicin. Intracellular doxorubicin, rather than doxorubicin concentration in the cell growth media, was demonstrated as the key determinant of cell proliferation inhibition. Whether the amount of intracellular doxorubicin was achieved by varying doxorubicin media concentration, treating cells with verapamil, or increasing treatment length was irrelevant. These results are consistent with previous studies of doxorubicin cellular pharmacodynamics.[52–56]

The doxorubicin single-cell IC_{50} values were 4 – 12 million intracellular doxorubicin molecules. To put this number in context, this represents ~ 3% loading of the total number of binding sites on doxorubicin's primary intracellular target, DNA, based on one doxorubicin molecule binding per ten DNA base pairs[57] and approximately three billion base pairs per cell in humans.[58] It is important to note that the quantification of intracellular doxorubicin molecules we report here is at the time of analysis, which is three days after ending doxorubicin treatment. During this incubation time, doxorubicin may efflux from the cell, be diluted by growth, or be degraded. Doxorubicin fluorescence is known to be quenched once bound to DNA, resulting in a 30-40 fold decrease in fluorescence signal.[43,59,60] It has also been shown that some doxorubicin degradation products fluoresce in the same emission wavelength window as doxorubicin.[59,61] Single-cell IC_{50} values provide a snapshot of the order of magnitude of intracellular doxorubicin molecules, but the interpretation of the exact quantitative values should consider these factors.

In this work, we assume that the intracellular doxorubicin is all available to bind to DNA; however, there may be a fraction of drug bound to proteins and lipids in the cell. The free drug (i.e. not bound to proteins or lipids) is the relevant quantity in relation to efficacy.[62] Since doxorubicin is a relatively hydrophilic drug ($\log D_{7.4} = -1.98$),[63] this cellular protein bound drug accounts for less of the intracellular drug than for more hydrophobic drugs, where drug bound to cellular proteins could account for more than 90% of the intracellular drug.[64] Plasma protein binding of drugs could be used as a correlate for cellular protein binding. Methods are established for plasma protein binding as well as published values for doxorubicin and a number of other drugs.[64–66] Hydrophobicity can also affect a drug's ability to diffuse into cells, which drives the difference between intracellular and extracellular drug concentrations.

Another key consideration when interpreting results from this assay is the fact that cells that have died by the time of analysis are not seen in the flow cytometry results. (The absence of dead cells is intrinsic to all clonogenic assays.) Thus, the reported intracellular doxorubicin values are for cells that are still intact. Likely, for many treatment conditions, there were cells that took up more doxorubicin and died before analysis was completed. Lower cell number and altered cell morphology as indicated by forward and side scatter patterns were observed for cells treated at the highest doxorubicin concentrations.

Previous studies that have quantified intracellular doxorubicin report 10^7 – 5 x 10^9 intracellular doxorubicin molecules after 2 – 12 h treatment periods.[39,67–71] Many of these reported values are higher than the single-cell IC_{50} values shown here, because the respective studies use higher doxorubicin media concentrations for treatment and the intracellular doxorubicin was quantified immediately after treatment rather than after a three-day growth period as in this assay. Most of the previous intracellular doxorubicin quantification studies were not correlated with cell proliferation. However, Kerr et al. reported a LD_{90} (lethal dose for 90% of colonies) of 39 million intracellular doxorubicin molecules.[54] This value corresponds well with single-cell IC_{50} values reported here.

Delivery of tens of millions of doxorubicin molecules to a cell, although easily accomplished via diffusion of the free drug, could be harder to achieve with an antibody-drug conjugate (ADC). ADCs are designed to carry a drug payload specifically to cancer cells and release the drug once internalized into the cell. Consider a cell with high antigen expression at 10^6 surface antigens per cell and an internalization half time of 12 h. With a drug-to-antibody ratio of 4, a cell would internalize ~ 4 million drug molecules per day. This estimated delivery is below many of the reported single-cell IC_{50} values for doxorubicin and doesn't take into account the additional processing steps between ADC internalization and doxorubicin binding to DNA. The single-cell IC_{50} values measured in this work for doxorubicin support the generally accepted rule that ADCs need a potent drug to be successful.[4,6,72,73] This assay provides a method for determining the required amount of drug that must be delivered intracellularly via an ADC.

This flow cytometric clonogenic assay can be generalized to study any fluorescent drug or fluorescently-tagged drug. Fluorescent analogs of drugs can be very useful tools for tracking cellular uptake of a drug in assays such as this flow cytometric assay and others.[74,75] However, fluorescent analogs may be difficult to synthesize, have reduced potency, and have different

trafficking behavior when compared to the parent drug. Drug delivery systems that are taken up by cells, such as liposomes, nanoparticles, and ADCs, can also be used in this clonogenic assay with a fluorescent tag on the delivery system as proxy for how much drug was taken up, rather than using a fluorescent drug or fluorescent analog of a drug.

In conclusion, we have presented here a straightforward flow cytometric clonogenic assay using a cell tracing dye and a fluorescent drug. The first application of the assay revealed the single-cell potency of doxorubicin via single-cell IC_{50} values of 4 – 12 million intracellular doxorubicin molecules for the cancer cell lines evaluated. Single-cell potency is a key parameter for molecular design of targeting agents where subcellular trafficking and processing can be affected by altered design attributes.

Chapter 3: Determination of Cellular Processing Rates for a Trastuzumab-Maytasinoid Antibody-Drug Conjugate

The contents of this chapter will be submitted for publication[76] as a companion paper with the contents of chapter 4.

3.1 Abstract

Antibody-drug conjugates (ADCs) are a promising class of cancer therapeutics that combine the specificity of antibodies with the cytotoxic effects of payload drugs. A quantitative understanding of how ADCs are processed intracellularly can illustrate which processing steps most influence payload delivery, thus aiding the design of more effective ADCs. In this work, we develop a kinetic model for ADC cellular processing as well as generalizable methods based on flow cytometry and fluorescence imaging to parameterize this model. A number of key processing steps are included in the model: ADC binding to its target antigen, internalization via receptor-mediated endocytosis, proteolytic degradation of the ADC, efflux of the payload out of the cell, and payload binding to its intracellular target. The model was developed with a Trastuzumab-Maytansinoid ADC (TM-ADC) similar to Trastuzumab-Emtansine (T-DM1), which is used in the clinical treatment of HER2+ breast cancer. In three high-HER2-expressing cell lines (BT-474, NCI-N87, and SK-BR-3), we report for TM-ADC half-lives for internalization of 6 – 14 h, degradation of 18 – 25 h, and efflux rate of 44 – 73 h. Sensitivity analysis indicates that the internalization rate and efflux rate are key parameters for determining how much payload is delivered to a cell with TM-ADC. In addition, this model describing the cellular processing of ADCs can be incorporated into larger pharmacokinetics/pharmacodynamics models, as demonstrated in Chapter 4.

3.2 Introduction

Antibody-drug conjugates (ADCs) are an emerging modality for cancer treatment, designed to selectively deliver chemotherapeutic payload drugs to tumor cells and reduce systemic toxicity. ADCs are comprised of an antibody specific to a cancer-associated antigen, a chemotherapeutic drug, and a linker to connect the antibody and drug payload. There are currently two FDA-approved ADCs available in the US: Brentuximab Vedotin (Adcetris) and Trastuzumab Emtansine (T-DM1, Kadcyla),[77] with more than 30 ADCs in clinical trials.[78] Key ADC design parameters include target antigen, antigen expression level (in normal tissue and tumor), linker type, conjugation site, conjugation chemistry, drug-to-antibody ratio (DAR), and payload drug potency.[4,79]

Previous studies have shown that an ADC will traffic through the body very similarly to its parent antibody, unless the ADC has a high DAR.[15] When an ADC reaches a tumor, the ADC binds its target antigen on the cancer cell surface. Next, the ADC is internalized via receptor-mediated endocytosis. Inside the endosomal/ lysosomal compartments, the ADC is degraded and the payload is released from the antibody. The payload can then bind its intracellular target, resulting in cell death. These processing steps are widely accepted in the field,[4,11,80] but they have not been combined in a complete quantitative model. The aim of this work is to fill this gap.

In order to develop a model of ADC processing in cells, we used a trastuzumab-maytansinoid antibody-drug conjugate (TM-ADC), similar to T-DM1, as the model ADC. The antibody component of T-DM1 is the antibody Trastuzumab (Herceptin), which binds HER2, a member of the human epidermal growth factor receptor family that is often overexpressed on breast cancer cells.[32] T-DM1 takes advantage of the therapeutic nature of the antibody itself; upon Trastuzumab binding to HER2, downstream growth signaling is blocked. The payload component of T-DM1 is emtansine (DM1), a potent microtubule-binding maytansine drug. DM1 is conjugated to lysine residues in Trastuzumab via a non-cleavable linker.

A number of models have been developed previously to describe T-DM1 pharmacokinetics/pharmacodynamics (PK/PD). [81–86] However, these models have focused on PK/PD at an organism or tissue-specific level and do not incorporate the cellular-level mechanisms of ADC processing. For our model, we have focused on the cellular processing of ADCs, an area which is fundamental to how ADCs work and are designed. Understanding which

intracellular processing steps influence ADC payload delivery, as well as how ADC design parameters affect the rate of these intracellular processing steps, may enable more rational design of safe and effective ADCs. The established model and parameters for TM-ADC intracellular processing described here have also been incorporated into a larger-scale PK/PD model in collaboration with Professor Dhaval Shah and Aman Singh at the University of Buffalo and Alison Betts and Chethana Kulkarni at Pfizer as described in Chapter 4.

3.3 Materials and Methods

3.3.1 *Cell Lines and Materials*

BT-474, NCI-N87 (N87), and SK-BR-3 cell lines were obtained from ATCC. BT-474 and N87 cells were grown in RPMI 1640 medium (Corning) supplemented with 10 % FBS and 1 % penicillin-streptomycin. SK-BR-3 cells were grown in McCoy's 5A Medium Modified, with L-Glutamine (Lonza) supplemented with 10 % FBS and 1 % penicillin-streptomycin. Trastuzumab labeled with Alexa Fluor 647 (Tras-647) was prepared as described previously.[33] The Trastuzumab-Maytansinoid ADC (TM-ADC), which is structurally similar to T-DM1, was also prepared as described previously.[87,88] MATLAB software (Mathworks) was used for model predictions and parameter fits. GraphPad Prism software was also used for parameter fits. Flow cytometry was performed using a BD Accuri C6 Flow Cytometer.

3.3.2 *Alexa Fluor 647 Labeling of TM-ADC (TM-ADC-647)*

TM-ADC was labeled using an Alexa Fluor 647 Protein Labeling Kit (Life Technologies) following the product manual recommendations, with purification on an AKTA size exclusion chromatography system (GE Healthcare). The fluorophore-to-antibody ratio was 2 – 7.5 based on absorbance at 280 nm and 647 nm.

3.3.3 *Model Development*

We used standard biomolecular kinetic methods[89] to develop material balances for each species as given in Equations 3.1 – 3.6. The variables used in the model are as follows:

[Ab] – concentration of ADC in cell growth media (M)

R – number of free surface receptors (HER2) per cell (#/cell)

C – number of ADC-receptor complexes per cell (#/cell)

I – number of internalized, intact ADCs per cell (#/cell)

D – number of degraded ADCs per cell (#/cell)

N – concentration of cells in well (# cells/ L)

The model parameters are as follows:

k_{on} – association rate constant (h^{-1} M^{-1})

k_{off} – dissociation rate constant (h^{-1})

K_D – equilibrium dissociation constant (M)

k_e – net internalization rate constant (h^{-1})

k_{deg} – degradation rate constant (h^{-1})

k_{out} – efflux rate constant (h^{-1})

μ – cell growth rate (h^{-1})

V_s – receptor synthesis rate (#/(cell h))

HER2 – total number of HER2 receptors per cell (#/cell)

N_{av} – Avogadro's number (6.02 x 10^{23} # / mol)

$$\frac{dR}{dt} = -k_{on}\left[Ab\right]R + k_{off}C + V_s - k_eR - \mu R \tag{3.1}$$

$$\frac{dC}{dt} = k_{on}\left[Ab\right]R - k_{off}C - k_eC - \mu C \tag{3.2}$$

$$\frac{dI}{dt} = k_eC - k_{\deg}I - \mu I \tag{3.3}$$

$$\frac{dD}{dt} = k_{\deg}I - k_{out}D - \mu D \tag{3.4}$$

$$\frac{d\left[Ab\right]}{dt} = \left(k_{off}C - k_{on}R\left[Ab\right]\right)\frac{N}{N_{Av}} \tag{3.5}$$

$$\frac{dN}{dt} = \mu N \tag{3.6}$$

The terms $k_{on}[Ab]R$ and $k_{off}C$ represent the association of ADC to the surface receptor (HER2) and dissociation of ADC from receptor, respectively. The equilibrium dissociation constant, K_D, is equal to k_{off}/k_{on}. The internalization of receptor or antibody-receptor complex are given by k_eR or k_eC, respectively. Note that there may be recycling of the receptor or antibody-receptor complex back to the cell surface; however, the internalization rate used here is the net internalization, i.e., the internalization in excess of that rapidly recycled back to the cell surface.

As cells grow, their cellular contents are diluted with each cell division. The terms μR, μC, μI, and μD represent this dilution by growth. The degradation of the intact ADC and release of the payload is given by $k_{\deg} I$. Once the payload is released from the antibody, it may leave the cell. The term $k_{out} D$ represents the efflux of payload from the cell. The receptor synthesis rate, V_s, is determined assuming a constant HER2 expression level and the steady state material balance (from Equation 1) for receptor with no ADC present; thus, $V_s = (\mu + k_e) HER2$. Note that most of the species are described in units of "number per cell" to correspond with per cell measurements made by flow cytometry. Equations 1 – 4 can be converted to concentrations based on the concentration of cells in a manner similar to Equation 5. Antibody in the media is described as a concentration (M) rather than a per cell basis.

3.3.4 *Determination of K_D and k_{off}*

To determine the apparent K_D of Trastuzumab, we treated fixed SK-BR-3 cells with a range (0.6 – 320 pM) of Tras-647 overnight at 37 °C. Cells were fixed to prevent internalization. Cells were washed twice with 1 mL cold stain buffer (PBS, pH 7.4, 0.2 % BSA, 0.09 % sodium azide, filtered), and fluorescence signal was read via flow cytometry. We minimized depletion effects using a minimal number of cells and large suspension volumes. See also Appendix B.7.

To determine k_{off}, we treated fixed cells (BT-474, N87, and SK-BR-3) with 10 nM TM-ADC-647 at least overnight at 37 °C. At each time point (between 0 and 78 h), cells were washed with cold stain buffer and resuspended in stain buffer with 100 nM Trastuzumab in order to compete with any TM-ADC-647 that had dissociated from cells. After the time course, all cells were washed with cold stain buffer and read on the flow cytometer.

3.3.5 *Determination of HER2 Expression Levels*

The HER2 expression levels for each cell line were determined using Quantum Simply Cellular anti-Human IgG Quantitation beads (Bangs Lab). Beads were prepared following the product manual and stained with 10 µL of Tras-647 to give a final concentration of 0.8 µM. Fixed cells were stained with 10 nM Tras-647 overnight at 37 °C. Fixation was performed using Cytofix Buffer (BD Biosciences) at 4 °C for 25 min as described in the product manual. The fluorescence signals for beads and cells (triplicate per cell line) were read via flow cytometry.

Using the calibration spreadsheet provided by Bangs Lab, the average fluorescence intensity for each cell line was converted to number of HER2 receptors on the surface of each cell. See also Appendix B.6.

3.3.6 *Determination of Cell Growth Rate*

Cell growth rates for untreated cells were determined by plating 2 x 10^5 cells per well in 6-well plates. At each time point, cells were washed with PBS, detached from the plate using 0.25 % Trypsin/ EDTA (Corning), pelleted, and resuspended in 250 µL of PBS supplemented with 5 % FBS. To each sample, 50 µL of CountBright Absolute Counting Beads (Life Technologies) were added. The cell counts were determined via flow cytometry using gating on forward scatter (FSC) and side scatter (SSC). The average of the triplicates for each time point was used to fit an exponential growth rate.

3.3.7 *Determination of Net Internalization Rate*

The methods used to measure the net internalization rates were adapted from those published previously.[9,90,91] To determine what fraction of the total signal from Tras-647 or TM-ADC-647 was from surface-bound antibody rather than internalized antibody, we used an anti-human antibody rather than acid stripping or quenching antibodies. In 24-well plates, 10^5 cells per well were plated and left to adhere overnight. Cells were treated with 10 – 20 nM of Tras-647 or TM-ADC-647 for time points between 0 – 9 h. Based on the dissociation and association rates, this concentration range ensures a rapid equilibration rate and the resulting equilibrium favors saturated surface receptors. After treatment, cells were washed once with PBS, and then detached from the plate using 0.25 % Trypsin/ EDTA. Cells were pelleted at 1000 x g for 5 min and then resuspended in stain buffer with 10 µL of Alexa Fluor 488 Goat anti-Human IgG (H+L) (Life Technologies). Cells were incubated at 4 °C on a rotator for 30 min and then washed twice with 500 µL of stain buffer. The mean fluorescence intensity (MFI) was measured via flow cytometry. This MFI was normalized as described in the next paragraph.

In order to determine the Alexa Fluor 647 signal which corresponds to fully saturated surface receptors, an additional 10^5 cells per cell line were fixed to prevent internalization. The fixed cells were then stained with 10-20 nM Tras-647 or TM-ADC-647 for at least 1 h at 37 °C. The difference in MFI of the stained fixed cells versus unstained fixed cells was used to

normalize the Alexa Fluor 647 signal for cells treated for internalization. New cells were fixed and stained at the same time as each experimental replicate to account for any variations in HER2 expression level. To normalize the Alexa Fluor 488 signal, the average of the Alexa Fluor 488 signal (besides the initial time point) was considered a fully saturated surface. The internalized fraction was determined by subtracting the normalized Alexa Fluor 488 signal (surface-bound antibody) from the normalized Alexa Fluor 647 signal (total antibody). A global fit of the data from triplicate independent experiments was used to determine the net internalization rate. Equation 3.7 demonstrates the linear function used for the fit. See also Appendix B.8.

$$I(t_2) = k_e \int_{t_1}^{t_2} C dt + I(t_1) \tag{3.7}$$

To test whether non-specific uptake is significant, cells were treated for at least 20 min with 800 nM (40-fold excess) or 500 nM (25-fold excess) of unlabeled Trastuzumab or unlabeled TM-ADC, respectively. After pre-treatment, Tras-647 or TM-ADC-647 was added to a final concentration of 20 nM. At various time points, the cells were washed and the Alexa Fluor 647 MFI was measured using flow cytometry. See also Appendix B.9.

3.3.8 *Determination of Degradation Rate*

Degradation rate was measured using a time course of cell lysate samples prepared from cells treated with TM-ADC-647. In 6-well tissue culture plates, 10^5 cells were plated and allowed to adhere overnight. Then cells were treated for 30 min with 10 nM TM-ADC-647 at 37 °C. Cells were washed twice with PBS, and media was replaced with fresh media. At each time point, cells were washed once with PBS, and 100 µL of ice-cold cell lysis buffer (150 nM NaCl, 50 mM Tris-HCl, 1 % Triton X-100 plus freshly added proteases inhibitors, "cOmplete, mini, EDTA-free Protease Inhibitor Cocktail Tablets" (Roche), with 1 tablet per 10 mL buffer) was added to each well. Cells were scraped from the well, and the suspension of cells in lysis buffer was transferred to a microcentrifuge tube. Samples were placed on a rotator at 4 °C for 30 min, centrifuged at 12,000 rpm for 20 min, and the resulting supernatant was stored at 4 °C.

After all time points were collected, 12 µL of each sample was mixed with 3 µL of non-reducing, no dye SDS loading buffer (0.125 M Tris-HCl, 0.35 M sodium dodecyl sulfate, 50 % by volume glycerol). From this mixture, 10 µL was added to each lane in a 4 – 12 % Bis-Tris

Protein Gel (Life Technologies). Gels were run in MOPS buffer at 250 V for 15 min. They were then imaged for Alexa Fluor 647 signal using a Typhoon Imager (GE). Intact antibody bands were quantified using ImageJ software (NIH). Data were normalized to the initial time point, which was taken immediately after the treatment period. Using the model described in the model development section, the degradation rate was fit by minimizing the difference between data and model predictions for the sum of C, intact antibody in complex with HER2 on the surface of the cell, and I, the intact (non-degraded) antibody inside the cell. Since the cell lysate samples measure from the population of cells rather than individual cells, the total intact antibody from all cells (C x N, # / L) was used to compare the model predictions and data. See also Appendix B.10.

3.3.9 *Determination of Efflux Rate*

The efflux rate was determined using the total fluorescence signal in cells over time as measured by flow cytometry. Cells were plated in 6-well tissue culture plates (10^5 cells per well) and allowed to adhere overnight. Then cells were treated for 30 min with 10 nM TM-ADC-647 at 37°C. Cells were washed twice with PBS and media was replaced with fresh media. At each time point, cells were washed once with PBS, detached from the plate using 0.25 % Trypsin/ EDTA, pelleted, and resuspended in PBS supplemented with 5 % FBS. Total Alexa Fluor 647 fluorescence signal was read via flow cytometry and normalized to the fluorescence signal at the initial time point, immediately after treatment. Using the complete model described in the model development section, the efflux rate was fit by minimizing the measured normalized total fluorescence signal and the normalized total amount of TM-ADC in cells from the model. The total amount of TM-ADC is the sum of TM-ADC in complex with HER2 on the surface of the cell (C), internalized intact TM-ADC (I), and degraded products (D).

Loss of fluorescence signal in cells is mainly due to efflux of degraded products and dilution by growth. To ensure an accurate fit of the efflux rate constant, independent of dilution by growth, we measured the cell growth rate (μ) during each experiment using counting beads and fit using an exponential growth model. See also Appendix B.11.

3.3.10 *Sensitivity Analysis*

To determine the model sensitivity to each of the model parameters, we calculated the local sensitivity based on 10 % perturbations from the established parameters as described by Equation 3.8. The area under the curve (AUC) for the degraded products (payload) at different parameter values, k_i, was calculated and the difference normalized to the AUC at the established parameter values. The treatment regimen used for determining AUC was 10 days at surface saturating concentrations of ADC (10 nM ADC).

$$\text{Sensitivity}\left(k_i\right) = \frac{AUC\left(k_i \cdot (1.1)\right) - AUC\left(k_i \cdot (0.9)\right)}{0.1\left(AUC\left(k_i\right)\right)} \tag{3.8}$$

The parameters k_e and HER2 were analyzed as one parameter since these parameters do not act independently when there are saturating antibody conditions.

To define the length of time required to reach steady state, we used the time at which the concentration of degraded antibody inside the cell was equal to 95% of the concentration of degraded antibody after 100 days of treatment, with antibody concentration in the media maintained at 10 nM (saturating for the cell surface) and no cell growth.

3.3.11 *Incorporation of Payload Binding to Target*

Payload binding to target can be incorporated in the model as shown in Equation 3.9, where $k_{on}^{\text{PL-Target}}$ is the association rate constant for payload (DM1) binding to its intracellular target (tubulin) in (# / cell)$^{-1}$ h^{-1}, $k_{off}^{\text{PL-Target}}$ is the dissociation rate constant in h^{-1}, T is the amount of target (tubulin) in cells in # / cell, and Q is the number of drug-target complexes per cell.

$$\frac{dD}{dt} = k_{\text{deg}} I - k_{out} D - \mu D - k_{on}^{\text{PL-Target}} TD + k_{off}^{\text{PL-Target}} Q \tag{3.9}$$

For these analyses, we used the following previously reported values:[92,93] $K_D^{\text{PL-Target}}\left(= k_{on}^{\text{PL-Target}} / k_{off}^{\text{PL-Target}}\right)$ of 930 nM, $k_{on}^{\text{PL-Target}}$ of 0.44 M^{-1} h^{-1}, and T of 65 nM. To convert the amount of payload drug (D) from # / cell to an intracellular concentration, we assumed the cell volume was 1000 μm^3.

3.4 Results

3.4.1 *Model Development*

Fig. 3.1 illustrates the model schema for this work. With the model equations established, we proceeded to parameterize the model. Parameters were measured in a sequential manner in order to guide the design of experiments for rate constant measurements for later processing steps. The apparent equilibrium binding constant, K_D, measured via a cell-based assay was 38 ± 16 pM, as illustrated in Fig. 3.2A. The measured dissociation rate constant, k_{off}, was 0.014 ± 0.016 h^{-1}, as illustrated in Fig. 3.2B. Flow cytometry quantitation beads were used with Tras-647 to determine the HER2 expression levels. The measured HER2 expression levels for each cell line were 2.71 x 10^6, 3.25 x 10^6, and 3.55 x 10^6 HER2/cell for BT-474, N87, and SK-BR-3 cells, respectively. We observed some variability in the precise expression level with time in culture. These HER2 expression levels are similar to those reported previously for these cell lines.[94–96] In addition, the untreated cell growth rate was 0.013 ± 0.003 h^{-1}, 0.019 ± 0.007 h^{-1}, 0.011 ± 0.002 h^{-1} for BT-474, N87, SK-BR-3 cells, respectively, as shown in Fig. 3.3.

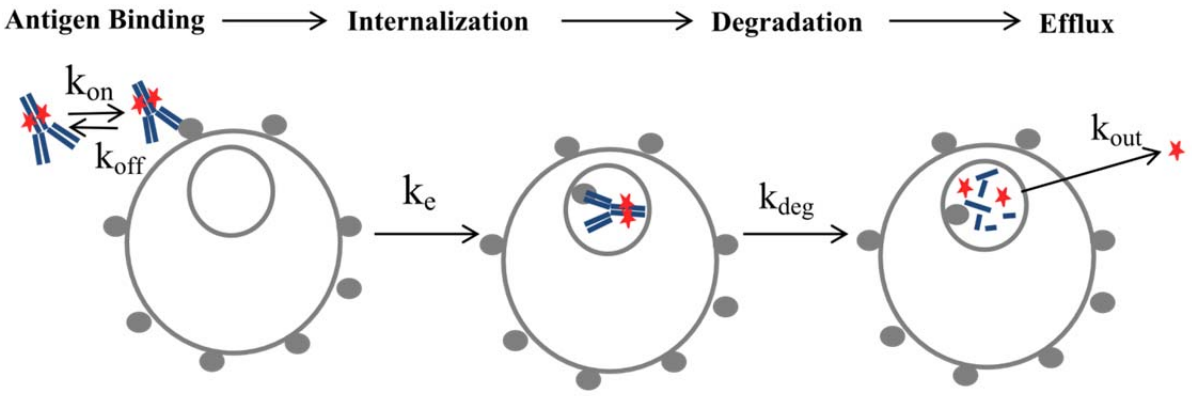

Figure 3.1 Schematic of kinetic model for ADC cellular processing, including ADC association, dissociation, internalization, degradation, and efflux. Model parameter descriptions are provided in the Methods section, under Model Development.

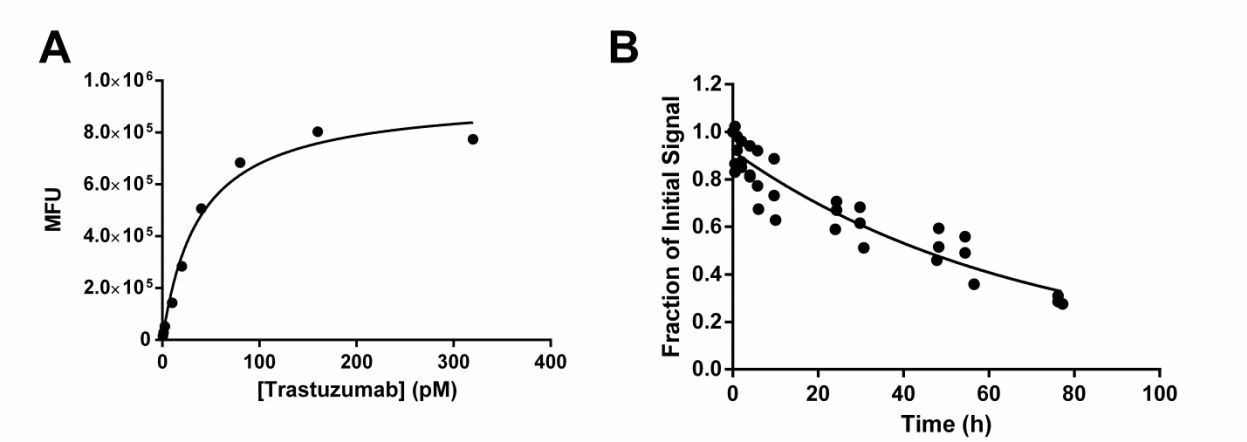

Figure 3.2 Curve fits for (A) the apparent K_D of Tras-647 on SK-BR-3 cells and (B) k_{off} for Tras-647 on BT-474, N87, and SK-BR-3 cells.

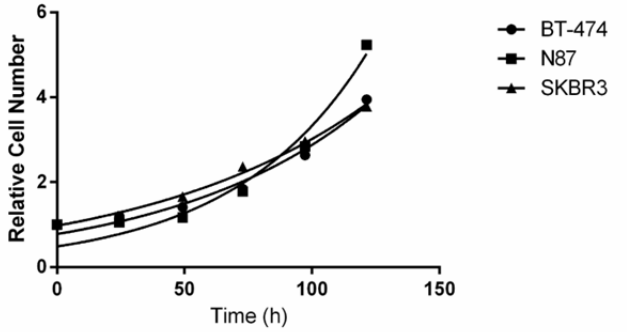

Figure 3.3 Cell growth rates for untreated cells

3.4.2 *Determination of Internalization Rate Constant*

The net internalization rate constant, k_e, was determined for both Trastuzumab and TM-ADC, using Tras-647 and TM-ADC-647, respectively. The Alexa Fluor 647 signal from labeled Trastuzumab or TM-ADC was used as a measure of total antibody in the cell, i.e., both on the surface and internalized within cells. The amount of surface-bound antibody was detected using an Alexa Fluor 488 anti-human antibody. In order to correlate the Alexa Fluor 647 and Alexa Fluor 488 signal, both signals were normalized to that of cells with saturated surface receptors. The difference in the normalized signal between the total antibody and surface-bound antibody is the signal arising from internalized antibody.

Fig. 3.4A depicts a representative example of the total, surface-bound, and internalized signal versus time for cells treated with TM-ADC-647. The unbound HER2 and TM-ADC

quickly equilibrate between the initial time point and the 1.5 h time point. The surface-bound signal remains constant after 1.5 h, indicating there is little down-regulation of HER2 during this time period, as observed previously,[97] and that there is no depletion of ADC in the media. Within the 9 h time course, we assume the rate of degradation is negligible compared to the rate of internalization. Tests of non-specific uptake showed that less than 2 % of the total Alexa Fluor 647 signal measured for unblocked cells was observed with cells that were pre-blocked with unlabeled Trastuzumab or unlabeled TM-ADC.

Fig. 3.4B illustrates the global fit of triplicate experiments for BT-474 cells treated with TM-ADC-647 based on the surface integral and internalized fraction from plots such as Fig. 3.4A. The equivalent graphs for other cell lines are shown in Fig. 3.5. A summary of the net internalization rates, k_e (± 95 % confidence intervals), measured for three different cell lines are shown in Table 3.1. The half-times, $t_{1/2}$, for internalization, which were calculated using $t_{1/2} = \ln(2)/ k_e$, are also shown. The range spans the 95 % confidence intervals of the net internalization rate.

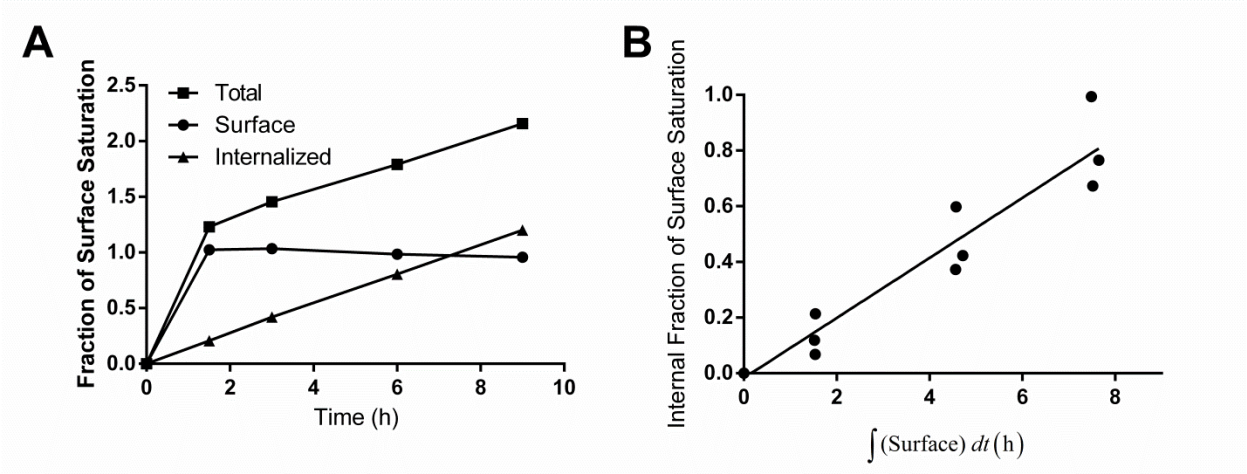

Figure 3.4 Example of internalization rate constant (k_e) fit. (A) Representative plot of the normalized Alexa Fluor 647 signal (total antibody), normalized Alexa Fluor 488 signal (surface-bound antibody), and internalized (total – surface) antibody versus time for BT-474 cells treated with 10 nM TM-ADC-647 and stained with an Alexa Fluor 488 anti-human antibody. The y-axis is fraction of the normalized surface saturation level, which is either Alexa Fluor 647 or Alexa Fluor 488 MFI normalized as described in the Methods section. (B) Fit of internalization rate using the internalized fraction of TM-ADC-647 versus surface integral as given by Equation 3.7. A representative plot for TM-ADC-647 internalization in BT-474 cells is shown here. The equivalent plots for other cell lines and Tras-647 are shown in Fig. 3.5. Fit values for the internalization rate constants for Tras-647 and TM-ADC-647 are presented in Table 3.1.

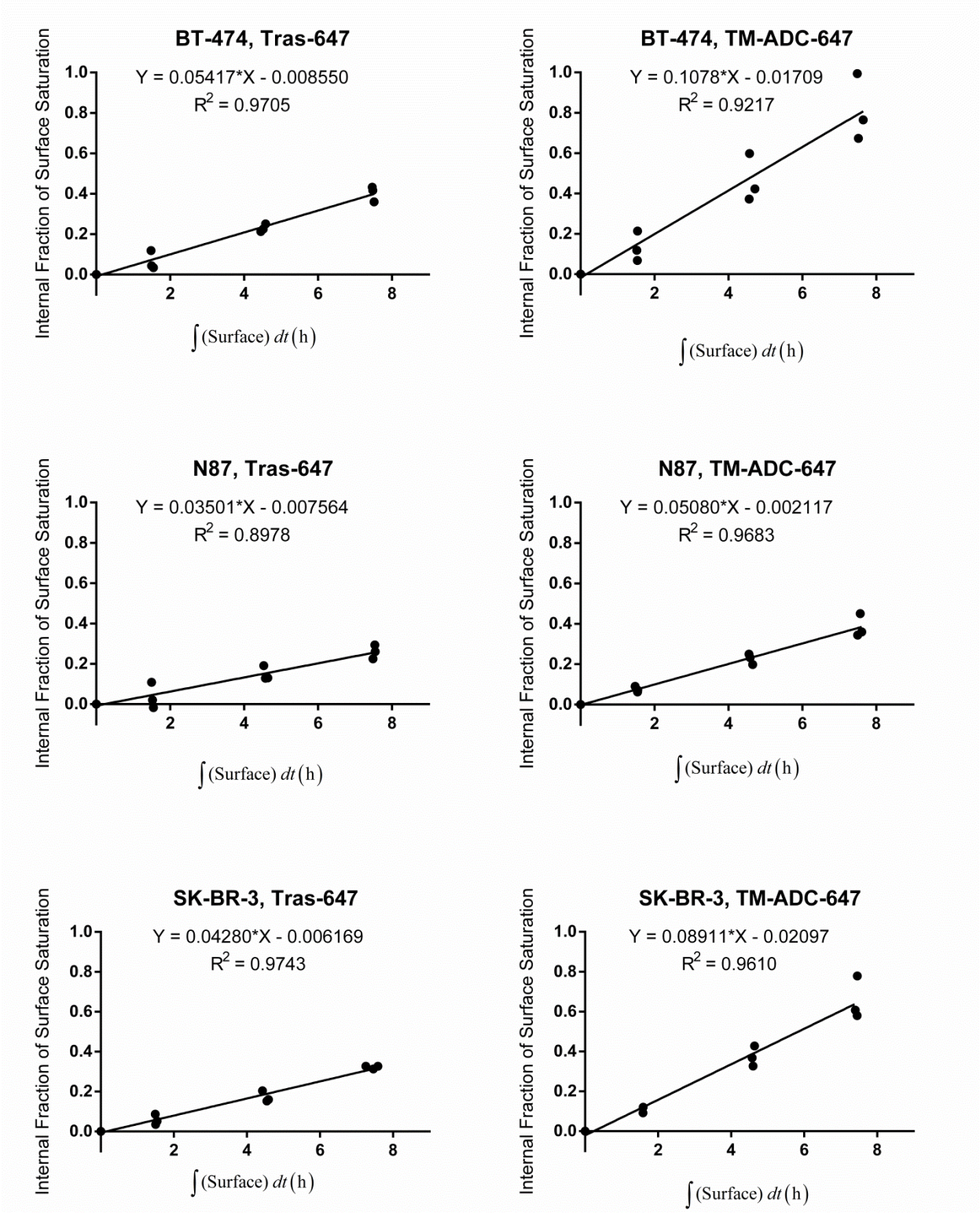

Figure 3.5 Internalization rate constant (k_e) fit for Tras-647 and Tras-ADC-647 in three cell lines (BT-474, N87, and SK-BR-3). The linear fit equations are reported for each fit at the top of the graph. Data points represent triplicate independent experiments.

Table 3.1 Net Internalization Rates (k_e) and Half-Lives ($t_{1/2}$) for Tras-647 and TM-ADC-647

	Tras-647		**TM-ADC-647**		**Significantly Different?** p value
Cell Line	$k_e\left(h^{-1}\right)$	$t_{1/2}\left(h\right)$	$k_e\left(h^{-1}\right)$	$t_{1/2}\left(h\right)$	
BT-474	0.054 ± 0.007	12.8	0.11 ± 0.02	6.3	<0.0001
NCI-N87	0.035 ± 0.008	19.8	0.051 ± 0.006	13.6	<0.01
SK-BR-3	0.043 ± 0.005	16.1	0.09 ± 0.01	7.7	<0.000001

3.4.3 *Determination of Degradation Rate Constant*

In TM-ADC, DM1 is conjugated to Trastuzumab via a non-cleavable linker, succinimidyl 4-(N-maleimidomethyl)cyclohexane-1-carboxylate (SMCC). Thus, the drug metabolite of TM-ADC is lysine-N^{ε}-SMCC-DM1, which is the payload, linker, and residual amino acid (lysine) to which the linker-payload was conjugated.[28,98] This metabolite results from complete proteolytic degradation of the antibody component of TM-ADC in lysosomal compartments after internalization. Thus, the degradation rate we measure describes the rate of proteolytic degradation of the antibody, which results in release of the payload.

In order to measure the degradation rate constant, k_{deg}, we developed a gel-based imaging assay. Cell lysate samples were collected at different time-points (0 – 130 h) after cells were treated for 30 min with 10 nM TM-ADC-647. These samples were then run on a non-reducing SDS-PAGE gel, which was imaged for fluorescence. The fluorescence signal from the intact antibody was quantified. Fig. 3.6A depicts a typical gel image with BT-474 cell lysate samples collected from different time points (0 – 130 h) after treatment. The higher band corresponds to full antibody, as confirmed by running samples in a gel with a protein ladder, as illustrated in Fig. 3.7. The main band at approximately 150 kDa seen in Fig. 3.7 corresponds to intact full antibody, based on comparison to the protein ladder and the positive control of TM-ADC-647 in lysis buffer (Lane 4). The signal at the very bottom runs at the small molecule front and includes Alexa Fluor 647-Lysine that has been released via degradation of the ADC. In addition, some minor bands are seen which correspond to aggregates (> 200 kDa) and the dissociated heavy (50 kDa) and light (25 kDa) chains of the antibody.

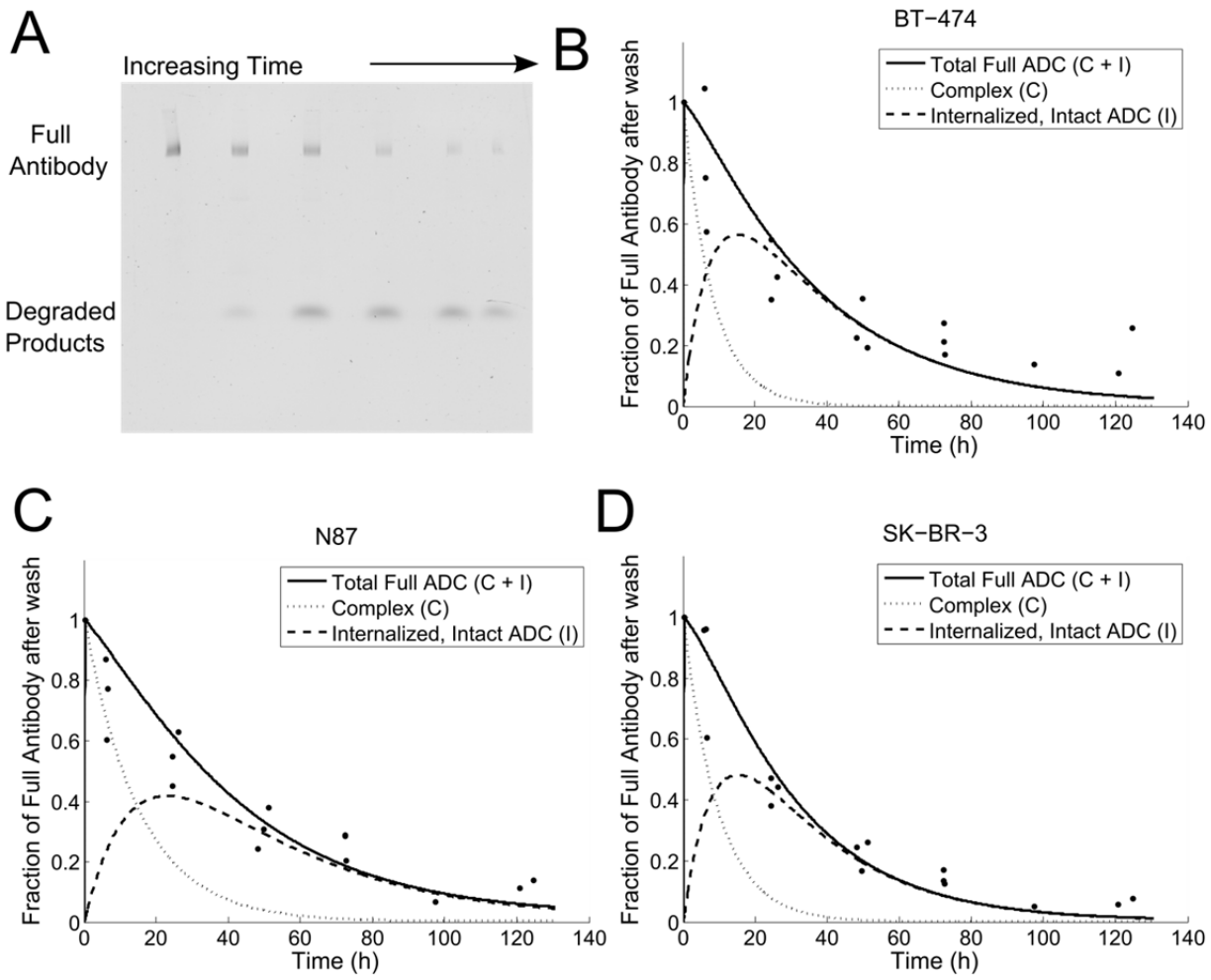

Figure 3.6 Degradation rate constant (k_{deg}) fit. (A) Image of native SDS-PAGE gel with cell lysate samples over 0 – 130 h after BT-474 cells were treated for 30 min with 10 nM TM-ADC-647. The full antibody at each time point was quantified from images such as this. The decay over time of the full antibody signal was used to fit the degradation rate constant for (B) BT-474, (C) N87, and (D) SK-BR-3 cells. The full antibody signal is the sum of the full antibody in complex with receptors on the cell surface and the intact antibody that has been internalized into the cell but not yet degraded. The model predictions for these two species are shown in dashed lines as indicated by the legend. Data points are from triplicate independent experiments.

Only the total full antibody was quantified from gels such as Fig. 3.6A. The total full antibody is the sum of both antibody on the cell surface in complex with HER2 and intact antibody that has been internalized. The predicted contributions of both of these components to the total antibody signal are shown in dashed lines in Fig. 3.6B – D. The amount of internalized, intact ADC in the cells increases initially due to internalization of ADC in complex with HER2

and then decreases due to degradation of the ADC. The antibody in complex on the cell surface decreases due to antibody internalization and dissociation. The experimental set-up was chosen to isolate the process of degradation as much as possible. By briefly dosing cells with TM-ADC-647, we quickly saturate the HER2 receptors on the cell surface. At later time points, there is no longer ADC on the surface to be internalized and the decay in signal comes from degradation. In Fig. 3.6B, 3.6C, and 3.6D, the fit curves for BT-474, N87, and SK-BR-3, respectively, are shown. The degradation rate was fit using the total intact antibody signal, normalized to the initial signal from cells collected immediately after wash at the end of the 30 min treatment period. The degradation rate constants and half-lives are shown in Table 3.2. The degradation rate of TM-ADC-647 is similar across the three cell lines tested, with half-lives on the order of one day.

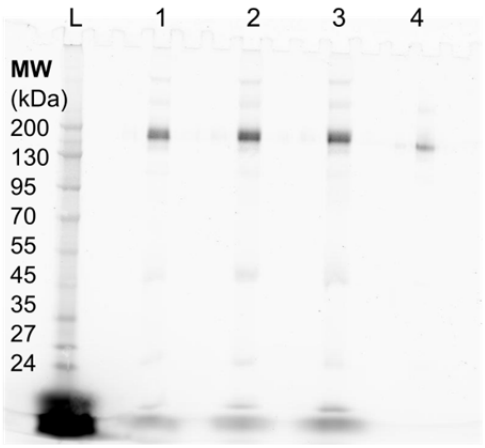

Figure 3.7 Image of native SDS-PAGE gel for degradation rate (k_{deg}) determination with cell lysate samples from cells treated for 30 min with 10 nM TM-ADC-647. Lanes are as follows: L – ladder, 1, 2, 3 – cell lysate from BT-474, N87, SK-BR-3 cells (respectively) 19 h after treatment with TM-ADC-647, 4 – positive control of TM-ADC-647 in cell lysis buffer.

Table 3.2 Degradation Rates (k_{deg}) and Half-Lives ($t_{1/2}$) for TM-ADC-647

Cell Line	$k_{deg}\left(h^{-1}\right)$	$t_{1/2}\left(h\right)$
BT-474	0.03 ± 0.01	23.3
NCI-N87	0.027 ± 0.008	25.4
SK-BR-3	0.038 ± 0.009	18.0

3.4.4 *Determination of Efflux Rate Constant*

With the internalization and degradation rate constants established, we next turned to measurement of the efflux rate constant, k_{out}, which describes the rate at which the payload metabolite exits the cell after the ADC is internalized and degraded. This model parameter encompasses a number of possible mechanisms for payload release from the cell, including passive efflux, such as diffusion of payload across the cell membrane, and active efflux, such as pumping of the payload out of the cell via multi-drug resistance pumps. Efflux of payload from the cell may also be due to lysosomal fusion with the cell membrane[99] or exosomes.[100–102] A recent study of residualization rates showed a surprising similarity of efflux rate for a number of different fluorophores,[103] suggesting that fluorophore efflux mechanisms may be independent of fluorophore structure and characteristics.

To determine the efflux rate constant, we tracked the total cell fluorescence over time using flow cytometry following a 30 min treatment period with TM-ADC-647 to saturate the surface receptors. The loss of total fluorescence signal over time is due to dissociation of surface-bound ADC, efflux of fluorophore metabolites from degraded ADCs, and dilution by growth. Internalization and degradation change the form of the ADC, but do not decrease the total fluorescence signal due to ADC in the cell. Using the complete model, which takes into account the contributions from dissociation and dilution by growth, we fit the efflux rate based on decay of the total cell fluorescence over time. Here, we tracked efflux of the fluorophore metabolite as a proxy for the maytansinoid metabolite. Fig. 3.8A – C show the curves used to fit the efflux rate constant for degraded products from cells treated with TM-ADC-647. The cell growth rate was measured during each experimental replicate as illustrated in Fig. 3.9. The fit efflux rate constants and corresponding half-lives are listed in Table 3.3.

Table 3.3 Efflux Rates (k_{out}) and Half-Lives ($t_{1/2}$) of Metabolites for TM-ADC-647

Cell Line	$k_{out}\left(h^{-1}\right)$	$t_{1/2}\left(h\right)$
BT-474	0.009 ± 0.004	75.3
NCI-N87	0.022 ± 0.009	31.7
SK-BR-3	0.015 ± 0.006	45.3

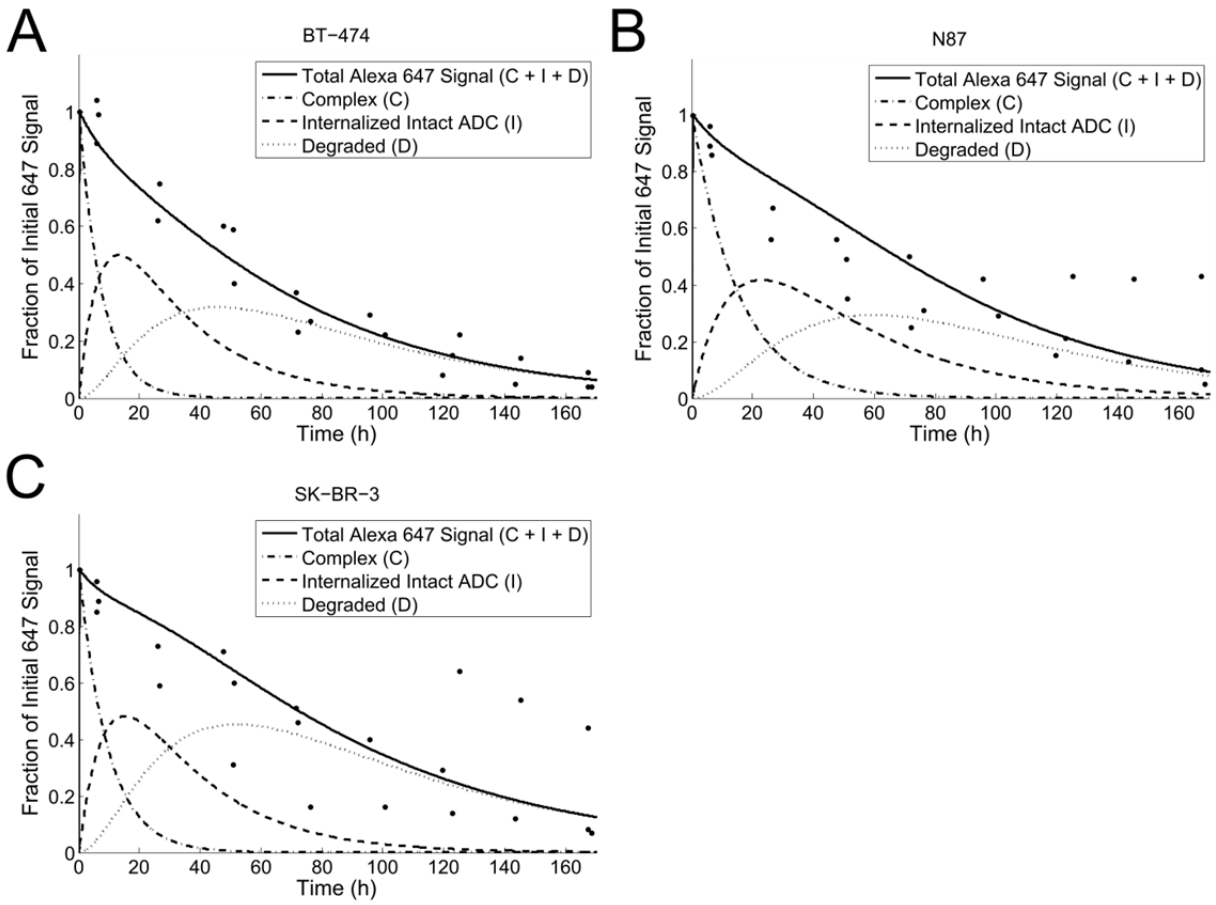

Figure 3.8 Efflux rate constant (k_{out}) fit. The decay over time of the total fluorescence signal as measured by flow cytometry from cells treated with 10 nM TM-ADC-647. The fit curves are shown for (A) BT-474, (B) N87, and (C) SK-BR-3 cells. The total fluorescence signal is the sum of the signal from antibody in complex with receptors on the cell surface (C), intact ADC (I), and degraded products (D). The model predictions for these species are shown as indicated in the legend for each graph. Data points are from triplicate independent experiments.

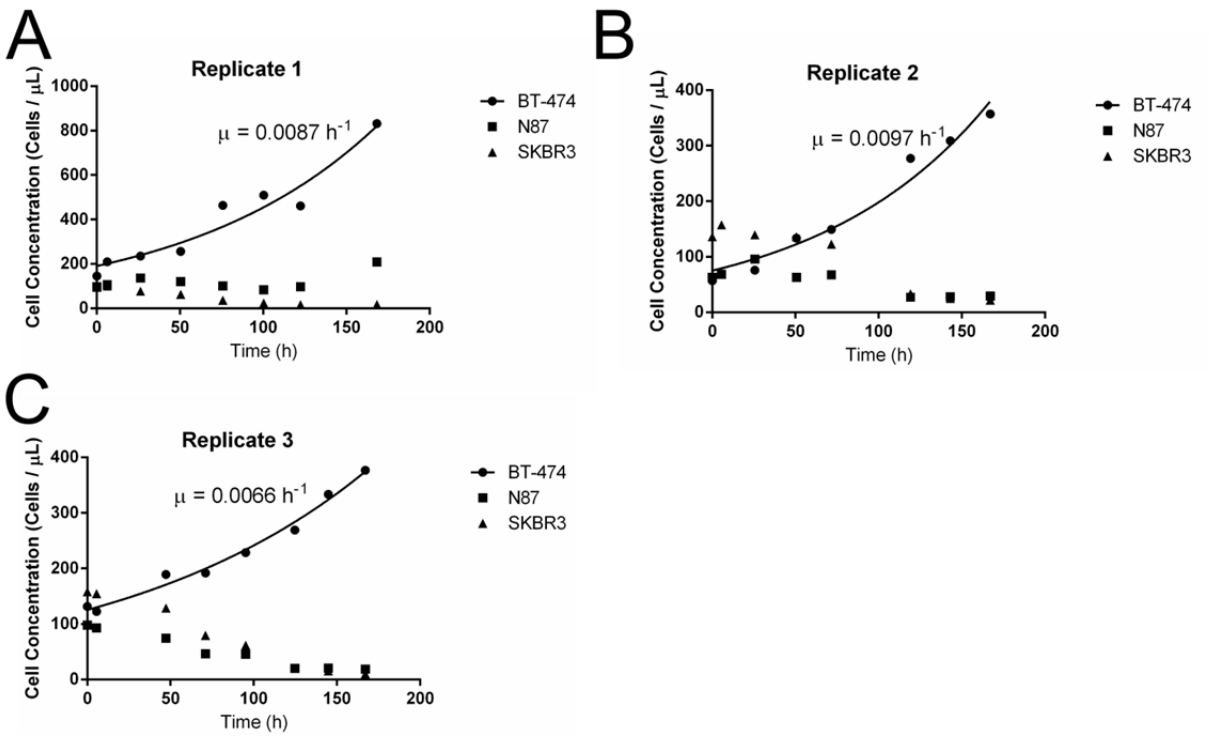

Figure 3.9 Cell growth rates for efflux rate experiments. For the treated cells, a cell growth rate was only fit for BT-474 cells because the other cell lines did not demonstrate growth.

3.4.5 *Sensitivity Analysis*

Once we established all of the model parameters, we performed a local sensitivity analysis in order to determine which parameters have the largest impact on the amount of payload delivered into cells. Fig. 3.10 illustrates the model sensitivity for each of the model parameters for cells treated with TM-ADC for 10 days at surface saturating conditions, which is physiologically relevant for cancer patients treated with tumor targeting antibodies.[93,104] Fig. 3.10A includes dilution by cell growth assuming a growth rate equal to that of untreated cells. Alternatively, if a sufficiently large quantity of payload is delivered, then cell growth would cease; Fig. 3.10B presents the same sensitivity analysis, but with no cell growth ($\mu = 0$). In both cases, the internalization rate (k_eHER2) and efflux rate (k_{out}) are key parameters for determining how much payload is delivered to cells.

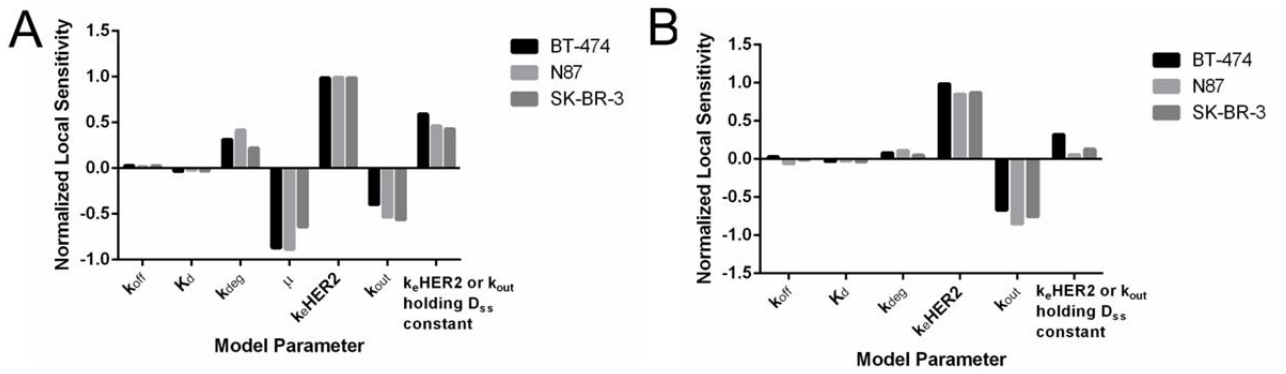

Figure 3.10 Local sensitivity analysis for model parameters (A) with cell growth rate (μ) equal to untreated cell growth rate or (B) with no cell growth. Sensitivity was calculated based on variations in the area under the curve for released payload after 10 days of treatment with 10 nM TM-ADC-647 with 10 % perturbations in the indicated model parameter.

Another way to evaluate how effectively an ADC delivers payload to a cell is to consider the payload concentration within cells at steady state with constant exposure to ADC. Assuming sufficiently high ADC concentration to saturate HER2 receptors on the cell surface, the expression for steady state payload concentration is given in Equation 3.10.

$$D_{ss} = \frac{k_{\deg} k_e HER2}{\left(k_{\deg} + \mu\right)\left(k_{out} + \mu\right)} \tag{3.10}$$

Assuming no cell growth in addition to sufficiently high ADC concentration to saturate HER2 receptors on the cell surface, the steady state expression of payload drug is simplified to Equation 3.11.

$$D_{ss} = \frac{k_e HER2}{k_{out}} \tag{3.11}$$

Equation 3.11 illustrates the crucial balance between the amount of drug that enters the cell via internalization and that which leaves the cell. This expression also demonstrates that expression level and internalization rate do not act independently of one another, rather the product of the two dictate the amount of ADC internalized. Although the amount of payload at steady state (D_{ss}) captures the key parameters, it is important to note that it would take 8 – 15 days for cells to reach steady state with continuous exposure to surface saturating levels of ADC, based on the

parameters measured for TM-ADC-647 in the three cell lines tested as described in the methods section. Fig. 3.11 illustrates the amount of each species in the cell over time to reach steady state. The number of slow processing steps results in this long approach to steady state. Fig. 3.10A and 3.10B also include the model sensitivity to modifications of k_eHER2 and k_{out} when holding D_{ss} constant. For the case with no cell growth (Fig. 3.10B), although the model is sensitive to the internalization rate (k_eHER2) and efflux rate (k_{out}) independently, it is relatively insensitive to changes to these parameters if D_{ss} is held constant.

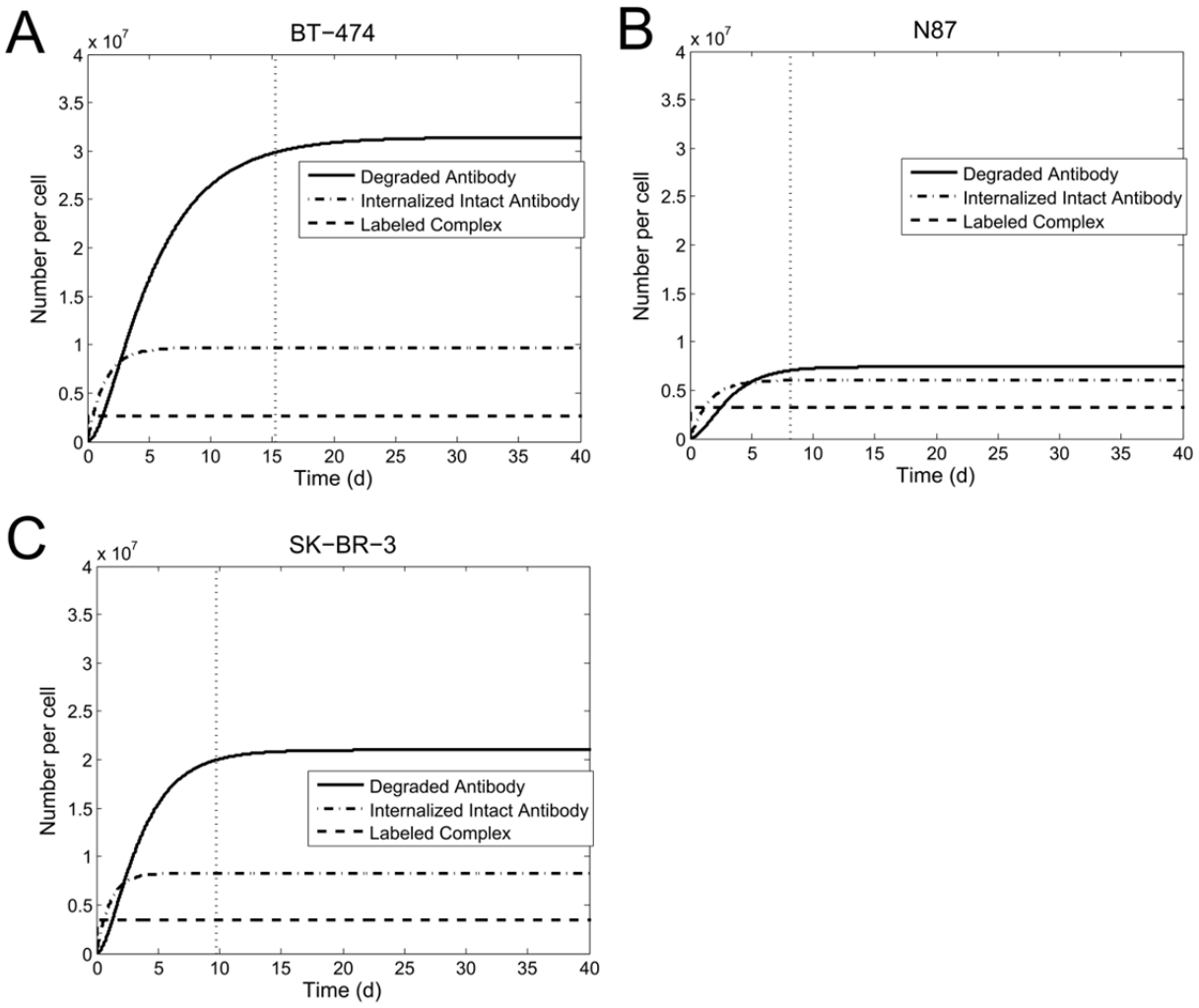

Figure 3.11 Plot of species quantity in cells over time as steady state is approached. The species (antibody in complex on the cell surface, internalized antibody, and degraded antibody) over time are shown for three cell lines: (A) BT-474, (B) N87, and (C) SK-BR-3. The vertical dashed line corresponds to the time at which steady state is reached as defined in the methods section. Note that one degraded antibody corresponds to the release of the DAR of drug molecules, i.e. one degraded antibody equals release of two drug molecules if the ADC has a DAR of 2.

3.4.6 *Incorporation of Payload Binding to Target*

Another processing step we have incorporated into the model is payload binding to its intracellular target. DM1 binding to its target, tubulin, provides an additional sink that could reduce the amount of payload that effluxes from cells. The balance between target binding and efflux has been demonstrated previously with D and L isomers of the maytansinoid DM4.[28] The K_D for DM1 binding to microtubules has been measured experimentally,[92] and the on rate and concentration of tubulin in a tumor have been estimated via a large scale PK/PD model.[93]

Based on the developed model and parameter estimates, the concentration of payload metabolites in the cell reaches 1 – 3 μM after 1 day of treatment at surface saturating concentrations of TM-ADC. This concentration of payload metabolite is in the range of previously reported IC_{50} values for DM1 inhibition of microtubule growth[92] and experimentally determined catabolite concentrations for other antibody-SMCC-DM1 conjugates.[105] At these concentrations, the quantity of DM1 present in a cell is 50 – 2500 times greater than the number of tubulin binding sites, which is on the order of 1,000 – 10,000 sites per cell.[93,106] Thus, accounting for payload binding to target does not dramatically affect the free payload concentration in the cell. However, it is important to note these calculations assume all of the drug payload catabolite escapes the lysosome and is in the cytosol. As others have suggested,[105,107] it is possible that some payload metabolite may be trapped in endosomal/ lysosomal compartments. Thus, payload concentration in the cytosol may be lower than payload concentration inside the endosomal/ lysosomal compartments; however, payload concentration in the cytosol is the relevant value to dictate how much payload ultimately reaches its target.

3.5 Discussion

In this work, we have developed a model for the cellular processing of ADCs, and we have reported generalizable methods to measure the model parameters. A Trastuzumab-maytansinoid ADC (TM-ADC), which is similar to a clinically relevant ADC, T-DM1 (Kadcyla), was used to establish this model. For TM-ADC, we found the internalization rate to be moderate relative to other antibodies[108] (half-life of 6 – 14 h), the degradation rate to be slower than internalization (half-life of 18 – 25 h), and the efflux rate to be the slowest rate (half-life of 32 – 75 h). Since degradation of the ADC is required to release the active payload component, the payload is not available for target binding as rapidly as the internalization rate might suggest. The balance between these different rates determines how effectively an ADC delivers its payload.

In order to track the processing of TM-ADC, we used Alexa Fluor 647 labeled TM-ADC. The use of a fluorescent label offers a number of advantages: the label enables tracking of the ADC in a quantitative manner; fluorescent labels can be easily applied to different ADCs of interest; fluorescence signal can be measured using multiple approaches; and fluorescent labeling is safer than radiolabeling, a common alternative. On the other hand, fluorescence labeling also has disadvantages, including susceptibility to photobleaching and environmental sensitivity; however, Alexa fluorophores are relatively stable and environmentally insensitive. An additional caveat to note is that the addition of any type of label may perturb the structure and behavior of an ADC.

At a single-cell level, efflux of payload from cells is not ideal, considering that the desired outcome after ADC treatment is the payload binding to its target to cause cell death. However, on the scale of a whole tumor, efflux of payload could be beneficial due to the so-called bystander effect.[28,109] Cell killing via the bystander effect involves a tumor cell taking up an ADC, then releasing free drug payload into the surroundings, where it can diffuse freely into nearby cells. The bystander effect can affect both tumor cells and stroma.

We hypothesize that escape of an ADC drug payload from endosomes and lysosomes is a key factor that affects how much payload actually reaches its intracellular target. Our analysis of intracellular payload concentrations indicates that if endosomal escape is not limited, then the concentration of DM1 in the cell is around the IC_{50} for DM1 binding to tubulin when cells are treated for one day with T-DM1 at cell surface saturating conditions. However, if only 10 % of

the payload metabolite escapes endosomes, then it will take ~4 times longer for cells to reach intracellular payload concentrations equal to the IC_{50}. A more detailed understanding of how payload escapes the endosomal/ lysosomal compartments could improve ADC design for more efficient payload delivery.

One limitation of our analysis is that we were unable to track the payload, DM1, itself once it was separated from the antibody component of TM-ADC. Instead, we tracked efflux of the fluorophore metabolite as a proxy for the DM1 metabolite. This assumption is reasonable given that the molecular weight and hydrophobicity of the fluorophore metabolite and DM1 metabolite are similar; in TM-ADC-647, both DM1 and the Alexa Fluor 647 dye were attached to Trastuzumab via lysine residues. The use of fluorescent drug payloads or fluorescent drug analogs could be better suited for studying payload trafficking. However, fluorescent drug analogs could be processed differently by cells depending on the modifications, and they are generally challenging to access synthetically. In ongoing work, we are studying ADCs bearing fluorescent drug payloads to enable tracking of the actual payload metabolite.

In conclusion, a quantitative understanding of ADC cellular processing allows one to compare the rates at which different processing steps occur and appreciate how these rates are related to one another. This level of understanding may be useful for improving ADC design. The cellular mechanisms of ADC processing can be integrated into larger PK/PD models, as described in Chapter 4.

Chapter 4: Extension of Antibody-Drug Conjugate Tumor Disposition Model to Predict Preclinical Tumor Pharmacokinetics of Trastuzumab-Emtansine (T-DM1)

The work discussed in this chapter[110] was completed as a close collaboration with Aman Singh and Professor Dhaval Shah at the University of Buffalo. I contributed to the model design and refinement, interpretation of data and results, data presentation, and manuscript editing.

4.1 Abstract

A mathematical model that can accurately characterize intracellular disposition of Antibody-Drug Conjugates (ADCs) is essential for predicting unconjugated drug concentrations inside the tumor. The objectives of the work described in this chapter were to: (a) extend a previously published ADC cellular disposition model with more intracellular details to characterize the disposition of T-DM1 in HER2 expressing cell lines, (b) integrate the modified cellular model with the ADC tumor disposition model to predict DM1 concentrations in a preclinical tumor model, and (c) identify prominent pathways and sensitive parameters associated with intracellular activation. The cellular disposition model was augmented by incorporating processes such as intracellular ADC degradation and passive diffusion of unconjugated drug through tumor cells. Biomeasures and chemomeasures for T-DM1, quantified in Chapter 3 and from published results in the literature, were incorporated in the modified model to characterize *in vitro* pharmacokinetics of T-DM1 in three HER2+ cell lines. When the updated cellular model was integrated with the tumor disposition model, the model was able to predict tumor DM1 concentrations in xenograft mice. Local sensitivity analysis revealed that non-specific deconjugation and passive diffusion of the drug through tumor cell are the most sensitive parameters for tubulin bound drug inside a cell. Pathway analysis suggested differential relative contribution of antigen-mediated and passive diffusion pathways for unconjugated drug exposure in a tumor cell *in vitro* versus *in vivo*. A more detailed model for intracellular processing of ADCs has been proposed to highlight how ADCs may be processed differently as endosomes mature into lysosomes.

4.2 Introduction

The past decade has seen an emergence of Antibody-Drug Conjugates (ADCs) as a successful treatment modality for cancer. More than 50 ADCs are already in clinical development, against diverse targets encompassing various hematological malignancies and solid tumors.[111] These "armed antibodies" are a chemical combination of monoclonal antibodies (mAbs) and chemotherapeutic agents, attached via a linker. The targeting capability of a mAb along with the cell-killing potential of a chemotherapeutic agent renders increased efficacy and minimal toxicity for ADCs *in vivo*, leading to widened therapeutic window. The typical mechanism for an ADC involves specific high-affinity binding of the mAb to highly expressed cell surface antigens on tumor cells, followed by receptor-mediated endocytosis. Following internalization, degradation of the linker results in release of the drug, which subsequently exhibits the cytotoxic effect. Once the ADC is administered *in vivo*, the mAb and the released drug exhibit distinctive dispositional characteristics, making it challenging to characterize the pharmacokinetics (PK) and resultant pharmacodynamics (PD) of ADCs. Thus, to generate a translatable multiscale PK models for ADCs, it is imperative to integrate all the processes that determine the disposition of an ADC and its components, especially the intracellular processes that determine drug release inside the cell. Once developed, these models can be used to further identify the important pathways and rate-limiting steps for ADC drug delivery, modulations of which could result in the development of better ADCs.[112,113]

Previously, a multiscale mechanistic PK model for tumor disposition of ADCs has beed described, which has been applied to two different ADCs, brentuximab vedotin[93] and A1mcMMAF.[104] While both of these ADCs were anatomically very similar (i.e. auristatin based ADCs conjugated via random conjugation at inter-chain disulfide bonds), they differed in their linker chemistry. Brentuximab-vedotin consists of anti-CD30 mAb (cAC10) attached to a potent tubulin polymerization inhibiting payload Monomethyl Auristatin E (MMAE) via a cleavable linker valine-citrulline (vc). Whereas, A1mcMMAF consists of an anti-5T4 mAb (A1) linked to Monomethyl Auristatin F (MMAF) via a non-cleavable linker maleimidocaproyl (mc). In this work, we have augmented the ADC tumor disposition model and have extended its application to a lysine based ADC, ado-Trastuzumab-Emtansine (T-DM1, Kadcyla®). T-DM1 is a clinically approved ADC for the treatment of patients with human epidermal growth factor receptor 2

(HER2)-positive metastatic breast cancer, who have been previously treated with Trastuzumab (Herceptin®) as a monotherapy or in combination with other chemotherapeutic agents.[98] T-DM1 is composed of a humanized anti-HER2 mAb Trastuzumab attached to DM1 (a derivative of maytansine), via a non-cleavable thioether linker succinimidyl-trans-4-[maleimidylmethyl] cyclohexane-1-carboxylate (SMCC). Overexpression of HER2 (ErbB2) in 20-25% of breast cancer patients along with the easy accessibility of its extracellular domain makes it an ideal target for antibody-based therapeutics.[28] The mechanisms of action for Trastuzumab include inhibition of PI3K/AKT signaling pathway, inhibition of HER2 shedding, and antibody-dependent cellular cytotoxicity (ADCC).[114] T-DM1 retains these mechanisms of Trastuzumab, along with the additional cytotoxic effect of DM1. Proteolytic degradation of T-DM1 results in different catabolites composed of a combination of DM1, the linker SMCC, and the conjugating amino acid lysine. Preclinical and clinical studies have confirmed MCC-DM1 and lysine-MCC-DM1 as the two major active catabolites generated following intracellular processing of T-DM1.[82,115] These catabolites and DM1 are expected to inhibit microtubule polymerization with similar potencies (IC_{50} ~ 1 μM).[92] Since most T-DM1 catabolites do not readily permeate cell membranes, they are expected to result in minimal bystander effect.[28]

In this chapter, we propose a more mechanistic cellular disposition model for ADCs that explicitly accounts for intracellular proteolytic degradation as well as passive diffusion of DM1 across the tumor cell membrane. The cellular model has been validated using cellular disposition data of T-DM1 in different cell lines and various biomeasures reported in Chapter 3. The cellular model has been integrated into the *in vivo* ADC tumor disposition model, and the ability of this augmented model in predicting tumor PK of T-DM1 and its components is assessed.

4.3 Materials and Methods

4.3.1 *Cellular Disposition of T-DM1*[82] *Dataset*

Intracellular PK of T-[H]^{3}DM1 has been investigated by Erickson et al.[82] in three different HER2 expressing cell lines: BT-474EEI (resistant to Trastuzumab), SK-BR-3, and MCF-7/neoHER2. Briefly, they introduced a stable tritium label in the C-20 methoxy group of DM1. Cells were cultured in a T-75 flask and were treated with T-[H]^{3}DM1 (30-40 nM) for 2 h at 4^{o}C. Drug containing medium was then exchanged with fresh medium at room temperature and radioactivity associated with maytansinoids (in media and cell pellet) was assessed using liquid scintillation counting (LSC) over the period of 24 h. Cellular disposition data for conjugated and unconjugated maytansinoids in intracellular and extracellular space of 3 cell lines were digitized and used for the validation of improved cellular disposition model.[82]

4.3.2 *Plasma PK of T-DM1 and DM1 Dataset*

Plasma PK for T-DM1 in both tumor bearing and non-tumor bearing mice has been investigated by several groups. It has been demonstrated that there is no significant difference in the PK of T-DM1 in tumor-bearing vs. non-tumor bearing mice. Hence, two different datasets were utilized to build a plasma PK model for T-DM1. Erickson et al.[28] studied PK of total Trastuzumab and T-DM1 after intravenous administration of T-DM1 at two different dose levels (2 and 3 mg/kg) in non-tumor bearing mice. Whereas, Jumbe et al.[83] investigated plasma PK of T-DM1 in tumor-bearing mice after intravenous administration at three different dose levels (0.3, 3, and 15 mg/kg). Datasets from both the studies were simultaneously used to fit the plasma PK model for T-DM1. The Tumor PK model (described in Section 4.3.6) also has the plasma PK model for the released drug integrated into it. Thus, in order to develop the systemic disposition model for T-DM1, we employed plasma PK data of DM1 reported by Shen et al.,[115] who investigated plasma PK of radioactive DM1 in rats at a single dose level. All three datasets were digitized and fit simultaneously using the integrated systemic disposition model of ADC described in Fig. 4.1A. DM1 PK parameter estimates in rats were scaled down to mice assuming the principles of allometry, using the equations 4.1 – 4.4.

$$CL_{mice} = CL_{rats}\left[\frac{25g}{100g}\right]^{0.75} \tag{4.1}$$

$$CLD_{mice} = CLD_{rats}\left[\frac{25g}{100g}\right]^{0.75} \tag{4.2}$$

$$V1_{mice} = V1_{rats}\left[\frac{25g}{100g}\right]^{1} \tag{4.3}$$

$$V2_{mice} = V2_{rats}\left[\frac{25g}{100g}\right]^{1} \tag{4.4}$$

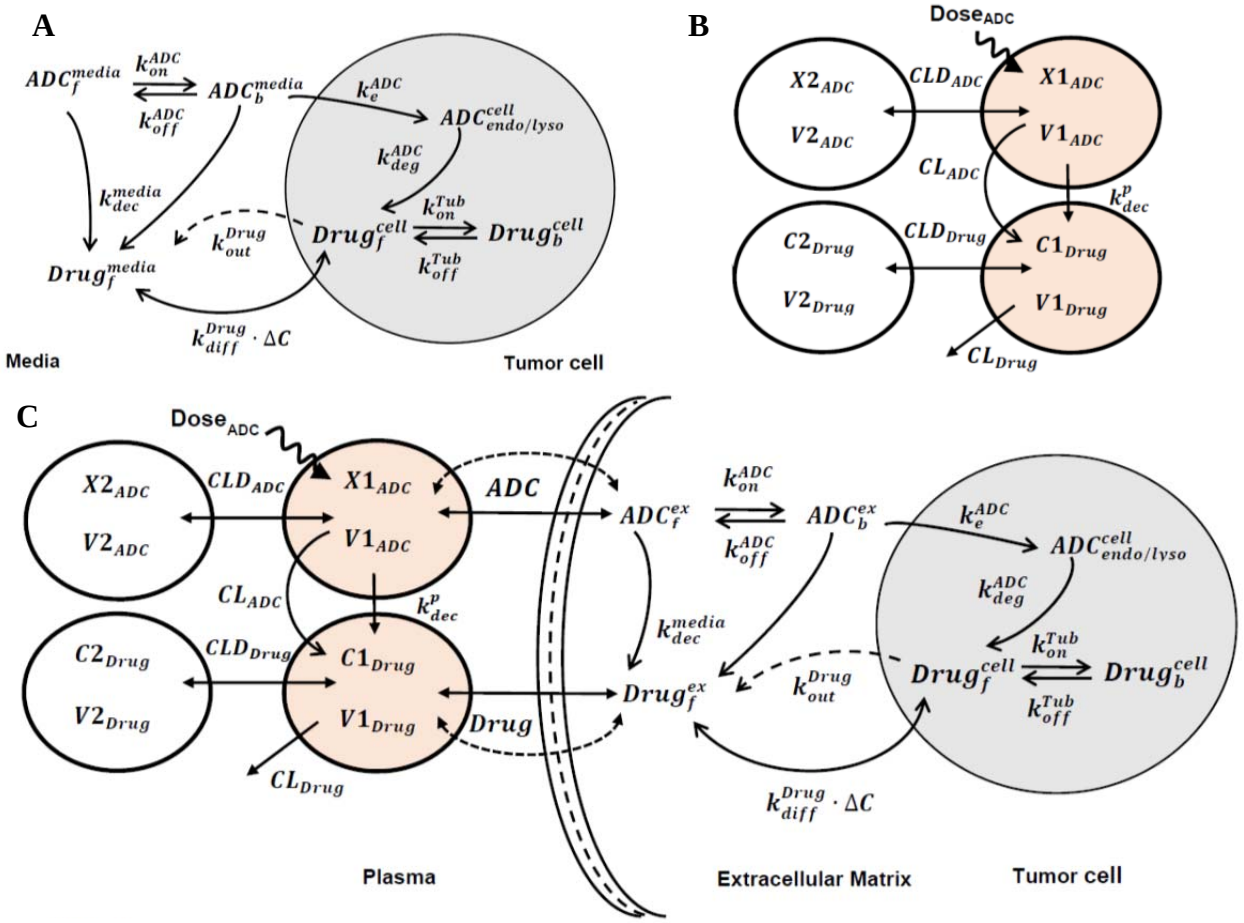

Figure 4.1 Schematics of PK models used to characterize the disposition of T-DM1. (A) Cellular disposition model for T-DM1 characterizing the intracellular processing and release of DM1 catabolites in the intracellular and extracellular space. (B) A combined PK model consisting of two integrated 2-compartment models characterizing the disposition of T-DM1 and released DM1 catabolites simultaneously. (C) Full multiscale mechanistic tumor PK model capable of predicting tumor concentrations of released DM1 catabolites based on plasma T-DM1 PK.

4.3.3 *Tumor PK of T-DM1 Dataset*

In vivo catabolism studies for T-DM1 have been performed by Erickson et al.[82] (also well described in Wada et al.[81]) in BT-474EEI tumor bearing xenograft models. Briefly, tumor bearing mice were treated with an intravenous dose of T-[H]^{3}DM1 (300 µg/kg DM1 based dose) upon achieving the tumor volume of ~250 mm^3. After treatment, mice were sacrificed at different time points up to 7 days to measure total plasma maytansinoids and tumor maytansinoids concentrations (total and unconjugated) using liquid scintillation counting (LSC). The dataset was used to validate the predictions made using the complete Tumor PK model (Fig. 4.1C), as described in Section 4.3.5.

4.3.4 *Cellular Disposition Model*

Fig. 4.1A describes the cellular disposition model which was used to capture the intracellular processing of T-DM1. All the state variables drawn in the model diagram have been defined in Table 4.1. Some of the key processes captured in the model includes cell surface binding (k_{on}^{ADC} and k_{off}^{ADC}) of T-DM1 in media to HER2 receptors (Ag_{total}) followed by internalization (k_e^{ADC}) and degradation in the endosomal/lysosomal compartment. Upon degradation, each molecule of T-DM1 is assumed to yield unconjugated maytansinoids (DM1 catabolites) equivalent to the Drug-Antibody Ratio (DAR) at that time. Free DM1 catabolites are assumed to escape into the cytoplasm where they are subjected to binding to intracellular tubulin (k_{on}^{tub} and k_{off}^{tub}) or diffuse (k_{diff}^{drug}) outside the cells into the media. Non-specific deconjugation of drug in the media from T-DM1 (free or bound to HER2) was characterized using k_{dec}^{media} parameter. The model equations are as listed as equations 4.5 – 4.11.

Table 4.1 Glossary of the state variables and model parameters used to build the model

Symbol	Definition	Unit
$ADC_f^{media}, ADC_b^{media}$, ADC_f^{ex}, ADC_b^{ex}	Free (f) and bound (b) concentrations of ADC in the media or extracellular space (ex)	nM
$ADC_{endo/lyso}^{cell}$	Concentration of ADC internalized in the endosome/lysosome of a tumor cell	nM
$Drug_f^{cell}, Drug_b^{cell}$	Intracellular concentrations of the unconjugated drug free (f) and bound (b) to tubulin	nM
$Drug_f^{media}, Drug_f^{ex}$	Free drug concentrations in the media or extracellular space	nM
$k_{on}^{ADC}, k_{off}^{ADC}$	Association and dissociation rate constants between ADC and tumor antigen	1/nM/d, 1/d
$k_{dec}^{media}, k_{dec}^{p}$	Rate constant of drug deconjugation from ADC in the cell culture media and plasma (p) respectively	1/d
$k_{out}^{drug}, k_{diff}^{drug}$	Rate constants for active efflux (out) and passive diffusion (diff)of drug between tumor cell and extracellular matrix	1/d
k_e^{ADC}	Internalization rate of the antigen inside the cell	1/d
$k_{\deg}^{ADC}$	Endosomal degradation rate constant of the ADC to release free drug	1/d
$k_{on}^{tub}, k_{off}^{tub}$	Association and dissociation rate constants for drug binding to intracellular tubulin	1/nM/d, 1/d
$\overline{DAR}, \overline{DAR}^0$	Average Drug to Antibody Ratio (DAR) values at time 't' and time 0	Unitless
$X1_{ADC}, X1_{mAb}, X1_{drug}$	Amount of ADC, total mAb and drug in the systemic circulation	nmol
$X2_{ADC}, X2_{mAb}, X2_{drug}$	Amount of ADC, total mAb and drug in the peripheral circulation	nmol
$V1_{ADC}, V1_{mAb}, V1_{drug}$	Volume of distribution in the central compartment for ADC, mAb and drug	L
$CL_{ADC}, CL_{mAb}, CL_{drug}$	Central Clearance of ADC, mAb and drug	L/d
$V2_{ADC}, V2_{mAb}, V2_{drug}$	Volume of distribution in the peripheral compartment for ADC, mAb and drug	L
$CLD_{ADC}, CLD_{mAb}, CLD_{drug}$	Distributional Clearance of ADC, mAb and drug	L/d
$C1_{drug}, C2_{drug}$	Concentration of drug in central (1) or peripheral (2) compartment	nM
R_{cap}, R_{Krogh}	Radius of the tumor blood capillary (cap), and an average distance between two capillaries (known as Krogh radius)	mm
P_{ADC}, D_{ADC}	Permeability and diffusion coefficient of ADC across and around the tumor blood vessels	μm/d, cm^2/d
P_{drug}, D_{drug}	Permeability and diffusion coefficient of released drug across and around the tumor blood vessels	μm/d, cm^2/d
$\varepsilon_{ADC}, \varepsilon_{drug}$	Tumor void volume for ADC and drug	Unitless
R_{tumor}	Radius of the tumor	cm
Ag_{tot}, Tub_{total}	Total antigen concentration and tubulin concentration	nM

$$\frac{d\left(ADC_f^{media}\right)}{dt} = -k_{on}^{ADC} ADC_f^{media}\left(Ag_{tot} - ADC_b^{media}\right) + k_{off}^{ADC} ADC_b^{media} - k_{dec}^{media} ADC_f^{media} \quad (4.5)$$

$$\frac{d\left(ADC_b^{media}\right)}{dt} = k_{on}^{ADC} ADC_f^{media}\left(Ag_{tot} - ADC_b^{media}\right) - k_{off}^{ADC} ADC_b^{media} - k_e^{ADC} ADC_b^{media} - k_{dec}^{media} ADC_b^{media} \quad (4.6)$$

$$\frac{d\left(ADC_{endo/lyso}^{cell}\right)}{dt} = k_e^{ADC} ADC_b^{media} - k_{\deg}^{ADC} ADC_{endo/lyso}^{cell} \quad (4.7)$$

$$\frac{d\left(Drug_f^{cell}\right)}{dt} = k_{\deg}^{ADC} \overline{DAR}\left(ADC_{endo/lyso}^{cell}\right) - k_{on}^{tub} Drug_f^{cell}\left(Tub_{tot} - Drug_b^{cell}\right) + \quad (4.8)$$

$$k_{off}^{tub} Drug_b^{cell} - k_{out}^{drug} Drug_f^{cell} + k_{diff}^{drug}\left(Drug_f^{media} - Drug_f^{cell}\right)$$

$$\frac{d\left(Drug_b^{cell}\right)}{dt} = k_{on}^{tub} Drug_f^{cell}\left(Tub_{tot} - Drug_b^{cell}\right) - k_{off}^{tub} Drug_b^{cell} \quad (4.9)$$

$$\frac{d\left(Drug_f^{media}\right)}{dt} = k_{out}^{drug} Drug_f^{cell} + k_{dec}^{media} \overline{DAR}\left(ADC_f^{media} + ADC_b^{media}\right) - k_{diff}^{drug}\left(Drug_f^{media} - Drug_f^{cell}\right) \quad (4.10)$$

$$\frac{d\left(\overline{DAR}\right)}{dt} = -k_{dec}^{media} \overline{DAR} \quad (4.11)$$

4.3.5 *Plasma PK Model*

Fig. 4.1B describes the plasma PK model for T-DM1. The biexponential profile of T-DM1 in mice is captured by a two-compartment PK model with linear clearance (CL_{ADC}) from central compartment and distributional clearance (CLD_{ADC}) to peripheral compartment. An extra clearance component, k_{dec}^{p} (non-specific deconjugation of DM1 in systemic circulation), accounts for faster clearance of conjugated antibody (T-DM1) versus total antibody (Trastuzumab). The disposition of released DM1, generated either by proteolytic degradation of T-DM1 (CL_{ADC}) or via non-specific deconjugation (k_{dec}^{media}), is also characterized using a 2-compartment model with linear clearance (CL_{drug}) and distributional clearance (CLD_{drug}). Total clearance of T-DM1 as well as dissociation clearance (via k_{dec}^{p}) feeds as an input to the DM1 PK model. The integrated PK model was then used to fit the PK datasets for T-DM1 PK in tumor-bearing and non-tumor bearing mice and DM1 PK in rats to get parameter estimates. The associated model equations are as listed in equations 4.12 – 4.18.

$$\frac{d\left(X1_{mAb}\right)}{dt} = -\frac{CL_{mAb}}{V1_{mAb}} X1_{mAb} - \frac{CLD_{mAb}}{V1_{mAb}} X1_{mAb} + \frac{CLD_{mAb}}{V2_{mAb}} X2_{mAb} \quad (4.12)$$

$$\frac{d\left(X2_{mAb}\right)}{dt} = \frac{CLD_{mAb}}{V1_{mAb}} X1_{mAb} - \frac{CL_{mAb}}{V2_{mAb}} X2_{mAb} \quad (4.13)$$

$$\frac{d\left(X1_{ADC}\right)}{dt} = -\frac{CL_{ADC}}{V1_{ADC}} X1_{ADC} - \frac{CLD_{ADC}}{V1_{ADC}} X1_{ADC} + \frac{CLD_{ADC}}{V2_{ADC}} X2_{ADC} - k_{dec}^{p} X2_{ADC} \quad (4.14)$$

$$\frac{d\left(X2_{ADC}\right)}{dt} = \frac{CLD_{ADC}}{V1_{ADC}} X1_{ADC} - \frac{CL_{ADC}}{V2_{ADC}} X2_{ADC} \quad (4.15)$$

$$\frac{d\left(C1_{drug}\right)}{dt} = -\frac{CL_{drug}}{V1_{drug}} C1_{drug} - \frac{CLD_{drug}}{V1_{drug}} C1_{drug} + \frac{CLD_{drug}}{V1_{drug}} C2_{drug} + \frac{k_{dec}^{p} X1_{ADC} \overline{DAR}}{V1_{drug}} + \frac{CL_{ADC} \overline{DAR}\left(\frac{X1_{ADC}}{V1_{ADC}}\right)}{V1_{drug}} \quad (4.16)$$

$$\frac{d\left(C2_{drug}\right)}{dt} = \frac{CLD_{drug}}{V1_{drug}} C1_{drug} - \frac{CLD_{drug}}{V2_{drug}} C2_{drug} \quad (4.17)$$

$$\frac{d\left(\overline{DAR}\right)}{dt} = -k_{dec}^{p} \overline{DAR} \quad (4.18)$$

4.3.6 *Tumor PK Model*

Fig. 4.1C describes the complete tumor disposition model for ADCs, which is used to predict tumor T-DM1 PK in a preclinical xenograft model. All state variables are defined in Table 4.1 and a detailed description of model has been published in previous work.[93,104] Briefly, after administration in a tumor bearing mouse, T-DM1 and DM1 disposition in the systemic circulation and peripheral tissues is described by the PK model described earlier (Fig. 4.1B). Both T-DM1 and released DM1 catabolites in the systemic circulation are distributed to the tumor extracellular space using permeability and diffusion associated terms depending on the molecular weights of the two entities. Size of the tumor determines the extent of distribution via either surface exchange or vascular exchange. At lower tumor sizes, surface exchange dominates whereas at higher tumor sizes, the vascular exchange dominates. Within the tumor extracellular space, T-DM1 binds to HER2 receptors on the cell-surface and gets internalized. Internalized T-DM1 is degraded in the endosomal/lysosomal compartment yielding DM1 catabolites which are free to either bind to intracellular tubulin or diffuse (via k_{diff}^{drug}) into the extracellular space. The effluxed or generated DM1 (via non-specific deconjugation from free or bound T-DM1) in the extracellular space can distribute back into the systemic circulation via tumor exchange

$$\frac{d\left(X1_{ADC}\right)}{dt}=-\frac{CL_{ADC}}{V1_{ADC}}X1_{ADC}-\frac{CLD_{ADC}}{V1_{ADC}}X1_{ADC}+\frac{CLD_{ADC}}{V2_{ADC}}X2_{ADC}-\left(\frac{2P_{ADC}R_{cap}}{R_{Krogh}{}^{2}}+\frac{6D_{ADC}}{R_{tumor}{}^{2}}\right)\left(\varepsilon_{ADC}\frac{X1_{ADC}}{V1_{ADC}}-ADC_{f}^{ex}\right)TV \tag{4.19}$$

$$\frac{d\left(X2_{ADC}\right)}{dt}=\frac{CLD_{ADC}}{V1_{ADC}}X1_{ADC}-\frac{CL_{ADC}}{V2_{ADC}}X2_{ADC} \tag{4.20}$$

$$\frac{d\left(ADC_{f}^{ex}\right)}{dt}=\left(\frac{2P_{ADC}R_{cap}}{R_{Krogh}{}^{2}}+\frac{6D_{ADC}}{R_{tumor}{}^{2}}\right)\left(\varepsilon_{ADC}\frac{X1_{ADC}}{V1_{ADC}}-ADC_{f}^{ex}\right)-k_{on}^{ADC}ADC_{f}^{ex}\left(Ag_{tot}-ADC_{b}^{ex}\right)+k_{off}^{ADC}ADC_{b}^{media}-k_{dec}^{media}ADC_{f}^{media} \tag{4.21}$$

$$\frac{d\left(ADC_{b}^{ex}\right)}{dt}=k_{on}^{ADC}ADC_{f}^{ex}\left(Ag_{tot}-ADC_{b}^{ex}\right)-k_{off}^{ADC}ADC_{b}^{ex}-k_{e}^{ADC}ADC_{b}^{ex}-k_{dec}^{media}ADC_{b}^{ex} \tag{4.22}$$

$$\frac{d\left(ADC_{endo/lyso}^{cell}\right)}{dt}=k_{e}^{ADC}ADC_{b}^{ex}-k_{\deg}^{ADC}ADC_{endo/lyso}^{cell} \tag{4.23}$$

$$\frac{d\left(Drug_{f}^{cell}\right)}{dt}=k_{\deg}^{ADC}\overline{DAR}\left(ADC_{endo/lyso}^{cell}\right)-k_{on}^{tub}Drug_{f}^{cell}\left(Tub_{tot}-Drug_{b}^{cell}\right)+k_{off}^{tub}Drug_{b}^{cell}-k_{out}^{drug}Drug_{f}^{cell}+k_{diff}^{drug}\left(Drug_{f}^{ex}-Drug_{f}^{cell}\right) \tag{4.24}$$

$$\frac{d\left(Drug_{b}^{cell}\right)}{dt}=k_{on}^{tub}Drug_{f}^{cell}\left(Tub_{tot}-Drug_{b}^{cell}\right)-k_{off}^{tub}Drug_{b}^{cell} \tag{4.25}$$

$$\frac{d\left(Drug_{f}^{ex}\right)}{dt}=\left(\frac{2P_{drug}R_{cap}}{R_{Krogh}{}^{2}}+\frac{6D_{drug}}{R_{tumor}{}^{2}}\right)\left(\varepsilon_{drug}C1_{drug}-Drug_{f}^{ex}\right)+k_{out}^{drug}Drug_{f}^{cell}+k_{dec}^{media}\overline{DAR}\left(ADC_{f}^{ex}+ADC_{b}^{ex}\right)-k_{diff}^{drug}\left(Drug_{f}^{ex}-Drug_{f}^{cell}\right) \tag{4.26}$$

$$\frac{d\left(C1_{drug}\right)}{dt}=-\frac{CL_{drug}}{V1_{drug}}C1_{drug}-\frac{CLD_{drug}}{V1_{drug}}C1_{drug}+\frac{CLD_{drug}}{V2_{drug}}C2_{drug}-\left(\frac{2P_{drug}R_{cap}}{R_{Krogh}{}^{2}}+\frac{6D_{drug}}{R_{tumor}{}^{2}}\right)\left(\varepsilon_{drug}C1_{drug}-Drug_{f}^{ex}\right)+\frac{k_{dec}^{p}X1_{ADC}\overline{DAR}}{V1_{drug}}+\frac{CL_{ADC}\overline{DAR}\left(\frac{X1_{ADC}}{V1_{ADC}}\right)}{V1_{drug}} \tag{4.27}$$

$$\frac{d\left(C2_{drug}\right)}{dt}=\frac{CLD_{drug}}{V1_{drug}}C1_{drug}-\frac{CLD_{drug}}{V2_{drug}}C2_{drug} \tag{4.28}$$

$$\frac{d\left(\overline{DAR}\right)}{dt}=-k_{dec}^{p}\overline{DAR} \tag{4.29}$$

processes described earlier.[108,116,117] The parameters obtained from earlier two analysis (i.e. cellular disposition model and plasma PK model) were fixed in this final step to predict the tumor concentration of DM1 catabolites. All model equations are as listed in equations 4.19 – 4.29. The tumor volume (TV) was calculated from the tumor radius, R_{tumor}, assuming a spherical shape.

4.3.7 *Biomeasures and Chemomeasures*

Determination of the T-DM1 binding coefficients (k_{on}^{ADC} and k_{off}^{ADC}) to HER2, the antigen-antibody internalization rate (k_e^{ADC}), and the lysosomal degradation rate ($k_{\deg}^{ADC}$) were measured as described in Chapter 3[76]. The rest of the parameters were either extracted from literature or were estimated using the model (Table 4.2).

4.3.8 *Modeling and Simulation*

All datasets were digitized from original publications using Grab It! ® software package. Models were simulated using the software Berkeley Madonna (University of California at Berkeley, CA) and were fit to the data using maximum likelihood (ML) estimation methods in ADAPT-5 software (Biomedical Simulations Resource, CA). For the model fitting, the variance model shown in equation 4.30 was used, where $\sigma_{\text{intercept}}$ refers to the additive error to the data and σ_{slope} refers to the error proportional to the model output.

$$\text{var}(t) = \left(\sigma_{\text{intercept}} + \sigma_{slope} \cdot Y(t)\right)^2 \tag{4.30}$$

Table 4.2 Estimated, experimentally obtained, or literature derived values for model parameters

Parameters	Value (CV %)	Unit	Source
Intracellular Model Parameters			
k_{on}^{ADC}	0.37	1/nM/h	(76)
k_{off}^{ADC}	0.014	1/h	(76)
k_{e}^{ADC}	0.011	1/h	(76)
$k_{\deg}^{ADC}$	0.03	1/h	(76)
k_{on}^{tub}	0.03	1/nM/h	(104)
k_{off}^{tub}	10.6	1/h	(118)
Tub_{tot}	65	nM	(104)
k_{dec}^{media}	0.0226	1/h	(119)
k_{diff}^{drug}	0.092 (17.4%)	1/h	Estimated
k_{out}^{drug}	0	1/h	Fixed
$Ag_{tot}^{BT-474EEI}$	0.594 (12.4%)	nM	Estimated
$Ag_{tot}^{SK-BR-3}$	1.6 (11.3%)	nM	Estimated
$Ag_{tot}^{MCF-7/neoHER2}$	1.96 (11.8%)	nM	Estimated
Systemic PK Parameters			
CL_{ADC}	0.0093 (4.4 %)	L/d	Estimated
CLD_{ADC}	0.118 (12.6 %)	L/d	Estimated
$V1_{ADC}$	0.043 (7.3 %)	L	Estimated
$V2_{ADC}$	0.0948 (5.2 %)	L	Estimated
CL_{drug}	11.29 (78.2%)	L/d	Estimated
CLD_{drug}	155.4	L/d	Fixed
$V1_{drug}$	3.30 (48 %)	L	Estimated
$V2_{drug}$	2.01	L	Fixed
k_{dec}^{p}	0.241 (8.8%)	1/d	Estimated
Tumor Distribution Parameters:-			
R_{cap}	8	mm	(104)
R_{Krogh}	75	mm	(104)
P_{ADC}	334	µm/d	(104)
P_{drug}	21000	µm/d	(104)
D_{ADC}	0.022	cm^2/d	(104)
D_{drug}	0.25	cm^2/d	(104)
ε_{ADC}	0.24	Unitless	(104)

4.3.9 *Local sensitivity and Pathway Analysis*

Local sensitivity analysis was performed on our proposed cellular PK model (Fig. 4.1A). The changes in relevant state variables were assessed with sequential changes in the parameter values. Model based exposures ($AUC_{(0-24h)}$) of total ($ADC_f^{media} \cdot \overline{DAR} + Drug_f^{media}$) and unconjugated maytansinoids ($Drug_f^{media}$) in the extracellular space as well as free unconjugated ($Drug_f^{cell}$) and tubulin-bound unconjugated maytansinoids ($Drug_b^{cell}$) in the intracellular space were simulated based on 0.1-10 fold change in parameter values. Percent changes in the exposure of each variable were plotted against the changes in the parameter values, to identify the most sensitive model parameters. Pathway analysis was performed on the cellular disposition model (Fig. 4.1A) and tumor disposition model (Fig. 4.1C) to quantify the relative contribution of antigen-mediated and passive diffusion pathway in leading the amount of unconjugated drug inside a cell.

4.4 Results

4.4.1 *Cellular Disposition Model*

Fig. 4.2 shows the observed and model generated profiles of total, conjugated, and unconjugated DM1 inside the cells, and unconjugated and total DM1 in the media, after treating BT-474EEI, SK-BR3, and MCF-7/neoHER2 cells with T-DM1. The cell volumes of 3955, 3823 and 3648 μm^3 for BT-474EEI, SK-BR3 and MCF-7/neoHER2 cells were accounted for in the model while predicting the intracellular and extracellular concentrations of DM1. The washing step after 2 h of treatment (as described in experimental design) was captured in the model by resetting the media state variables to zero at that time. All the fixed parameters obtained experimentally or from the literature, as well as fitted parameter estimates, are reported in Table 4.2. Since many studies have demonstrated that the major metabolite of T-DM1 (i.e. lysine-MCC-DM1) has minimal active transport via efflux transporters, the active efflux parameter (k_{out}^{drug}) was assumed to be minimal and was fixed to zero while characterizing the data.

4.4.2 *Plasma PK Model*

Fig. 4.3 shows the observed and model generated plasma PK profiles of T-DM1 and DM1 in mice and rats, respectively. The model shown in Fig. 4.1B was fit to all data simultaneously. Fig. 4.3A and 4.3B show the average PK data of total Trastuzumab and T-DM1 in non-tumor bearing mice after IV administration of 2 and 3 mg/kg doses. Fig. 4.3C shows the average PK profile of T-DM1 in tumor bearing mice after IV administration of 0.3, 3, and 15 mg/kg doses. Fig. 4.3D shows the model fit DM1 profile in rats, which was used to obtain mouse parameters following allometric scale-down. All parameter estimates are reported in Table 4.2.

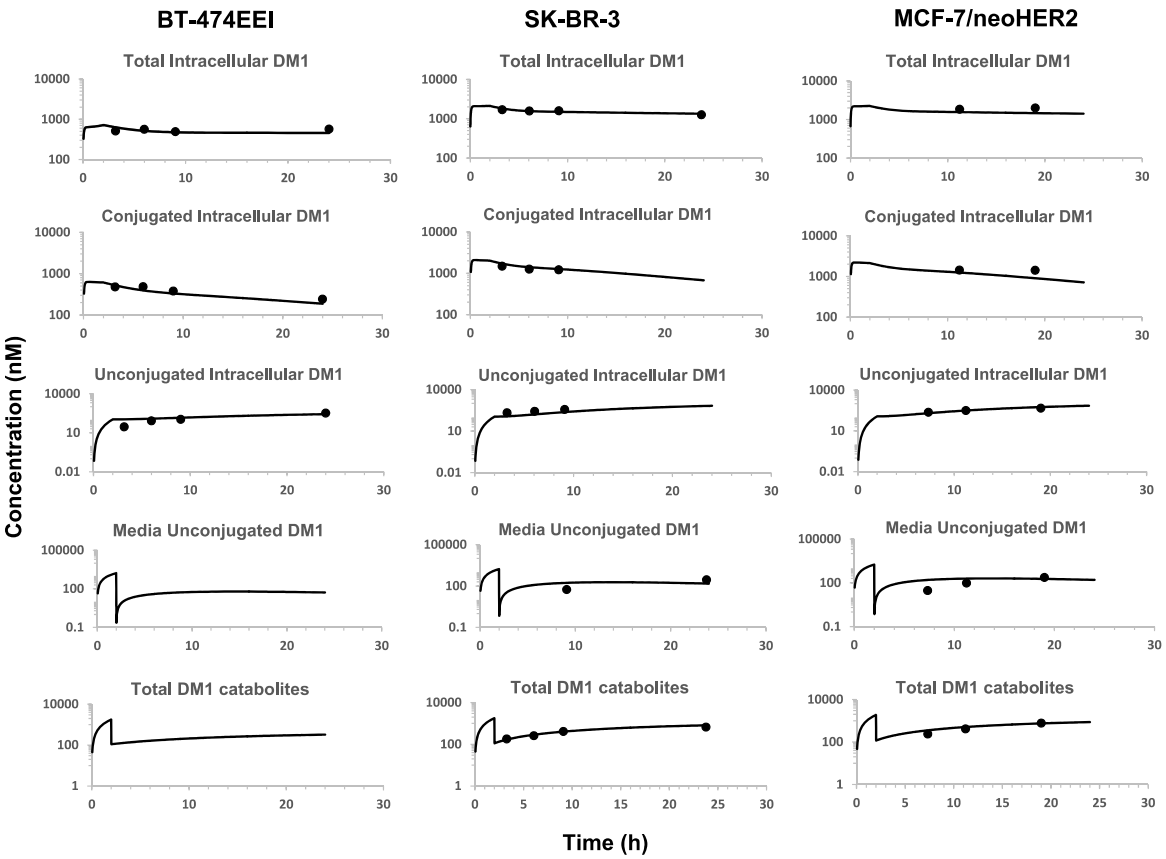

Figure 4.2 Observed and model generated profiles of total, conjugated, and unconjugated maytansinoids inside the cells, and unconjugated and total DM1 in the media, after treating BT-474EEI, SK-BR3, and MCF-7/neoHER2 cells with DM1.[82]

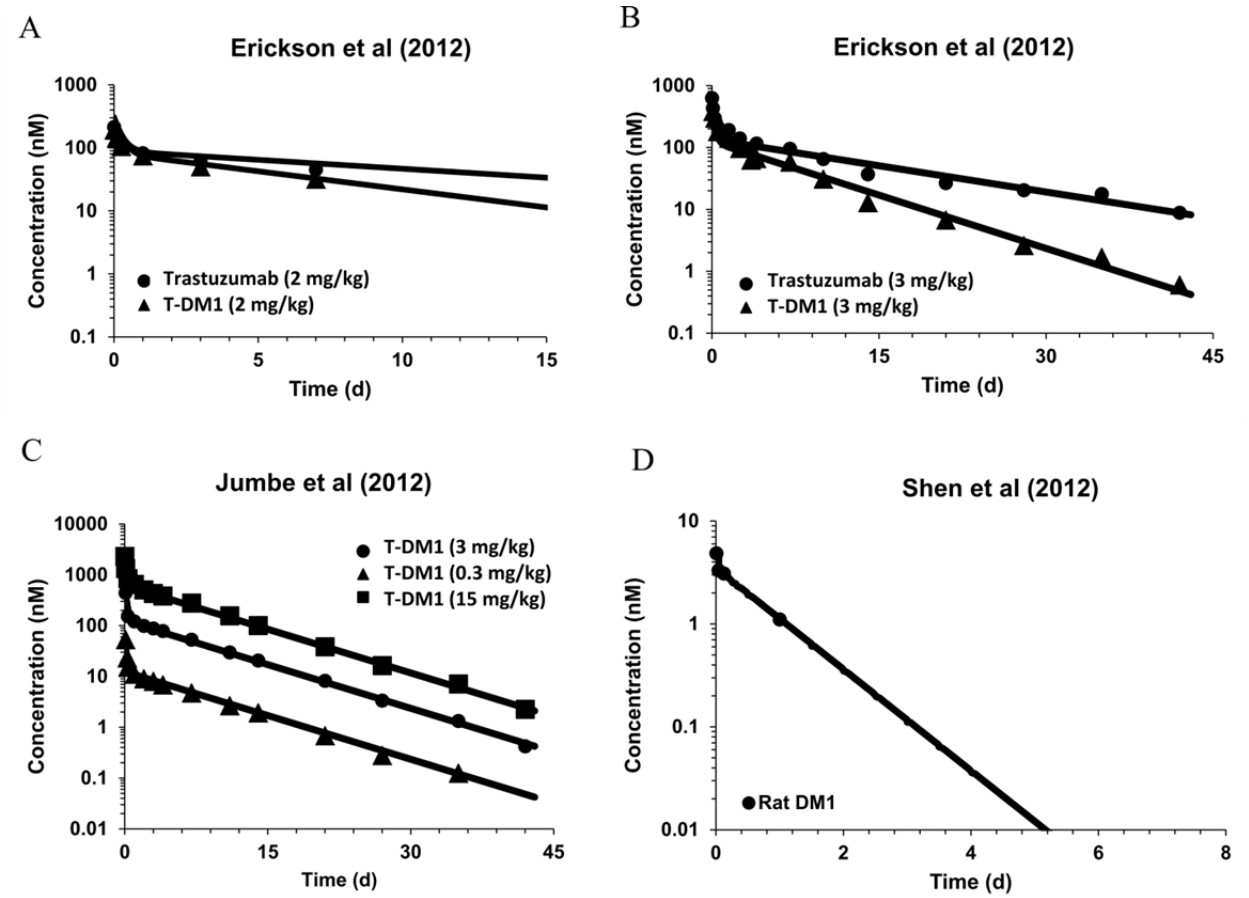

Figure 4.3 Observed[28] and model generated plasma PK profiles of total Trastuzumab and T-DM1, after (A) 2 mg/kg and (B) 3 mg/kg dose of T-DM1 in non-tumor bearing mice. (C) Observed[83] and model generated plasma PK profile of T-DM1 after 0.3, 3, and 15 mg/kg intravenous dose of T-DM1 in tumor bearing mice. (D) Observed[115] and model generated plasma PK profile of DM1 after intravenous DM1 administration in rats.

4.4.3 *Predictions of Tumor PK*

Fig. 4.4 shows the model predicted PK profiles of total maytansinoids (i.e. T-DM1 + unconjugated DM1) in the tumor and plasma, as well as unconjugated DM1 profile in the tumor. The model predictions were overlaid with experimentally obtained data in a BT-474EEI xenograft, after IV administration of 300µg/kg $[H]^3$DM1-based dose of T-$[H]^3$DM1.[81,82] While making predictions, the cellular disposition parameters specific to BT-474EEI cell line as well as the plasma PK parameters for T-DM1 were fixed to estimates obtained in the previous sections. The tumor distribution parameters associated with T-DM1 and DM1 were fixed to what have reported in previous work.[93,104] A diffusion rate constant (k_{diff}^{drug}) was introduced and estimated characterizing the passive diffusion of drug through a tumor cell. Since there is no finite value

reported for this parameter in the literature, the estimated uncertainty in cellular model fitting (i.e. CV% of 17.4) was used to run Monte-Carlo simulations and generate 5th and 95th percentile confidence intervals around the median. The percent prediction error (% PE) on observed and predicted exposure ($AUC_{(0-24h)}$) using the expression, $\frac{|Predicted-Observed|}{Predicted} \times 100$, was calculated to be 2.5%, 20.5% and 22.8% for plasma, total tumor and unconjugated tumor maytansinoids. The parameter values associated with the final model are listed in Table 4.2.

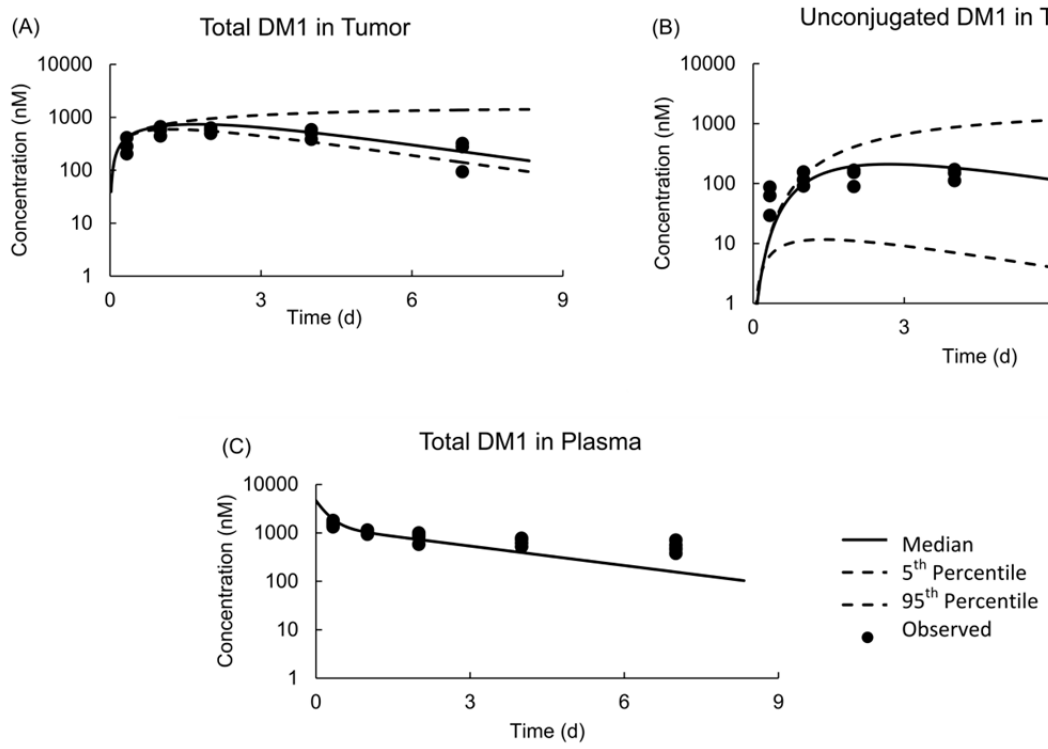

Figure 4.4 Observed and model predicted profiles of total maytansinoids (A) and unconjugated maytansinoids (B) in the tumor and total plasma maytansinoids (C) obtained after IV administration of 300 µg/kg [H]^{3}DM1-based dose of T-[H]^{3}DM1 in BT-474EEI tumor bearing mice.[81,82]

4.4.4 *Local Sensitivity and Pathway Analysis of Cellular Disposition Model*

Fig. 4.5A shows the local sensitivity analysis profile for tubulin-bound drug inside the cell ($Drug^{b}_{cell}$) generated using the improved cellular disposition model for ADC shown in Fig. 4.1A. The non-specific deconjugation rate (k^{media}_{dec}) and passive diffusion rate (k^{drug}_{diff}) were identified as the most sensitive parameters for free and bound unconjugated maytansinoid exposures in the intracellular space. Additionally, total and unconjugated maytansinoid levels in

the extracellular space were also dependent on the total antigen expression (Ag_{tot}). The sensitivity analysis for other state variables is provided in the Fig. 4.6. Fig 4.5B and 4.5C reveals the pathway analysis profiles of cellular model (Fig. 4.1A) and full tumor PK model (Fig. 4.1C) respectively as a function of ADC dose. Both antigen-mediated and passive diffusion pathways start out with approximately equal contribution in an *in vitro* setting (Fig. 4.5B) with saturation of antigen-mediated pathway with increasing ADC dose. However, most of the diffusion mediated drug transport is driven outside the tumor in an *in vivo* situation (Fig. 4.5C) rendering majority of the drug transported via antigen-mediated pathway inside tumor cell.

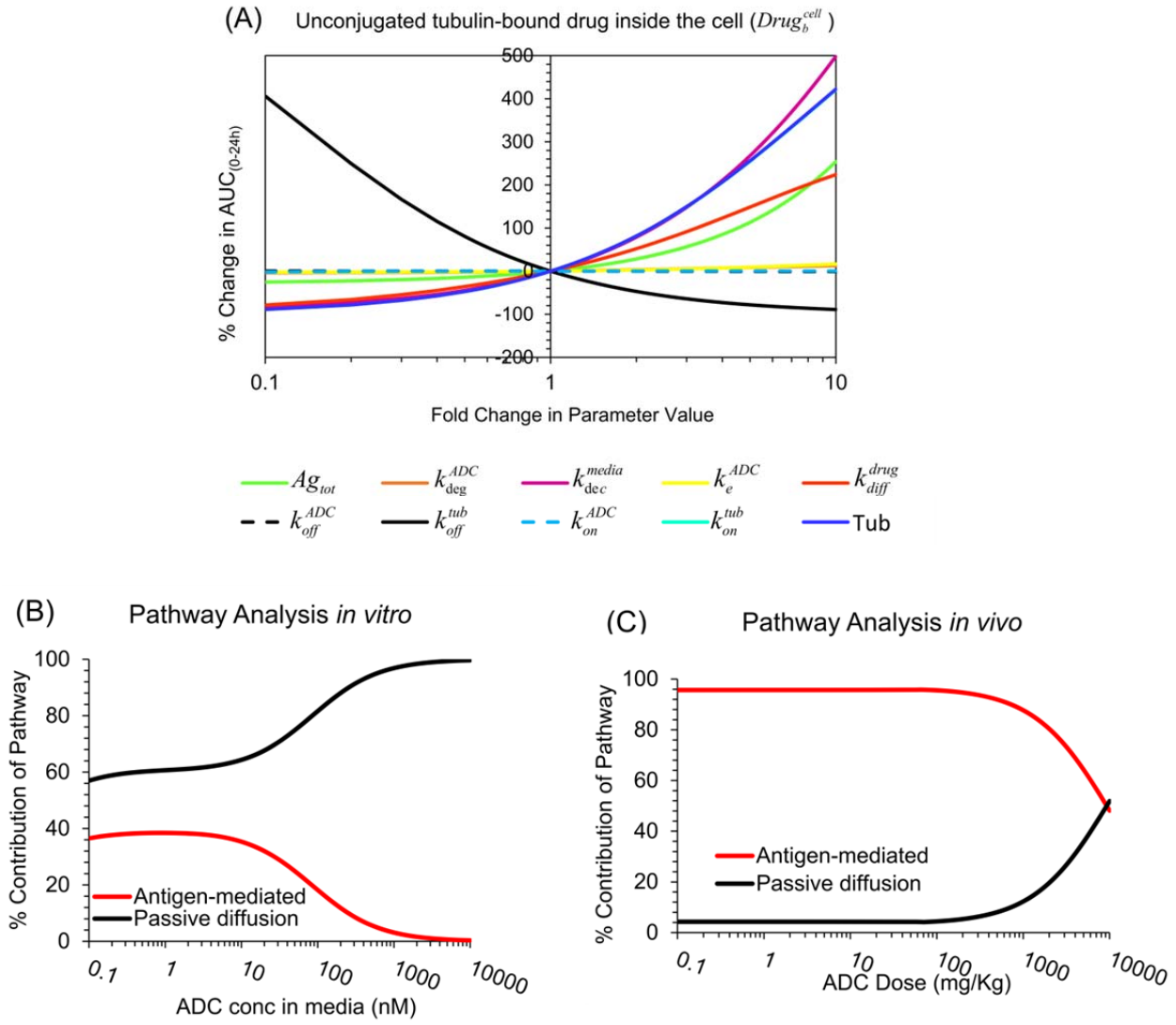

Figure 4.5 Local sensitivity (A) and pathway analysis (B & C) of the improved cellular disposition model for ADCs.

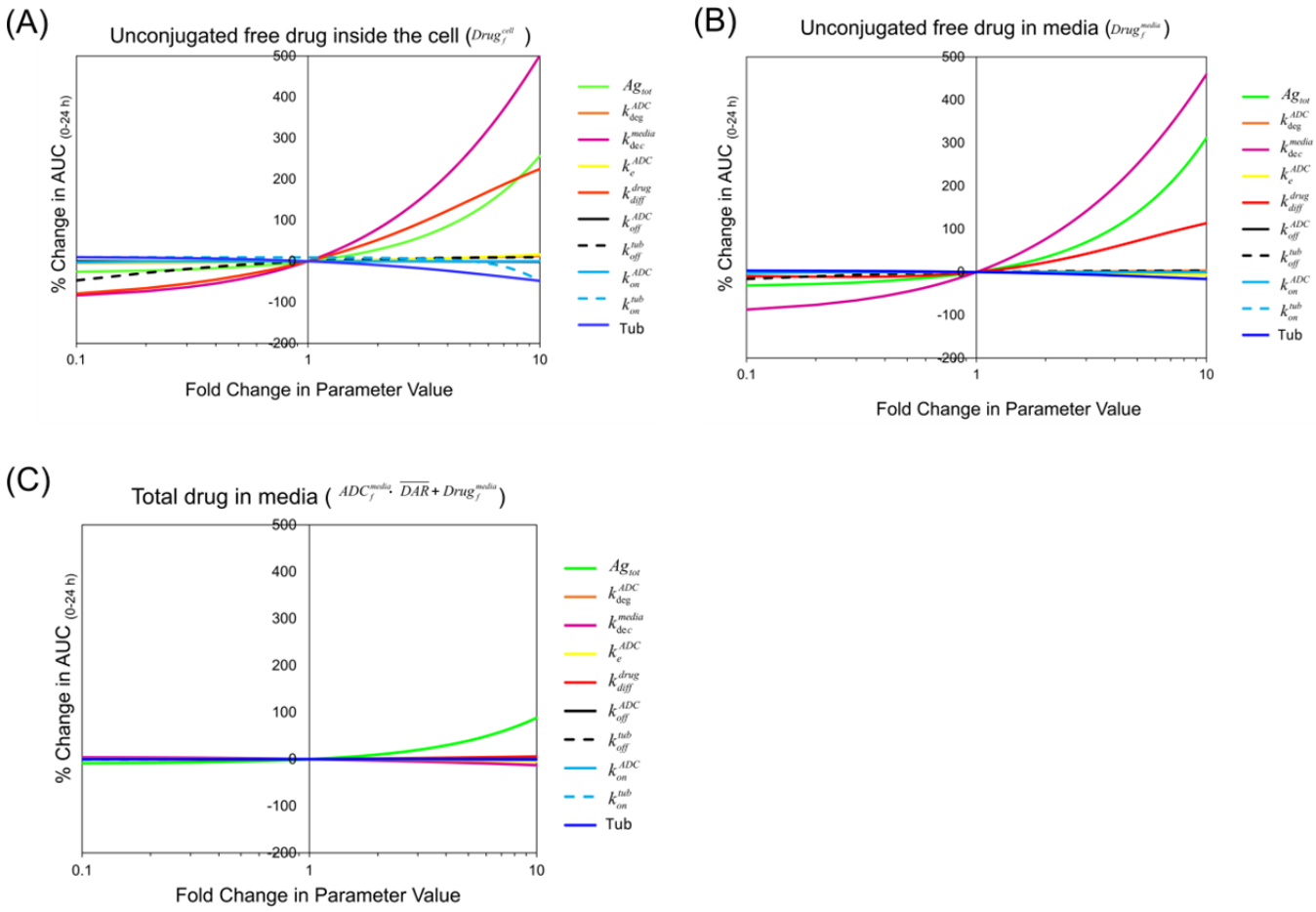

Figure 4.6 Sensitivity Analysis for (A) unconjugated free drug inside cells, (B) unconjugated free drug in the media, and (C) Total drug in media.

4.5 Discussion

In this work, we have extended a PK model for ADCs to include cellular-level processing. We have evaluated the application of this model to T-DM1 by using the experimental data obtained from Erickson et al.,[82] who studied intracellular processing of T-DM1 in different cell lines.

In order to characterize the data, we incorporated experimentally obtained values of different biomeasures[118,119] and estimated unknown parameters such as passive diffusion rate of drug inside the cell (k_{diff}^{drug}). We assume these parameters to be ADC/drug-specific and expect them to differ based on the linker design and cytotoxic agent. To experimentally obtain k_{diff}^{drug}, one needs to perform cellular uptake studies using the observed drug metabolite (e.g. lysine-MCC-DM1 for T-DM1). We also estimated the antigen expression levels in different cell lines. The reported values were consistent with the reported values by Erickson et al.[82]. This developed model could be expanded to incorporate multiple cell populations (e.g. antigen positive and antigen negative), and to account for dynamically changing cell numbers with time, similar to the single-cell kinetic model reported by Krippendorff et al.[120].

From the local sensitivity analysis, we identified non-specific deconjugation rate (k_{dec}^{media}), passive diffusion rate of drug (k_{diff}^{drug}), and antigen expression levels (Ag_{tot}) as the most sensitive parameters associated with the exposure of total and unconjugated maytansinoids (DM1) in the media and inside cell. Additionally, the dissociation rate of DM1 (k_{off}^{tub}) from the tubulin-DM1 complex and concentration of tubulin (Tub) were also important parameters determining the extent of bound DM1 exposure in the intracellular space. The importance of the ADC degradation rate ($k_{\deg}^{ADC}$) is underrepresented in this analysis because increases in degradation rate past a threshold result in the net internalization rate (k_e^{ADC}) becoming rate-limiting, restricting the net change in unconjugated DM1 exposure. A global sensitivity analysis of this model will be more adequate to highlight the sensitivity of this parameter.

The model was able to predict maytansinoid levels in plasma and tumors well with the median estimate going through the middle of the data and the majority of the data in the 95% confidence interval. Some of the observed deviations in the plasma PK predictions of total maytansinoids may be due to the fact that disposition of DM1 in mice was characterized using

PK parameters scaled down from rat. In addition, in the absence of average DAR vs. time profile for T-DM1 in mice, we estimated the drug deconjugation rate, k_{dec}^{media}, based on total antibody and conjugated antibody profiles, which may not yield the most accurate parameter estimates for drug deconjugation. Our estimated k_{dec}^{media} parameter value was consistent with the reported value by other groups.[119] Moreover, the DM1 catabolites obtained after non-specific deconjugation (in systemic circulation or extracellular matrix) can be different than the DM1 catabolites obtained after intracellular processing (e.g. lysine-MCC-DM1). These different DM1 containing molecules may have significantly different disposition *in vivo*, which can also result in the deviation of model prediction from observed data. A dedicated systemic and tumor distribution study of DM1 metabolites (lysine-MCC-DM1) in xenograft mice could further bolster our understanding of PK parameters for the released drug. In this analysis, we fixed the active efflux rate, k_{out}^{drug}, to zero as most studies have reported no evidence of active transport of lysine-MCC-DM1 out of a tumor cells.[121,122] However, studies quantifying the active efflux rate *in vitro* could be performed by loading cancer cells with radiolabeled-lysine-MCC-DM1 and following the obtained radioactivity outside the cell over time.

Intracellular activation of ADCs entail cellular trafficking in different endosomal and lysosomal compartments, eventually leading to the release of conjugated drug that induces the cytotoxic effect. However, the currently available data on cellular disposition of ADCs limits our capability to mathematically characterize all these processes. Fig. 4.7 depicts the schematic of a proposed ADC PK model that incorporates the maturation of early endosomes to late endosomes and then lysosomes. The cellular processing rates could vary depending on the maturation stage of the endo/lysosomal compartment. For example, an acid-labile linker will cleave immediately following changes in pH in early endosomes; a valine-citrulline linker will be cleaved in the late endosome/lysosomes based on the abundance of the enzyme cathepsin B; a non-cleavable SMCC linker will be proteolytically degraded in lysosomes; and a disulfide linker will be cleaved by the cytoplasmic glutathione molecules. The rate (k_{esc}^{drug}) and extent (F_{esc}) of endosomal escape of the unconjugated drug/drug metabolite in the cytoplasm could be a salient factor determining an ADC's efficacy, as sequestration of weakly basic drugs in lysosomes is widely acknowledged.[123]

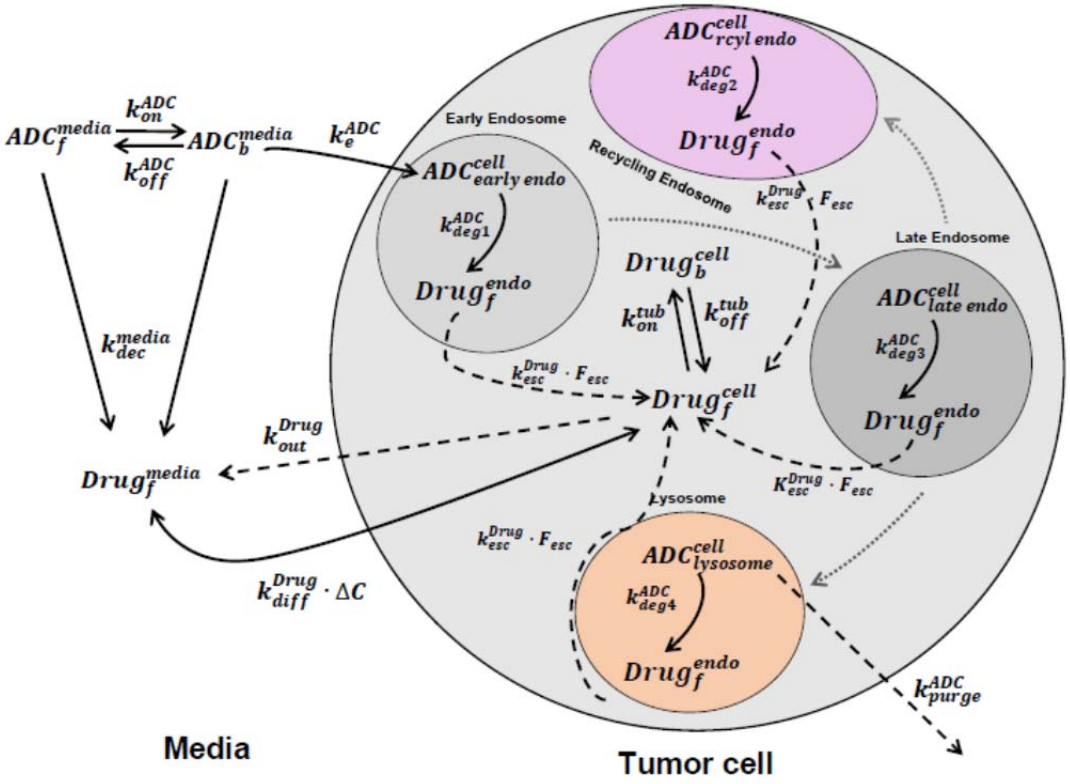

Figure 4.7 Schematics of a proposed more detailed model for intracellular processing of ADCs, which highlights how endosomal maturation may effect ADC degradation and drug escape from a endosomal/lysosomal compartment.

In summary, we have improved a previously published *in vivo* ADC tumor disposition model and have demonstrated the application of this augmented model to T-DM1. First, the cellular disposition model for ADCs was developed to incorporate more intracellular details for characterizing ADCs designed with non-cleavable linkers. The model was able to characterize the cellular disposition of T-DM1 in 3 different HER2 expressing cell lines. When integrated with the *in vivo* tumor disposition model, the new model was successfully able to predict tumor exposure of T-DM1 in a xenograft mouse model. In the future, the model could be extended to link the unconjugated tumor drug concentrations to T-DM1 efficacy data obtained in different xenografts to estimate the efficacy parameters.[83,124,125] The preclinical PK/PD model can then be translated to humans and evaluated using the clinical PK and efficacy data for T-DM1.[86]

Chapter 5: Lysosomal Escape May Limit Drug Target Binding when Delivered via an Antibody-Drug Conjugate

5.1 Abstract

Antibody-drug conjugates (ADCs) are a promising type of cancer therapeutic which uses the tumor specificity of an antibody to target small molecule chemotherapeutic drugs. Once an ADC binds its target antigen, the ADC gets internalized into endosomal/lysosomal compartments where it gets degraded, releasing the drug payload. However, the drug payload must first escape this compartment before it can bind its intracellular target. In this work, we used an established model for ADC cellular processing and processing rates measured for a Trastuzumab-Doxorubicin (Tras-Dox) ADC to demonstrate that more than 10 million doxorubicin molecules can be delivered to cells via the Tras-Dox ADC. However, we find based on fluorescence microscopy with Tras-Dox that cellular trafficking may limit the amount of drug that reaches its target (DNA in the nucleus) in the cell. When we compare cells treated with free doxorubicin to cells treated with the Tras-Dox ADC on an equimolar doxorubicin basis, the free doxorubicin accumulates in the nucleus whereas the Tras-Dox does not accumulate in nucleus. The doxorubicin is likely trapped in the endosomal/lysosomal compartment where the ADC is internalized and degraded. These results suggest that improving a drug's ability to escape the endosomal/lysosomal compartments may improve the efficacy of ADCs and that lysosomal escape should be characterized when developing an ADC.

5.2 Introduction

Antibody-drug conjugates (ADCs) are a promising class of cancer therapeutics,[26,73,77,126] which combine the specificity of a tumor targeting antibody with the potency of a chemotherapeutic drug. ADCs are designed to carry a drug payload to the site of the tumor and deliver inside the tumor cell. First, the antibody binds its target antigen on the tumor cell surface. Then, the ADC is internalized into endosomal/lysosomal compartments via receptor-mediated endocytosis. In these compartments the ADC is degraded in a mechanism dependent on the linker design and the drug component is released from the antibody. However, once the drug is separated from the antibody, it must still escape from the endosomal/lysosomal compartment before it can reach its intracellular target.

ADC linkers are typically designed to be degraded based on the conditions found in the endosomal/lysosomal compartment. Early generations of ADCs used the acidic conditions found in endosomes and lysosomes to cause the cleavage of linkers such as hydrazone linkers.[26,127,128] Later generations of ADCs use proteases found in the endosomes and lysosomes to cleave linkers such as peptide based linkers.[19,129–131] More recently, non-cleavable linkers have been used.[24,72,98] The drug component is released based on complete degradation of the antibody by proteases and the active drug catabolite is the drug, linker, and a residual amino acid such as a lysine or cysteine.[28,105,115]

Previous work[33] using a clonogenic assay based on flow cytometry has established that 4 – 12 million doxorubicin molecules need to be delivered to a cell to cause it to stop proliferating. In this work, we use the methods and model previously established[76] for T-DM1 and applied it to a Trastuzumab-Doxorubicin (Tras-Dox) ADC to predict whether the goal of doxorubicin molecules could theoretically be delivered. In addition, we used Tras-Dox with fluorescence microscopy in order to observe spatially where within the cell the drug payload (doxorubicin) trafficked as the ADC was processed. The drug doxorubicin was selected because it is naturally fluorescent[43] such that we could track the drug payload itself once it was released from the antibody. Tras-Dox was synthesized using a non-cleavable linker such that the release of doxorubicin is expected to occur once the whole ADC is degraded by proteases found in the lysosome. The hypothesized active metabolite is doxorubicin-linker-cysteine (the amino acid which is used for conjugation).

5.3 Materials and Methods

5.3.1 *Materials and Cell Lines*

The Trastuzumab-Doxorubicin (Tras-Dox) antibody-drug conjugate was synthesized as described previously (See Sections 2.3.8 and 2.3.9).[33] Briefly, the linker succinimidyl 4-[N-maleimidomethyl] cyclohexane-1-carboxylate (SMCC) was used. First, the SMCC linker was conjugated to doxorubicin via its amine group. Then, the doxorubicin-SMCC drug-linker was conjugated to an engineered cysteine site on Trastuzumab A114C using the maleimide handle of SMCC to form a stable thioether bond. Tras-Dox was aliquoted, flash frozen using liquid nitrogen, and stored at -80°C. New vials of Tras-Dox were thawed for each experiment and stored temporarily at 4°C.

Doxorubicin hydrochloride was purchased from Sigma (St. Louis, Missouri). The SK-BR-3 cell line was used in this work and was obtained from the American Type Culture Collection (ATCC) (Manassas, Virginia). The cells were grown in McCoy's 5A Medium Modified (Lonza, Basel, Switzerland) supplemented with 10% fetal bovine serum (FBS) and 5% penicillin–streptomycin. For live cell imaging experiments, media without Phenol Red was used to reduce background signal. MATLAB software (Mathworks) was used for model implementation and parameter fits. GraphPad Prism (La Jolla, California) software was also used for parameter fits. Image J (United States National Institutes of Health) was used for image analysis and processing.

5.3.2 *Alexa Fluor 647 Labeling of Tras-Dox*

Tras-Dox was labeled using the Alexa Fluor 647 NHS Ester (Succinimidyl Ester) dye (Life Technologies, ThermoScientific, Waltham, Massachusetts) to generate Tras-Dox-647. A 1M solution of sodium bicarbonate was added with a 1:10 ratio to Tras-Dox (1 mg/mL) in PBS. Then, Alexa Fluor 647 dye (at 10 mg/mL in DMSO) was added to reach a final concentration of 45 μg/mL. The reaction was left at room temperature for 30 minutes on a rotator. Then the mixture was immediately purified on an AKTA size exclusion chromatography system (GE Healthcare). The fluorophore-to-antibody ratio was less than 1 based on absorbance at 280 nm and 647 nm. See appendix B.5 for reference as well.

5.3.3 *Cellular Processing Rate Measurements*

The following cellular processing parameters were measured for Tras-Dox: equilibrium dissociation constant, K_D; net internalization rate constant, k_e; and degradation rate, k_{deg}. The methods used were similar to those used previously[76] (See Section 3.3.4, 3.37, and 3.3.8). For the K_D measurement, fixed cells were treated with a range of Tras-Dox (5 – 320 pM) overnight at 37°C. Cells were then washed with PBS and the fluorescence signal was read via a BD FACSCanto II flow cytometer.

In short, the net internalization rate constant was also measured by flow cytometry. Cells were treated with 10 nM Tras-Dox for various lengths of time. Cells were then put on ice to limit further uptake of Tras-Dox and stained for surface Tras-Dox using an Alexa Fluor 488 Goat anti-Human IgG (H+L) (Life Technologies). Fluorescence signal for total Tras-Dox and the surface anti-Human IgG were read by flow cytometry. The difference in the normalized total signal and surface signal gives the amount of internalized Tras-Dox at each time point. From the internalized signal over time, the net internalization rate constant was fit. In addition, non-specific uptake was measured as described previously[76] using blocking and competition with unlabeled Trastuzumab.

The degradation rate constant was measured using Tras-Dox-647 in the developed gel assay. Cells were treated with 10 nM Tras-Dox-647 for 30 mins at 37°C and then washed with PBS and allowed to growth. At various time points, cell lysate samples were collected. The cell lysates were run on a non-reducing SDS-PAGE Gel and the gel was imaged for Alex Fluor 647 signal. The band for full, intact antibody was quantified and the decay in this signal over time was used to fit the degradation rate constant.

5.3.4 *Model Predictions*

The model framework has been described in detail previously[76] (See Section 3.3.3). To predict how much doxorubicin is delivered to SK-BR-3 cells via Tras-Dox, we simulated treatment of 50,000 cells in a 4 mL volume of media with 10 nM Tras-Dox for 15 days. We used the cellular processing rate parameters measured for Tras-Dox and assumed other parameters (k_{off} and k_{out}) were the same as those for T-DM1. The cellular parameters HER2 (HER2 expression level) and μ (cell growth rate) were measured previously[76] for SK-BR-3. With this

model, we simulate the base case, where all values are as described/reported, as well as a case where there is no cell growth ($\mu = 0$), no efflux ($k_{out} = 0$) or neither cell growth nor efflux (both $\mu = 0$ and $k_{out} = 0$).

5.3.5 *Live Cell Microscopy*

Cells were plated with 10,000 cells per well in 8-well Nunc™ LabTek™ chambered cover glass (Thermo Scientific, Waltham, Massachusetts) and allowed to adhere overnight. Cells were then treated with 40 nM free doxorubicin or 20 nM Tras-Dox. Since the DAR of Tras-Dox is 2, these treatments are equimolar in terms of doxorubicin dose. After one day of treatment, untreated cells, cells treated with 20 nM Tras-Dox, and cells treated with 40 nM free doxorubicin were imaged. After 4 days of treatment, the media was replaced for untreated cells and cells treated with Tras-Dox. For the treated cells, the fresh media contained 20 nM Tras-Dox again. After 5 days of treatment, untreated cells and cells treated with Tras-Dox were imaged. In addition, cells treated with Tras-Dox for 5 days were treated with 40 nM free doxorubicin for 1 day and were imaged after a total of 6 days.

To prepare for imaging, cells were treated with 0.4 μg/mL of the nuclear stain Hoescht 33342 (Thermo Scientific) and 50 nM of the lysosomal stain LysoTracker® Deep Red (Life Technologies/ Thermo Scientific) for 30 mins at 37 °C. Cell were washed thrice with PBS and fresh media was added to each well. An Applied Precision DeltaVision Ultimate Focus Microscope was used for imaging with environmental control to maintain 37°C and 5% CO_2. Images were taken using a 60X objective. Images were deconvoluted using the DeltaVision Software and the 3D iterative constrained deconvolution method with 10 iterations.

Three channels for fluorescence detection were used: DAPI channel (excitation at 390 nm, emission at 435 nm), FITC/TRITC channel (excitation at 475 nm, emission at 594 nm) and Cy5 channel (excitation 632 nm, emission at 676 nm). The DAPI channel corresponds to the Hoescht nuclear stain; the FITC/TRITC channel corresponds to doxorubicin signal; and the Cy5 channel corresponds to Alexa 647 signal. The laser power and exposure times for each channel were as follows: DAPI, 5% power, 0.49 s; FITC/TRITC, 100%, 0.60 s; and Cy5, 5%, 0.25 s. A panel of images was taken for each treatment condition resulting in at least 16 images per condition. See also Appendix B.17.

5.3.6 *Quantification of Live Cell Images*

The signal from doxorubicin in the nucleus of cells was quantified using the CellProfiler Software[132]. First, a threshold was applied to each channel of each image. An Adaptive thresholding strategy using the Otsu method with two classes, weighted variance for the entropy, no smoothing, and a threshold correction factor of 1.0 was applied. Next, the nuclei in each image were identified using the "IdentifyPrimaryObjects" module. Objects outside the diameter range of 50 to 120 pixels (corresponds to 10.8 to 25.9 μm) and objects touching the image border were discarded. An adaptive background thresholding method was used with automatic smoothing and a threshold correction factor of 1.0. Clumped objects were distinguished based on intensity using the automatic methods to calculate the smoothing filter and minimum distance between local maxima. An illustration of the nucleus identification process is shown in Fig. 5.1.

The object intensity was determined using the "MeasureObjectIntensity" module and the results exported. This analysis was performed on all images for each treatment condition. The reported results provide the number of nuclei identified, the average signal intensity per nuclei and the standard deviation for the nuclear signal intensity per image. In order to convert the standard deviation for the nuclei from each image into a standard deviation for nuclei from all images in a given treatment group, we applied equation 5.1,[133] where s is the standard deviation for the combined group, n_x and n_y are the number of nuclei in group x and group y, s_x and s_y are the standard deviations for group x and group y, and $\overline{X}$ and $\overline{Y}$ are the mean nuclear signal for groups x and y, respectively. Equation 5.1 was applied serially to combined results from each image until results from each image for a given treatment condition was applied. The final standard deviation is used for the error bars in the reported results.

$$s^2 = \frac{n_x^2 s_x^2 + n_y^2 s_y^2 - n_y s_x^2 - n_y s_y^2 - n_x s_x^2 - n_x s_y^2 + n_y n_x s_x^2 + n_y n_x s_y^2 + n_x n_y \left(\overline{X} - \overline{Y}\right)^2}{\left(n_x + n_y - 1\right)\left(n_x + n_y\right)} \tag{5.1}$$

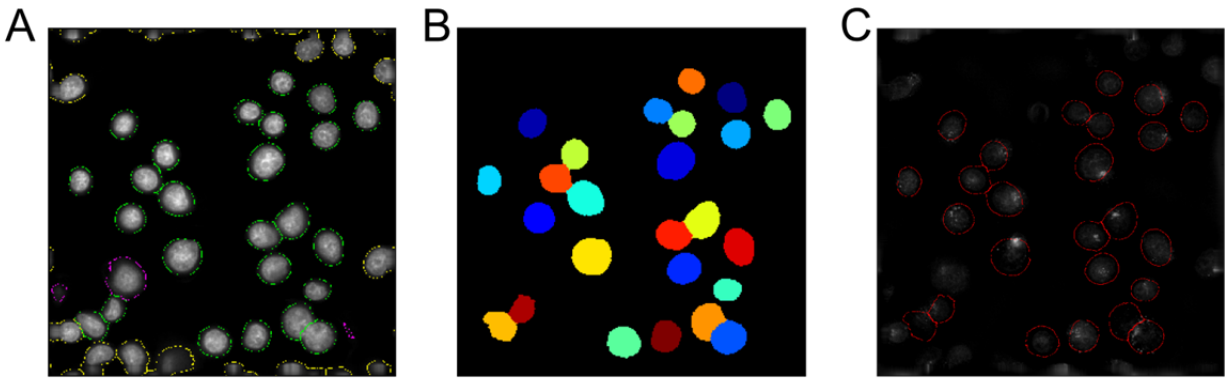

Figure 5.1 Example of nucleus identification process using CellProfiler. (A) Identification of cell nuclei based on Hoescht 33342 staining. The green outlines correspond to objects that were included in the final analysis. The yellow outlines are objects that were discarded because they border the image edge. The pink outlines are objects that were discarded based on size. (B) Display of all acceptable identified objects. (C) Overlay of identified objects (outlines shown in red) with the doxorubicin signal. This example uses a representative image of cells treated with 40 nM free doxorubicin.

5.4 Results

In order to determine whether it is theoretically possible to deliver the requisite 4-12 million doxorubicin molecules per cell[33] required to inhibit cell proliferation, we used our previously established model for ADC cellular processing[76] and measured each parameter for Tras-Dox. As shown in Fig. 5.2A, the equilibrium dissociation constant, $K_{D,}$ measured for Tras-Dox was 17 ± 2 pM, which is similar to what we measured before with Tras-647.[76] The net internalization rate constant, k_e, was 0.06 ± 0.02 h^{-1} as fit from Fig. 5.2B. In addition, the degradation rate constant, k_{deg}, for Tras-Dox was 0.04 ± 0.02 h^{-1}, as shown in Fig. 5.2C. These processing rates are similar to those previously measured for T-DM1, which is not surprising because the antibody component and linker are the same.

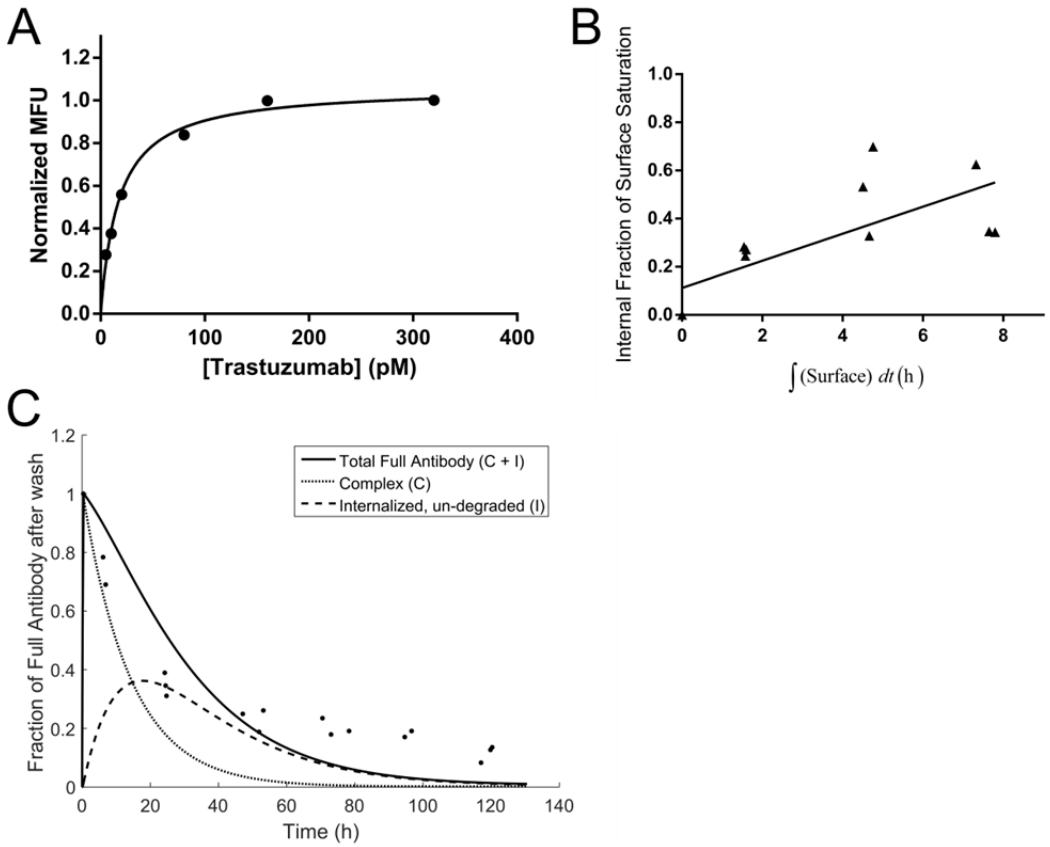

Figure 5.2 Parameter fits for cellular processing of Tras-Dox. (A) K_d fit, (B) Net internalization rate constant, k_e, fit, and (C) Degradation rate constant, k_{deg}, fit for SK-BR-3 cells.

Using the measured parameters for SK-BR-3 processing of Tras-Dox and the established ADC cellular processing model,[76] we predicted how many drug molecules would be delivered per cell as shown in Fig. 5.3. The base case includes binding, internalization, degradation, efflux, and dilution by cell growth. At steady state, drug uptake into the cell via the ADC internalization is balanced by dilution by cell growth and drug efflux from the cell. With the base case, the target of 4-12 million doxorubicin molecules[33] can barely be achieved at steady state. If there is no efflux of doxorubicin or no dilution by cell growth, a higher steady state number of drug molecules is achieved. However, if there is neither dilution by cell growth nor efflux, no steady state is achieved because there is only accumulation of drug and no loss of drug. Thus, the amount of drug within is a cell continues to increase over time. Note that Tras-Dox has a drug-to-antibody ratio (DAR) of 2. If an ADC was synthesized with the same processing kinetics, but a higher DAR, the number of drug molecules per cell would increase by the relative fold increase in the DAR.

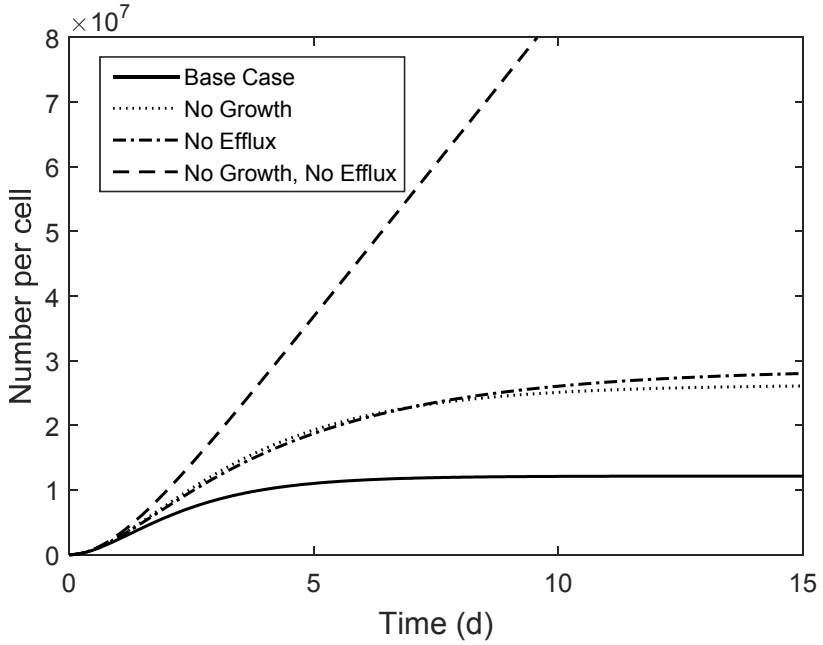

Figure 5.3 Predicted number of drug molecules delivered per cell via Tras-Dox.

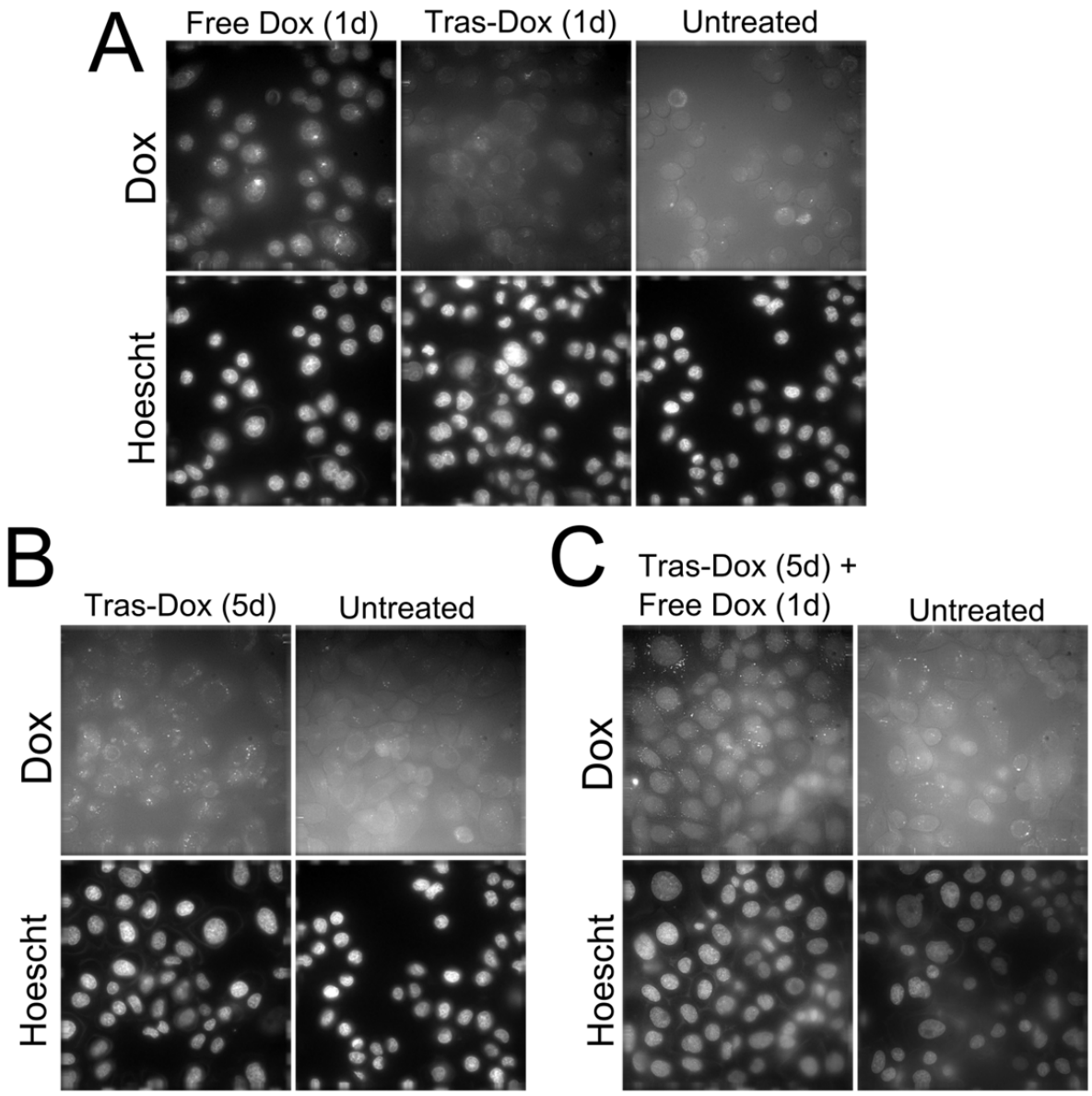

Figure 5.4 Fluorescence microscopy comparison of SK-BR-3 cells treated with free doxorubicin versus Tras-Dox on an equimolar doxorubicin basis. (A) Images of cells after one day of treatment of either 40 nM free doxorubicin, 20 nM Tras-Dox, or untreated. (B) Images of cells after 5 days of treatment with 20 nM Tras-Dox or untreated. (C) Images of cells after 5 days of treatment with 20 nM Tras-Dox followed by 1 day of treatment with 40 nM free doxorubicin or completely untreated. Images are representative of panels of images taken at each time point and treatment condition. Images from both the doxorubicin signal and Hoescht 33342 (nuclear stain) signal are shown for each time point.

As ADCs are internalized, they enter into endosomes/lysosomes, where the ADC is degraded, releasing the drug component from the antibody. The drug component must escape the lysosome before it can reach its intracellular target. The model used for Fig. 5.3 to predict the amount of doxorubicin delivered via Tras-Dox does not consider where within the cell the doxorubicin may be. We used fluorescence microscopy to observe where within the cell doxorubicin is delivered and if doxorubicin escapes the lysosome and makes it to its intracellular target, DNA in the cell nucleus.

In Fig. 5.4, we compare cells treated with free doxorubicin and Tras-Dox on an equimolar doxorubicin basis. The signal from the nuclear stain Hoescht 33342 is shown in the bottom panels and the signal from doxorubicin is shown in the upper panels. Fig. 5.4A illustrates what the drug distribution looks like when cells are treated for 1 day. When treated with free doxorubicin, the majority of the doxorubicin signal comes from the nucleus where doxorubicin binds the DNA. However, when treated with Tras-Dox for 1 day, we do not see the same distribution of doxorubicin to the nucleus. With only one day of treatment, it is not surprising that Tras-Dox does not deliver doxorubicin to its target, because the cellular processing (internalization and degradation) takes more than one day. However, even when cells are treated continuously for 5 days as shown in Fig. 5.4B, there is no significant accumulation of doxorubicin in the nucleus. To demonstrate the doxorubicin can in fact still get to the nucleus, we followed up 5 day treatment with Tras-Dox with a 1 day treatment of free doxorubicin as shown in Fig. 5.4C. Once the free doxorubicin is added, we do again see accumulation in the nucleus. The images shown in Fig. 5.4 are representative images. The doxorubicin signal in the nucleus was quantified from a panel of images for each treatment condition and summarized in Fig. 5.5. Only treatment with free doxorubicin resulted in significant accumulation of doxorubicin in the nucleus.

Based on the model predictions shown in Fig. 5.3, five days of treatment with Tras-Dox should result in close to the steady state amount of drug that could be delivered with Tras-Dox. To see whether we would see more accumulation of doxorubicin in the nucleus with longer treatment, we also treated cells continuously with Tras-Dox for 16 days. Even with this long length of treatment and replacement of the Tras-Dox in the media every two days, we did not see accumulation of doxorubicin in the nucleus.

In order to validate that Tras-Dox is actually binding cells and getting internalized, we used fluorescence microscopy with cells treated with Tras-Dox-647 as illustrated in Fig. 5.6. In Fig. 5.6A, we see most of the Alexa Fluor 647 signal comes from the cell surface because the Tras-Dox-647 has bound HER2 on the cell surface, but has not yet internalized. In Fig. 5.6B and 5.6C, we see over time that the Tras-Dox-647 does get internalized into the endosomes/lysosomes.

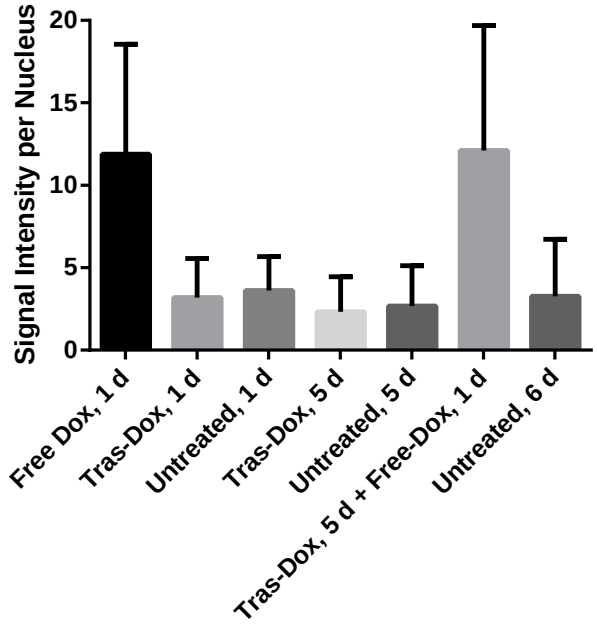

Figure 5.5 Quantification of doxorubicin signal in nuclei of cells treated with free doxorubicin (Free Dox) or Tras-Dox. The error bars represent the standard deviation of the mean signal intensity for all nuclei measured across multiple images for each treatment group.

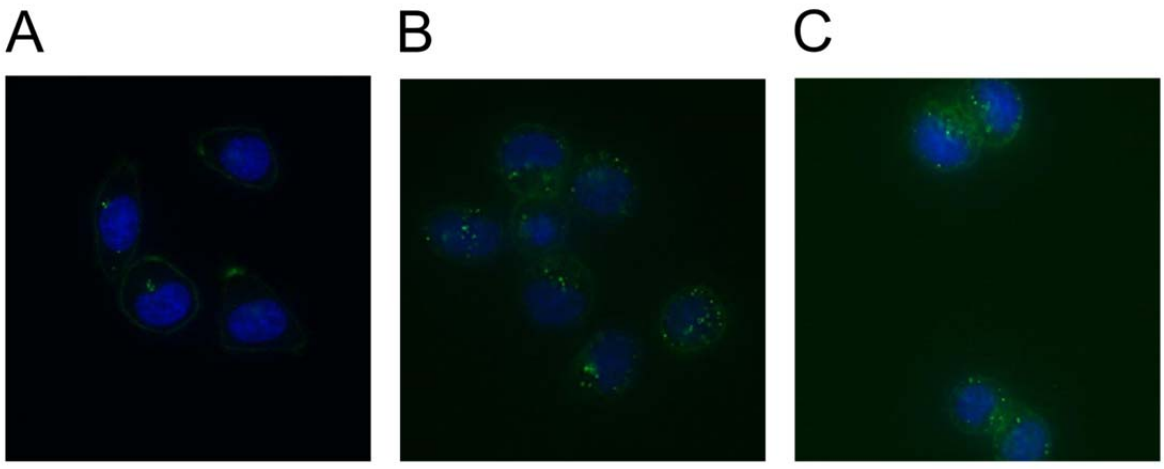

Figure 5.6 Images of cells treated with Tras-Dox-647 for (A) 6 h, (B) 24 h, and (C) 50 h. Blue is the signal from Hoescht 33342, the nuclear stain, and green is the signal from Alexa Fluor 647.

In order to determine our lower level of detection threshold, we treated cells for 24 h with free doxorubicin with a range of doxorubicin media concentrations as illustrated in Fig. 5.7. At 20 nM doxorubicin media concentration, we could still see distinct localization of signal from the nucleus. However, at 5 nM doxorubicin media concentration, the signal was distributed throughout cells, suggesting that the signal we were detecting is just background cell autofluorescence. Combined with previous work,[33] these results indicate that less than ~ 10^6 – 10^7 doxorubicin molecules in the nucleus may not be visible over the background signal.

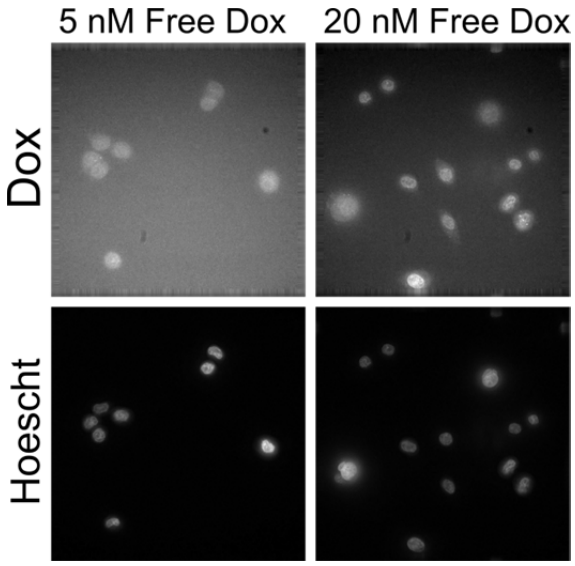

Figure 5.7 Evaluation of detection limit for doxorubicin in cell nucleus.

To overcome the dimness of doxorubicin's fluorescence, we tried a different approach based on the femtomolar fluorescein binder 4m5.3.[134] We generated an IgG-scFv bispecific construct based on previous topologies[135] with two 4m5.3 scFvs on the C-terminus of either the heavy or light chain of Trastuzumab. DNA sequences for these constructs are shown in Appendix A. The aim with these constructs was to use 4m5.3 binding of fluorescein to deliver the commercially available fluorescein conjugated drug, fluorescein-phalloidin, to the lysosomes of cells. Once the fluorescein-drug is delivered to the lysosome and released from 4m5.3, we could study the rate of lysosomal escape and target binding of the fluorescein-drug using fluorescence microcopy.

There are a few factors that made interpretation of images from these types of experiments difficult, including that fluorescein is quenched 95% upon 4m5.3 binding[134] and that

fluorescein is quenched in acidic conditions.[136] In addition, the target of fluorescein-phalloidin is actin, which can be distributed throughout a cell, making quantification of target binding more difficult than the drug in the nucleus for example. With these experiments, we also observed that it was necessary to use live cells for imaging rather than fixed cells because the fixation and permeablization procedures distributed fluorescein-phalloidin throughout the cells and did not preserve the original distribution. Because of these factors, we were unable to obtain conclusive results from this approach to measure the rate of lysosomal escape and target binding.

5.5. Discussion

As a general rule of thumb, it is assumed that a highly potent drug (sub-nanomolar IC_{50}) is required to have an effective ADC.[4,26,78] The results from this work suggest that one of the reasons you need a highly potent drug is because the escape of the drug payload from endosomal/lysosomal compartments is inefficient. If only a few drug molecules escape the lysosome, these molecules must be highly potent to result in effective cell killing. Inefficiency of drug escape from endosomal/lysosomal compartments has also been observed with other drug delivery systems such as nanoparticles and liposomes.[137–139] Previous studies suggest that about one in every million molecules escapes the endosomes/ lysosomes, as shown for the escape of the toxin Gelonin.[140]

Although doxorubicin is naturally fluorescent, it should be noted that doxorubicin is not as bright as commercially available fluorophores. During the course of this work, we ran into issues with the signal to noise ratio for the fluorescence of doxorubicin. The threshold for the number of doxorubicin molecules below which are not visible was higher than desirable. We chose to use doxorubicin since we could track the drug component itself based on doxorubicin's fluorescence. Alternatively, a fluorophore could be conjugated to the drug in order to make a fluorophore analogue. However, the addition of this fluorophore likely disturbs how the drug or drug metabolite traffics through the cell and its ability to escape the lysosome as well as the drug's potency. Fluorescently labeling the antibody component is a useful tool to track the ADC trafficking before the ADC is degraded, but is less useful once the ADC is degraded and trafficking of the drug component is no longer associated with trafficking of the fluorophore.

We expect that escape from endosomes and lysosomes occurs via both active transport and passive diffusion and is likely highly dependent on the chemical structure of the drug and linker used. Depending on the linker type used, the active drug catabolite might be just the drug, the drug plus a residual fraction of the linker, or in the case of non-cleavable linkers, the active catabolite is the drug, linker and the residual amino acid that was used for conjugation. Transport and diffusion properties likely differ depending on these differences in linker design. Differences based on linker choice in the ability of a drug catabolite to diffuse across a cell membrane and result in bystander killing have been demonstrated before.[28]

The design of an optimal linker results is selective linker degradation and release of drug only in the tumor. Ideally, a linker is quite stable during systemic circulation, but once the ADC reaches the tumor and is internalized, it quickly releases the drug. Previous work has established that lysosomal degradation is required to generate the active drug metabolite for certain linker types.[28,129] However, minimal work has been published describing how a drug or drug catabolite escapes the lysosome once delivered via an ADC.

In conclusion, the ability of the active drug catabolite from an ADC to escape from the endosomal /lysosomal compartments should be considered when designing an ADC. When comparing treatment with an equimolar dose of free doxorubicin versus a doxorubicin ADC (Tras-Dox), we observed that the free doxorubicin effectively accumulated in the nucleus, its intracellular target, whereas the Tras-Dox did not, suggesting that intracellular processing limits the efficacy of ADCs.

Chapter 6: Conclusions

In this thesis, we have explored how antibody drug conjugates get processed at a cellular level and developed a framework to understand how changes in ADC design affect how much drug gets to its target inside a tumor cell.

First, we described the development of a flow cytometric clonogenic assay and the application of this assay to determine doxorubicin's single cell potency. We found for the case of doxorubicin, a cell's ability to proliferate is only a function of the amount of drug inside the cell and is independent of the media drug concentration, length of treatment time, and treatment with the Pgp inhibitor, verapamil. The single-cell IC_{50} for doxorubicin is 4 – 12 million doxorubicin molecules. The developed flow cytometric clonogenic assay could be generalized for use with a fluorescent analogue of a drug or a fluorescently-labeled drug delivery system. We have applied this assay for use with fluorescently labeled antibody drug conjugates with mixed results.

When characterizing the potency of a drug for the potential use in an ADC, it is especially important to consider the potency on a single cell basis rather than the media drug concentration. The ability of a drug to cross cell membranes (based on the drug's permeability) will influence a drug's potency when measured on a media drug concentration. However, in the case of an ADC, the drug is carried across the cell membrane via internalization of the antibody. Understanding the number of drug molecules required to be delivered to any individual tumor cell gives a quantitative target for ADC delivery and can be a useful metric for determining if delivery of the required amount of drug is theoretically feasible.

Ten million drug molecules is a high target to achieve with an ADC. However, we've demonstrated that this number is theoretically possible with a Trastuzumab-Doxorubicin ADC. Using the clinically relevant ADC T-DM1, we measured half-lives for internalization of 6 – 14 h, degradation of 18 – 25 h, and efflux rate of 44 – 73 h. In addition, we established that the amount of drug delivered to a cell via an ADC at steady state depends on the amount of drug internalized (the product of the antigen expression level and the net internalization rate constant) and the amount of drug effluxed from the cell. In the case of a Trastuzumab ADC, the amount that gets internalized is towards the high end since HER2 has extremely high expression levels (~3 million HER2 per cell) and relatively rapid internalization ($t_{1/2}$ ~ 10 h).

The cellular level processing of ADCs can be incorporated into a larger PK/PD model as demonstrated with the model developed in collaboration with Aman Singh and Dhaval Shah at the University of Buffalo. In this model, the drug component could enter cells via two pathways: (1) receptor-mediated internalization and degradation as classically described for ADCs, and (2) passive diffusion of the drug into a cell after is has been released from the antibody in the tumor extracellular space via instability or non-specific deconjugation. The results with this model suggest that the amount of drug bound to its intracellular target depend on the drug target binding kinetics (target binding provides a sink to prevent drug efflux from the cell) as well as terms associated with both pathways for a drug to enter a cell. As noted with the pathway analysis when comparing *in vitro* versus *in vivo*, the passive diffusion of drug into a cell plays a much bigger role in *in vitro* studies whereas *in vivo*, free drug in the extracellular space is cleared more rapidly. This could be one explanation why *in vitro* studies with ADCs have had inconsistency in correlating with *in vivo* results.

It should be noted that the sensitivity analyses performed in this work were all local sensitivity analyses around the parameter values determined for these systems. Large changes in any of the parameters could dramatically affect which rates are the rate-limiting steps for a particular ADC.

Alternative methods to measure the cellular processing rates include mass spectrometry or the use of radiolabels. Mass spectrometry has the advantage that you can clearly distinguish relevant catabolites of the ADC; however, obtaining enough of the right species for calibration can be difficult. Radiolabels have the advantage of having very low background signals; however, they are more expensive and require more intensive safety precautions.

Once the drug payload is released from its antibody component, it must escape the endosomal/lysosomal compartment before it can reach its intracellular target. Our work with Tras-Dox demonstrates that the intracellular processing of ADCs can limit the efficient delivery of drug to its cellular target as compared to the free drug. Minimal work has been published on how a drug catabolite from an ADC leaves the endosomal/lysosomal compartment. We hypothesize that both passive diffusion across the lysosomal membrane and active transport contribute to a drug's ability to escape from endosomes and lysosomes. One potential approach to study drug accumulation and escape from lysosomes is with isolation of lysosomes via ultracentrifugation.

One future direction that would be very useful is to test the cellular processing rates for a number of different ADCs in order to make conclusions about how changes in ADC design (such as linker selection, drug conjugation site, etc.) affect the ADC cellular processing rates. The results of the work presented here point to characteristics about an ADC that should be measured when designing and selecting an ADC; however, we have not gone so far as to say how you could modify an ADC's design to improve various characteristics. Our difficulty in synthesizing our own ADCs in-house exemplifies the complexities involved with ADC synthesis. Expertise in small molecule chemical synthesis and purification as well as antibody production, purification, and conjugation are necessary.

Overall, ADCs are a unique type of cancer therapeutic, which aims to reduce the systemic toxicity of chemotherapeutic drugs using the tumor targeting specificity of antibodies. ADCs are a very active area of research and development in the pharmaceutical/biotechnology industry. However, there is still much to be learned about how ADCs get processed inside tumor cells. Elucidating how ADC design choices (such as linker design, drug payload, antibody target, etc.) affect how efficacious an ADC is (i.e. how much tumor cell killing results from treatment with the ADC) will help make ADC design more rational and improve the ADCs being developed.

References

1. Heron, M. Deaths: Leading Causes for 2012. *Natl. Vital Stat. Reports* **64,** 1–94 (2015).
2. Schrama, D., Reisfeld, R. A. & Becker, J. C. Antibody targeted drugs as cancer therapeutics. *Nat. Rev. Drug Discov.* **5,** 147–59 (2006).
3. Vanneman, M. & Dranoff, G. Combining immunotherapy and targeted therapies in cancer treatment. *Nat. Rev. Cancer* **12,** 237–51 (2012).
4. Carter, P. J. & Senter, P. D. Antibody-drug conjugates for cancer therapy. *Cancer J.* **14,** 154–69 (2008).
5. Luciani, F. *et al.* Effect of proton pump inhibitor pretreatment on resistance of solid tumors to cytotoxic drugs. *J. Natl. Cancer Inst.* **96,** 1702–13 (2004).
6. Teicher, B. a. Antibody-drug conjugate targets. *Curr. Cancer Drug Targets* **9,** 982–1004 (2009).
7. Tijink, B. M. *et al.* A phase I dose escalation study with anti-CD44v6 bivatuzumab mertansine in patients with incurable squamous cell carcinoma of the head and neck or esophagus. *Clin. Cancer Res.* **12,** 6064–72 (2006).
8. Tolcher, a W. *et al.* Randomized phase II study of BR96-doxorubicin conjugate in patients with metastatic breast cancer. *J. Clin. Oncol.* **17,** 478–84 (1999).
9. Schmidt, M. M., Thurber, G. M. & Wittrup, K. D. Kinetics of anti-carcinoembryonic antigen antibody internalization: effects of affinity, bivalency, and stability. *Cancer Immunol. Immunother.* **57,** 1879–90 (2008).
10. Perrino, E. *et al.* Curative properties of non-internalizing antibody-drug conjugates based on maytansinoids. *Cancer Res.* (2014). doi:10.1158/0008-5472.CAN-13-2990
11. Kovtun, Y. V & Goldmacher, V. S. Cell killing by antibody-drug conjugates. *Cancer Lett.* **255,** 232–40 (2007).
12. Kovtun, Y. V *et al.* Antibody-drug conjugates designed to eradicate tumors with homogeneous and heterogeneous expression of the target antigen. *Cancer Res.* **66,** 3214–21 (2006).
13. Zimmerman, E. S. *et al.* Production of Site-Speci fi c Antibody − Drug Conjugates Using Optimized Non-Natural Amino Acids in a Cell-Free Expression System. (2014).
14. Wang, L., Amphlett, G., Bla, W. A., Lambert, J. M. & Zhang, W. E. I. Structural characterization of the maytansinoid – monoclonal antibody immunoconjugate , huN901 – DM1 , by mass spectrometry. 2436–2446 (2005). doi:10.1110/ps.051478705.therapeutic
15. Hamblett, K. J. *et al.* Effects of drug loading on the antitumor activity of a monoclonal antibody drug conjugate. *Clin. Cancer Res.* **10,** 7063–70 (2004).
16. Lyon, R. P., Meyer, D. L., Setter, J. R. & Senter, P. D. *Conjugation of Anticancer Drugs Through Endogenous Monoclonal Antibody Cysteine Residues. Methods Enzymol.* **502C,** (Elsevier Inc., 2012).
17. Junutula, J. R. *et al.* Site-specific conjugation of a cytotoxic drug to an antibody improves the therapeutic index. *Nat. Biotechnol.* **26,** 925–32 (2008).
18. Shen, B. *et al.* Conjugation site modulates the in vivo stability and therapeutic activity of antibody-drug conjugates. *Nat. Biotechnol.* **30,** 184–9 (2012).
19. Senter, P. D. & Sievers, E. L. The discovery and development of brentuximab vedotin for use in relapsed Hodgkin lymphoma and systemic anaplastic large cell lymphoma. *Nat. Biotechnol.* **30,** 631–7 (2012).

20. Scott, A. M., Wolchok, J. D. & Old, L. J. Antibody therapy of cancer. *Nat. Rev. Cancer* **12,** 278–87 (2012).
21. Trail, P. a, King, H. D. & Dubowchik, G. M. Monoclonal antibody drug immunoconjugates for targeted treatment of cancer. *Cancer Immunol. Immunother.* **52,** 328–37 (2003).
22. Sarmay, G., Lund, J., Rozsnyay, Z., Gergely, J. & Jefferis, R. Mapping and comparison of the interaction sites on the Fc region of IgG responsible for triggering antibody dependent cellular cytotoxicity (ADCC) through different types of human Fc gamma receptor. *Mol. Immunol.* **29,** 633–9 (1992).
23. Dall'Acqua, W. Modulation of the effector functions of a human IgG1 through engineering of its hinge region. *J.* … (2006). at <http://www.jimmunol.org/content/177/2/1129.short>
24. Ritchie, M., Tchistiakova, L. & Scott, N. Implications of receptor-mediated endocytosis and intracellular trafficking dynamics in the development of antibody drug conjugates. *MAbs* **5,** 1–9 (2013).
25. Chari, R. V. J. Targeted cancer therapy: conferring specificity to cytotoxic drugs. *Acc. Chem. Res.* **41,** 98–107 (2008).
26. Ducry, L. & Stump, B. Antibody-drug conjugates: linking cytotoxic payloads to monoclonal antibodies. *Bioconjug. Chem.* **21,** 5–13 (2010).
27. Doronina, S. O. *et al.* Development of potent monoclonal antibody auristatin conjugates for cancer therapy. *Nat. Biotechnol.* **21,** 778–84 (2003).
28. Erickson, H. K. *et al.* Antibody-maytansinoid conjugates are activated in targeted cancer cells by lysosomal degradation and linker-dependent intracellular processing. *Cancer Res.* **66,** 4426–33 (2006).
29. Wang, J., Shen, W.-C. & Zaro, J. L. *Antibody-Drug Conjugates*. (2015).
30. Waller, E. Brentuximab Vedotin CD30-Directed Therapy for Hodgkin Lymphoma Oncologic Drugs Advisory Committee Brentuximab Vedotin Hodgkin Lymphoma Introduction. (2011).
31. LoRusso, P. M., Weiss, D., Guardino, E., Girish, S. & Sliwkowski, M. X. Trastuzumab emtansine: a unique antibody-drug conjugate in development for human epidermal growth factor receptor 2-positive cancer. *Clin. Cancer Res.* **17,** 6437–47 (2011).
32. Burris, H. a, Tibbitts, J., Holden, S. N., Sliwkowski, M. X. & Lewis Phillips, G. D. Trastuzumab emtansine (T-DM1): a novel agent for targeting HER2+ breast cancer. *Clin. Breast Cancer* **11,** 275–82 (2011).
33. Maass, K. F. *et al.* A Flow Cytometric Clonogenic Assay Reveals the Single-Cell Potency of Doxorubicin. *J. Pharm. Sci.* n/a–n/a (2015). doi:10.1002/jps.24631
34. Fotakis, G. & Timbrell, J. a. In vitro cytotoxicity assays: comparison of LDH, neutral red, MTT and protein assay in hepatoma cell lines following exposure to cadmium chloride. *Toxicol. Lett.* **160,** 171–7 (2006).
35. Weyermann, J., Lochmann, D. & Zimmer, A. A practical note on the use of cytotoxicity assays. *Int. J. Pharm.* **288,** 369–76 (2005).
36. Gottesman, M. M. Mechanisms of cancer drug resistance. *Annu. Rev. Med.* **53,** 615–627 (2002).
37. Pirie, C. M., Hackel, B. J., Rosenblum, M. G. & Wittrup, K. D. Convergent potency of internalized gelonin immunotoxins across varied cell lines, antigens, and targeting moieties. *J. Biol. Chem.* **286,** 4165–72 (2011).
38. Sundman-Engberg, B., Tidefelt, U., Liliemark, J. & Paul, C. Intracellular concentrations of anti cancer drugs in leukemic cells in vitro vs in vivo. *Cancer Chemother.* … 252–256 (1990).

39. Eliaz, R. E. Determination and Modeling of Kinetics of Cancer Cell Killing by Doxorubicin and Doxorubicin Encapsulated in Targeted Liposomes. *Cancer Res.* **64,** 711–718 (2004).
40. Sumantran, V. N. Cellular chemosensitivity assays: An overview. *Methods Mol. Biol.* **731,** 219–236 (2011).
41. Franken, N., Rodermond, H. & Stap, J. Clonogenic assay of cells in vitro. *Nat. Protoc.* **1,** 2315–2319 (2006).
42. Minotti, G., Menna, P., Salvatorelli, E., Cairo, G. & Gianni, L. Anthracyclines : Molecular Advances and Pharmacologic Developments in Antitumor Activity and Cardiotoxicity. **56,** 185–229 (2004).
43. Karukstis, K. & Thompson, E. Deciphering the fluorescence signature of daunomycin and doxorubicin. *Biophys.* … **73,** 249–263 (1998).
44. Saltiel, E. & McGuire, W. Doxorubicin (Adriamycin) Cardiomyopathy—A Critical Review. *West. J. Med.* **139,** 332–341 (1983).
45. Bénard, J. *et al.* Characterization of a Human Ovarian Adenocarcinoma Line , IGROV1 , in Tissue Culture and in Nude Mice Characterization of a Human Ovarian Adenocarcinoma Line , IGROV1 , in Tissue Culture and in Nude Mice1. *Cancer R* **45,** 4970–4979 (1985).
46. Chen, Q. & Gabathuler, R. Efficient Synthesis of Doxorubicin Melanotransferrin p97 Conjugates Through SMCC Linker. *Synth. Commun.* **34,** 2407–2414 (2004).
47. Holliday, D. L. & Speirs, V. Choosing the right cell line for breast cancer research. *Breast Cancer Res.* **13,** 215 (2011).
48. Spencer, S. L., Gaudet, S., Albeck, J. G., Burke, J. M. & Sorger, P. K. Non-genetic origins of cell-to-cell variability in TRAIL-induced apoptosis. *Nature* **459,** 428–432 (2009).
49. Gottesman, M. & Pastan, I. Biochemistry of multidrug resistance mediated by the multidrug transporter. *Annu. Rev. Biochem.* **62,** 385–427 (1993).
50. Shen, F. *et al.* Quantitation of Doxorubicin Uptake , Efflux , and Modulation of Multidrug Resistance (MDR) in MDR Human Cancer Cells. *Pharmacology* **324,** 95–102 (2008).
51. Lai, G.-M., Chen, Y.-N., Mickley, L. a., Fojo, A. T. & Bates, S. E. P-glycoprotein expression and schedule dependence of adriamycin cytotoxicity in human colon carcinoma cell lines. *Int. J. Cancer* **49,** 696–703 (1991).
52. Durand, R. & Olive, P. Flow cytometry studies of intracellular adriamycin in single cells in vitro. *Cancer Res.* **41,** 3489–3494 (1981).
53. El-Kareh, A. W. & Secomb, T. W. Two-Mechanism Peak Concentration Model for Cellular Pharmacodynamics of Doxorubicin. *Neoplasia* **7,** 705–713 (2005).
54. Kerr, D. J., Kerr, a M., Freshney, R. I. & Kaye, S. B. Comparative intracellular uptake of adriamycin and 4'-deoxydoxorubicin by non-small cell lung tumor cells in culture and its relationship to cell survival. *Biochem. Pharmacol.* **35,** 2817–23 (1986).
55. Praet, M., Stryckmans, P. & Ruysschaert, J. Cellular uptake, cytotoxicity, and transport kinetics of anthracyclines in human sensitive and multidrug-resistant K562 cells. *Biochem. Pharmacol.* **51,** 1341–1348 (1996).
56. Yu, T., Xiong, Z., Chen, S. & Tu, G. The use of models in 'target' theory to evaluate the survival curves of human ovarian carcinoma cell line exposure to adriamycin combined with ultrasound. *Ultrason. Sonochem.* **12,** 345–8 (2005).

57. Tarasiuk, J., Frézard, F., Garnier-Suillerot, a & Gattegno, L. Anthracycline incorporation in human lymphocytes. Kinetics of uptake and nuclear concentration. *Biochim. Biophys. Acta* **1013,** 109–17 (1989).
58. A Brief Guide to Genomics. *April 14, 2014* at <http://www.genome.gov/18016863>
59. Fiallo, M. & Laigle, A. Accumulation of degradation products of doxorubicin and pirarubicin formed in cell culture medium within sensitive and resistant cells. *Biochem. …* **45,** 659–665 (1993).
60. Hajian, R., Shams, N. & Mohagheghian, M. Study on the interaction between doxorubicin and Deoxyribonucleic acid with the use of methylene blue as a probe. *J. Braz. Chem. Soc.* **20,** 1399–1405 (2009).
61. Hovorka, O. *et al.* Spectral analysis of doxorubicin accumulation and the indirect quantification of its DNA intercalation. *Eur. J. Pharm. Biopharm.* **76,** 514–24 (2010).
62. Smith, D. a, Di, L. & Kerns, E. H. The effect of plasma protein binding on in vivo efficacy: misconceptions in drug discovery. *Nat. Rev. Drug Discov.* **9,** 929–939 (2010).
63. Law, V. *et al.* DrugBank 4.0: Shedding new light on drug metabolism. *Nucleic Acids Res.* **42,** 1091–1097 (2014).
64. Zhang, F., Xue, J., Shao, J. & Jia, L. Compilation of 222 drugs' plasma protein binding data and guidance for study designs. *Drug Discov. Today* **17,** 475–485 (2012).
65. Mateus, a, Matsson, P. & Artursson, P. Rapid measurement of intracellular unbound drug concentrations. *Mol. Pharm.* (2013). at <http://pubs.acs.org/doi/abs/10.1021/mp4000822>
66. Greene, R. F., Collins, J. M., Jenkins, J. F., Speyer, J. L. & Myers, C. E. Plasma Pharmacokinetics of Adriamycin and Adriamycinol : Implications for the Design of in Vitro Experiments and Treatment Protocols Plasma Pharmacokinetics of Adriamycin and Adriamycinol : Implications for the Design of in Vitro Experiments and Treatment. 3417–3421 (1983).
67. Anderson, A. B., Gergen, J. & Arriaga, E. a. Detection of doxorubicin and metabolites in cell extracts and in single cells by capillary electrophoresis with laser-induced fluorescence detection. *J. Chromatogr. B. Analyt. Technol. Biomed. Life Sci.* **769,** 97–106 (2002).
68. Deng, B. *et al.* Analysis of doxorubicin uptake in single human leukemia K562 cells using capillary electrophoresis coupled with laser-induced fluorescence detection. *Anal. Bioanal. Chem.* **401,** 2143–52 (2011).
69. Eichholtz-Wirth, H. Dependence of the cytostatic effect of adriamycin on drug concenration and exposure time in vitro. *Br. J. Cancer* 886–891 (1980).
70. Sakai-Kato, K., Saito, E., Ishikura, K. & Kawanishi, T. Analysis of intracellular doxorubicin and its metabolites by ultra-high-performance liquid chromatography. *J. Chromatogr. B. Analyt. Technol. Biomed. Life Sci.* **878,** 1466–70 (2010).
71. Xiong, G., Chen, Y. & Arriaga, E. a. Measuring the doxorubicin content of single nuclei by micellar electrokinetic capillary chromatography with laser-induced fluorescence detection. *Anal. Chem.* **77,** 3488–93 (2005).
72. Adair, J. R., Howard, P. W., Hartley, J. a, Williams, D. G. & Chester, K. a. Antibody-drug conjugates - a perfect synergy. *Expert Opin. Biol. Ther.* **12,** 1191–206 (2012).
73. Alley, S. C., Okeley, N. M. & Senter, P. D. Antibody-drug conjugates: targeted drug delivery for cancer. *Curr. Opin. Chem. Biol.* **14,** 529–37 (2010).
74. Thurber, G. M. *et al.* Single-cell and subcellular pharmacokinetic imaging allows insight into drug action in vivo. *Nat. Commun.* **4,** 1504 (2013).

75. Yang, J., Chen, H., Vlahov, I. R., Cheng, J.-X. & Low, P. S. Evaluation of disulfide reduction during receptor-mediated endocytosis by using FRET imaging. *Proc. Natl. Acad. Sci. U. S. A.* **103,** 13872–7 (2006).
76. Maass, K. F., Kulkarni, C., Betts, A. & Wittrup, K. D. Determination of Cellular Processing Rates for a Trastuzumab-Maytansinoid Antibody-Drug Conjugate (ADC) Points to Key Parameters for ADC Design. *(In Prep.*
77. Zolot, R. S., Basu, S. & Million, R. P. Antibody–drug conjugates. *Nat. Rev. Drug Discov.* **12,** 259–260 (2013).
78. Panowski, S., Bhakta, S., Raab, H., Polakis, P. & Junutula, J. R. Site-specific antibody drug conjugates for cancer therapy. *MAbs* **6,** 34–45 (2014).
79. McCombs, J. R. & Owen, S. C. Antibody Drug Conjugates: Design and Selection of Linker, Payload and Conjugation Chemistry. *AAPS J.* (2015). doi:10.1208/s12248-014-9710-8
80. Barok, M., Joensuu, H. & Isola, J. Trastuzumab emtansine: mechanisms of action and drug resistance. *Breast Cancer Res.* **16,** 209 (2014).
81. Wada, R. *et al.* Mechanistic pharmacokinetic/pharmacodynamic modeling of in vivo tumor uptake, catabolism, and tumor response of trastuzumab maytansinoid conjugates. *Cancer Chemother. Pharmacol.* **74,** 969–980 (2014).
82. Erickson, H. K. *et al.* The effect of different linkers on target cell catabolism and pharmacokinetics/pharmacodynamics of trastuzumab maytansinoid conjugates. *Mol. Cancer Ther.* **11,** 1133–42 (2012).
83. Jumbe, N. L. *et al.* Modeling the efficacy of trastuzumab-DM1, an antibody drug conjugate, in mice. *J. Pharmacokinet. Pharmacodyn.* **37,** 221–42 (2010).
84. Chudasama, V. L. *et al.* Semi-mechanistic population pharmacokinetic model of multivalent trastuzumab emtansine in patients with metastatic breast cancer. *Clin. Pharmacol. Ther.* **92,** 520–7 (2012).
85. Lu, D. *et al.* An integrated multiple-analyte pharmacokinetic model to characterize trastuzumab emtansine (T-DM1) clearance pathways and to evaluate reduced pharmacokinetic sampling in patients with HER2-positive metastatic breast cancer. *Clin. Pharmacokinet.* **52,** 657–672 (2013).
86. Girish, S. *et al.* Clinical pharmacology of trastuzumab emtansine (T-DM1): An antibody-drug conjugate in development for the treatment of HER2-positive cancer. *Cancer Chemother. Pharmacol.* **69,** 1229–1240 (2012).
87. Chari, R. V. J. *et al.* Immunoconjugates Containing Novel Maytansinoids : Promising Anticancer Drugs. *Cancer Res.* **52,** 127–131 (1992).
88. Loganzo, F. *et al.* Tumor Cells Chronically Treated with a Trastuzumab-Maytansinoid Antibody-Drug Conjugate Develop Varied Resistance Mechanisms but Respond to Alternate Treatments. *Mol. Cancer Ther.* **14,** 952–964 (2015).
89. Linderman, J. & Lauffenburger, D. *Receptors: Models for Binding, Trafficking, and Signaling*. (Oxford University Press, 1993).
90. Lund, K. A., Opresko, L. K., Starbuck, C., Walsh, B. J. & Wiley, H. S. Quantitative analysis of the endocytic system involved in hormone-induced receptor internalization. *J. Biol. Chem.* (1990).
91. Harper, J., Mao, S., Strout, P. & Kamal, A. in *Methods Mol. Biol.* (Ducry, L.) **1045,** 41–49 (Humana Press, 2013).

92. Lopus, M. *et al.* Maytansine and cellular metabolites of antibody-maytansinoid conjugates strongly suppress microtubule dynamics by binding to microtubules. *Mol. Cancer Ther.* **9,** 2689–99 (2010).
93. Shah, D. K., Haddish-Berhane, N. & Betts, A. Bench to bedside translation of antibody drug conjugates using a multiscale mechanistic PK/PD model: a case study with brentuximab-vedotin. *J. Pharmacokinet. Pharmacodyn.* **39,** 643–59 (2012).
94. Rusnak, D. W. *et al.* Assessment of epidermal growth factor receptor (EGFR, ErbB1) and HER2 (ErbB2) protein expression levels and response to lapatinib (Tykerb, GW572016) in an expanded panel of human normal and tumour cell lines. *Cell Prolif.* **40,** 580–94 (2007).
95. Hendriks, B. S. *et al.* Impact of tumor HER2/ERBB2 expression level on HER2-targeted liposomal doxorubicin-mediated drug delivery: multiple low-affinity interactions lead to a threshold effect. *Mol. Cancer Ther.* **12,** 1816–28 (2013).
96. Pillow, T. H. *et al.* Site-Speci fi c Trastuzumab Maytansinoid Antibody − Drug Conjugates with Improved Therapeutic Activity through Linker and Antibody Engineering. (2014).
97. Austin, C. D. *et al.* Endocytosis and Sorting of ErbB2 and the Site of Action of Cancer Therapeutics Trastuzumab and Geldanamycin. *Mol. Biol. Cell* **15,** 5268–5282 (2004).
98. Lewis Phillips, G. D. *et al.* Targeting HER2-positive breast cancer with trastuzumab-DM1, an antibody-cytotoxic drug conjugate. *Cancer Res.* **68,** 9280–90 (2008).
99. Rodríguez, A., Webster, P., Ortego, J. & Andrews, N. W. Lysosomes behave as Ca2+-regulated exocytic vesicles in fibroblasts and epithelial cells. *J. Cell Biol.* **137,** 93–104 (1997).
100. Safaei, R. *et al.* Abnormal lysosomal trafficking and enhanced exosomal export of cisplatin in drug-resistant human ovarian carcinoma cells. *Mol. Cancer Ther.* **4,** 1595–1604 (2005).
101. Federici, C. *et al.* Exosome release and low pH belong to a framework of resistance of human melanoma cells to cisplatin. *PLoS One* **9,** (2014).
102. Brinton, L. T., Sloane, H. S., Kester, M. & Kelly, K. a. Formation and role of exosomes in cancer. *Cell. Mol. Life Sci.* **72,** 659–671 (2014).
103. Cilliers, C., Liao, J., Atangcho, L. & Thurber, G. M. Residualization Rates of Near-Infrared Dyes for the Rational Design of Molecular Imaging Agents. *Mol. Imaging Biol.* (2015). doi:10.1007/s11307-015-0851-7
104. Shah, D. K. *et al.* A Priori Prediction of Tumor Payload Concentrations: Preclinical Case Study with an Auristatin-Based Anti-5T4 Antibody-Drug Conjugate. *AAPS J.* (2014). doi:10.1208/s12248-014-9576-9
105. Singh, R. & Salomon, P. L. A Sensitive ELISA Method for the Measurement of Catabolites of Antibody-Drug Conjugates (ADCs) in Target Cancer Cells. *Mol. Pharm.* 150304113735005 (2015). doi:10.1021/acs.molpharmaceut.5b00028
106. Spiegelman, B. M., Lopata, M. a & Kirschner, M. W. Multiple sites for the initiation of microtubule assembly in mammalian cells. *Cell* **16,** 239–252 (1979).
107. Loganzo, F. *et al.* Tumor cells chronically treated with a trastuzumab-maytansinoid antibody-drug conjugate develop varied resistance mechanisms but respond to alternate treatments. *Mol. Cancer Ther.* (2015). doi:10.1158/1535-7163.MCT-14-0862
108. Thurber, G. M., Schmidt, M. M. & Wittrup, K. D. Antibody tumor penetration: transport opposed by systemic and antigen-mediated clearance. *Adv. Drug Deliv. Rev.* **60,** 1421–34 (2008).
109. Okeley, N. M. *et al.* Intracellular activation of SGN-35, a potent anti-CD30 antibody-drug conjugate. *Clin. Cancer Res.* **16,** 888–97 (2010).

110. Singh, A. P. *et al.* Evolution of Antibody-Drug Conjugate Tumor Disposition Model to Predict Preclinical Tumor Pharmacokinetics of Trastuzumab-Emtansine (T-DM1). *(In Prep.*
111. Rostami, S., Qazi, I. & Sikorski, R. The Clinical Landscape of Antibody-drug Conjugates. *ADC Rev. / J. Antibody-drug Conjug.* (2014). doi:10.14229/jadc.2014.8.1.001
112. Singh, A. P., Shin, Y. G. & Shah, D. K. Application of Pharmacokinetic-Pharmacodynamic Modeling and Simulation for Antibody-Drug Conjugate Development. *Pharm. Res.* **32,** 3508–3525 (2015).
113. Lin, K. & Tibbitts, J. Pharmacokinetic considerations for antibody drug conjugates. *Pharm. Res.* **29,** 2354–2366 (2012).
114. Oroudjev, E. *et al.* Maytansinoid-antibody conjugates induce mitotic arrest by suppressing microtubule dynamic instability. *Mol. Cancer Ther.* **9,** 2700–13 (2010).
115. Shen, B.-Q. *et al.* Catabolic fate and pharmacokinetic characterization of trastuzumab emtansine (T-DM1): an emphasis on preclinical and clinical catabolism. *Curr. Drug Metab.* **13,** 901–10 (2012).
116. Thurber, G. M., Schmidt, M. M. & Wittrup, K. D. Factors determining antibody distribution in tumors. *Trends Pharmacol. Sci.* **29,** 57–61 (2008).
117. Schmidt, M. M. & Wittrup, K. D. A modeling analysis of the effects of molecular size and binding affinity on tumor targeting. *Mol. Cancer Ther.* **8,** 2861–2871 (2009).
118. Bhattacharyya, B. & Wolff, J. Maytansine binding to the vinblastine sites of tubulin. *FEBS Lett.* **75,** 159–62 (1977).
119. Bender, B. *et al.* A mechanistic pharmacokinetic model elucidating the disposition of trastuzumab emtansine (T-DM1), an antibody-drug conjugate (ADC) for treatment of metastatic breast cancer. *AAPS J.* **16,** 994–1008 (2014).
120. Krippendorff, B.-F., Oyarzún, D. A. & Huisinga, W. Predicting the F(ab)-mediated effect of monoclonal antibodies in vivo by combining cell-level kinetic and pharmacokinetic modelling. *J. Pharmacokinet. Pharmacodyn.* **39,** 125–139 (2012).
121. Erickson, H. K. *et al.* Tumor delivery and in vivo processing of disulfide-linked and thioether-linked antibody-maytansinoid conjugates. *Bioconjug. Chem.* **21,** 84–92 (2010).
122. Perez, H. L. *et al.* Antibody–drug conjugates: current status and future directions. *Drug Discov. Today* **19,** 869–881 (2014).
123. Zhitomirsky, B. & Assaraf, Y. G. Lysosomal sequestration of hydrophobic weak base chemotherapeutics triggers lysosomal biogenesis and lysosome-dependent cancer multidrug resistance. *Oncotarget* **6,** 1143–56 (2015).
124. Haddish-Berhane, N. *et al.* On translation of antibody drug conjugates efficacy from mouse experimental tumors to the clinic: a PK/PD approach. *J. Pharmacokinet. Pharmacodyn.* **40,** 557–71 (2013).
125. van der Lee, M. M. C. *et al.* The Preclinical Profile of the Duocarmycin-Based HER2-Targeting ADC SYD985 Predicts for Clinical Benefit in Low HER2-Expressing Breast Cancers. *Mol. Cancer Ther.* **14,** 692–703 (2015).
126. Chari, R. V. J., Miller, M. L. & Widdison, W. C. Antibody-drug conjugates: An emerging concept in cancer therapy. *Angew. Chemie - Int. Ed.* **53,** 3796–3827 (2014).
127. Willner, D. *et al.* (6-Maleimidocaproyl)hydrazone of doxorubicin--a new derivative for the preparation of immunoconjugates of doxorubicin. *Bioconjug. Chem.* **4,** 521–7 (1993).

128. Griffiths, G. L. *et al.* Cure of SCID Mice Bearing Human B-Lymphoma Xenografts by an Anti-CD74 Antibody-Anthracycline Drug Conjugate Cure of SCID Mice Bearing Human B-Lymphoma Xenografts by an Anti-CD74 Antibody-Anthracycline Drug Conjugate. 6567–6571 (2003).
129. Sutherland, M. S. K. *et al.* Lysosomal trafficking and cysteine protease metabolism confer target-specific cytotoxicity by peptide-linked anti-CD30-auristatin conjugates. *J. Biol. Chem.* **281,** 10540–7 (2006).
130. Francisco, J. a *et al.* cAC10-vcMMAE, an anti-CD30-monomethyl auristatin E conjugate with potent and selective antitumor activity. *Blood* **102,** 1458–65 (2003).
131. Jeffrey, S. C. *et al.* Dipeptide-based highly potent doxorubicin antibody conjugates. *Bioorganic Med. Chem. Lett.* **16,** 358–362 (2006).
132. Carpenter, A. E. *et al.* CellProfiler: image analysis software for identifying and quantifying cell phenotypes. *Genome Biol.* **7,** R100 (2006).
133. Headrick, T. *Statistical Simulation*. (Chapman and Hall/CRC, 2009). doi:10.1201/9781420064919
134. Boder, E. T., Midelfort, K. S. & Wittrup, K. D. Directed evolution of antibody fragments with monovalent femtomolar antigen-binding affinity. *Proc. Natl. Acad. Sci. U. S. A.* **97,** 10701–5 (2000).
135. Orcutt, K. D. *et al.* A modular IgG-scFv bispecific antibody topology. *Protein Eng. Des. Sel. PEDS* **23,** 221–228 (2010).
136. Martin, M. M. & Lindqvist, L. The pH dependence of fluorescein fluorescence. *J. Lumin.* **10,** 381–390 (1975).
137. Prokop, A. *Intracellular Delivery*. **5,** (Springer Netherlands, 2011).
138. Straubinger, R. M., Duzgunes, N. & Papahadjopoulos, D. pH-sensitive liposomes mediate cytoplasmic delivery of encapsulated macromolecules. *FEBS Lett.* **179,** 148–154 (1985).
139. Panyam, J., Zhou, W.-Z., Prabha, S., Sahoo, S. K. & Labhasetwar, V. Rapid endo-lysosomal escape of poly(DL-lactide-co-glycolide) nanoparticles: implications for drug and gene delivery. *FASEB J.* **16,** 1217–1226 (2002).
140. Yazdi, P. T. & Murphy, R. M. Quantitative analysis of protein synthesis inhibition by transferrin-toxin conjugates. *Cancer Res.* **54,** 6387–6394 (1994).

Appendices

Appendix A. DNA Sequences

The DNA sequences for Trastuzumab and Trastuzumab-4m5.3 in Gwiz plasmids are listed below. The Gwiz backbone is shown in black for the Trastuzumab Heavy Chain Gwiz plasmid in Appendix A.1. For all subsequent constructs, the same Gwiz backbone applies and only the insert is shown.

A.1 Gwiz Plasmid with Trastuzumab Heavy Chain

Gwiz Backbone – Trastuzumab Heavy Chain – Stop Codon – Gwiz Backbone

TCGCGCGTTTCGGTGATGACGGTGAAAACCTCTGACACATGCAGCTCCCGGAGACGGTCACA
GCTTGTCTGTAAGCGGATGCCGGGAGCAGACAAGCCCGTCAGGGCGCGTCAGCGGGTGTTG
GCGGGTGTCGGGGCTGGCTTAACTATGCGGCATCAGAGCAGATTGTACTGAGAGTGCACCAT
ATGCGGTGTGAAATACCGCACAGATGCGTAAGGAGAAAATACCGCATCAGATTGGCTATTG
GCCATTGCATACGTTGTATCCATATCATAATATGTACATTTATATTGGCTCATGTCCAACATT
ACCGCCATGTTGACATTGATTATTGACTAGTTATTAATAGTAATCAATTACGGGGTCATTAGT
TCATAGCCCATATATGGAGTTCCGCGTTACATAACTTACGGTAAATGGCCCGCCTGGCTGAC
CGCCCAACGACCCCCGCCCATTGACGTCAATAATGACGTATGTTCCCATAGTAACGCCAATA
GGGACTTTCCATTGACGTCAATGGGTGGAGTATTTACGGTAAACTGCCCACTTGGCAGTACA
TCAAGTGTATCATATGCCAAGTACGCCCCCTATTGACGTCAATGACGGTAAATGGCCCGCCT
GGCATTATGCCCAGTACATGACCTTATGGGACTTTCCTACTTGGCAGTACATCTACGTATTAG
TCATCGCTATTACCATGGTGATGCGGTTTTGGCAGTACATCAATGGGCGTGGATAGCGGTTT
GACTCACGGGGATTTCCAAGTCTCCACCCCATTGACGTCAATGGGAGTTTGTTTTGGCACCA
AAATCAACGGGACTTTCCAAAATGTCGTAACAACTCCGCCCCATTGACGCAAATGGGCGGTA
GGCGTGTACGGTGGGAGGTCTATATAAGCAGAGCTCGTTTAGTGAACCGTCAGATCGCCTGG
AGACGCCATCCACGCTGTTTTGACCTCCATAGAAGACACCGGGACCGATCCAGCCTCCGCGG
CCGGGAACGGTGCATTGGAACGCGGATTCCCCGTGCCAAGAGTGACGTAAGTACCGCCTAT
AGACTCTATAGGCACACCCCTTTGGCTCTTATGCATGCTATACTGTTTTTGGCTTGGGGCCTA
TACACCCCCGCTTCCTTATGCTATAGGTGATGGTATAGCTTAGCCTATAGGTGTGGGTTATTG
ACCATTATTGACCACTCCCCTATTGGTGACGATACTTTCCATTACTAATCCATAACATGGCTC
TTTGCCACAACTATCTCTATTGGCTATATGCCAATACTCTGTCCTTCAGAGACTGACACGGAC
TCTGTATTTTTACAGGATGGGGTCCCATTTATTATTTACAAATTCACATATACAACAACGCCG
TCCCCCGTGCCCGCAGTTTTTATTAAACATAGCGTGGGATCTCCACGCGAATCTCGGGTACG
TGTTCCGGACATGGGCTCTTCTCCGGTAGCGGCGGAGCTTCCACATCCGAGCCCTGGTCCCA
TGCCTCCAGCGGCTCATGGTCGCTCGGCAGCTCCTTGCTCCTAACAGTGGAGGCCAGACTTA
GGCACAGCACAATGCCCACCACCACCAGTGTGCCGCACAAGGCCGTGGCGGTAGGGTATGT
GTCTGAAAATGAGCGTGGAGATTGGGCTCGCACGGCTGACGCAGATGGAAGACTTAAGGCA
GCGGCAGAAGAAGATGCAGGCAGCTGAGTTGTTGTATTCTGATAAGAGTCAGAGGTAACTC
CCGTTGCGGTGCTGTTAACGGTGGAGGGCAGTGTAGTCTGAGCAGTACTCGTTGCTGCCGCG
CGCGCCACCAGACATAATAGCTGACAGACTAACAGACTGTTCCTTTCCATGGGTCTTTTCTG
CAGGCCGCCACCATGAAATGGAGCTGGGTCTTTCTCTTCCTGATGGCAATGGTTACAGGGGT
CAATTCAGAAGTGCAGCTGGTGGAATCCGGAGGTGGACTGGTGCAGCCTGGGGGAAGCCTG
AGACTGAGTTGTGCCGCATCTGGGTTTAACATTAAGGACACCTACATCCACTGGGTGCGACA
GGCTCCAGGCAAAGGGCTGGAGTGGGTCGCAAGAATCTACCCTACCAACGGATACACACGG

TATGCCGACTCCGTGAAGGGCAGATTCACAATCAGCGCAGATACTTCCAAAAACACCGCCTA
CCTGCAGATGAACAGCCTGAGGGCCGAAGATACTGCTGTCTACTATTGCAGTCGCTGGGGGG
GGGATGGGTTTTACGCTATGGATTACTGGGGGCAGGGCACTCTGGTGACTGTCTCCTCCGCT
AGCACCAAGGGCCCATCGGTCTTCCCCCTGGCACCCTCCTCCAAGAGCACCTCTGGGGGCAC
AGCGGCCCTGGGCTGCCTGGTCAAGGACTACTTCCCCGAACCGGTGACGGTGTCGTGGAACT
CAGGCGCCCTGACCAGCGGCGTGCACACCTTCCCGGCTGTCCTACAGTCCTCAGGACTCTAC
TCCCTCAGCAGCGTGGTGACCGTGCCCTCCAGCAGCTTGGGCACCCAGACCTACATCTGCAA
CGTGAATCACAAGCCCAGCAACACCAAGGTGGACAAGAAAGTTGAGCCCAAATCTTGTGAC
AAAACTCACACATGCCCACCGTGCCCAGCACCTGAACTCCTGGGGGGACCGTCAGTCTTCCT
CTTCCCCCCAAAACCCAAGGACACCCTCATGATCTCCCGGACCCCTGAGGTCACATGCGTGG
TGGTGGACGTGAGCCACGAAGACCCTGAGGTCAAGTTCAACTGGTACGTGGACGGCGTGGA
GGTGCATAATGCCAAGACAAAGCCGCGGGAGGAGCAGTACAACAGCACGTACCGTGTGGTC
AGCGTCCTCACCGTCCTGCACCAGGACTGGCTGAATGGCAAGGAGTACAAGTGCAAGGTCT
CCAACAAAGCCCTCCCAGCCCCCATCGAGAAAACCATCTCCAAAGCCAAAGGGCAGCCCCG
AGAACCACAGGTGTACACCCTGCCCCCATCCCGGGATGAGCTGACCAAGAACCAGGTCAGC
CTGACCTGCCTGGTCAAAGGCTTCTATCCCAGCGACATCGCCGTGGAGTGGGAGAGCAATGG
GCAGCCGGAGAACAACTACAAGACCACGCCTCCCGTGCTGGACTCCGACGGCTCCTTCTTCC
TCTACAGCAAGCTCACCGTGGACAAGAGCAGGTGGCAGCAGGGGAACGTCTTCTCATGCTC
CGTGATGCATGAGGCTCTGCACAACCACTACACGCAGAAGAGCCTCTCCCTGTCTCCGGGTA
AATGATAAGTCGACACGTGTGATCAGATATCGCGGCCGCTCTAGACCAGGCGCCTGGATCCA
GATCACTTCTGGCTAATAAAAGATCAGAGCTCTAGAGATCTGTGTGTTGGTTTTTTGTGGATC
TGCTGTGCCTTCTAGTTGCCAGCCATCTGTTGTTTGCCCCTCCCCCGTGCCTTCCTTGACCCTG
GAAGGTGCCACTCCCACTGTCCTTTCCTAATAAAATGAGGAAATTGCATCGCATTGTCTGAG
TAGGTGTCATTCTATTCTGGGGGGTGGGGTGGGGCAGCACAGCAAGGGGGAGGATTGGGAA
GACAATAGCAGGCATGCTGGGGATGCGGTGGGCTCTATGGGTACCTCTCTCTCTCTCTCTCTC
TCTCTCTCTCTCTCTCTCTCTCGGTACCTCTCTCTCTCTCTCTCTCTCTCTCTCTCTCTCTC
TCGGTACCAGGTGCTGAAGAATTGACCCGGTTCCTCCTGGGCCAGAAAGAAGCAGGCACAT
CCCCTTCTCTGTGACACACCCTGTCCACGCCCCTGGTTCTTAGTTCCAGCCCCACTCATAGGA
CACTCATAGCTCAGGAGGGCTCCGCCTTCAATCCCACCCGCTAAAGTACTTGGAGCGGTCTC
TCCCTCCCTCATCAGCCCACCAAACCAAACCTAGCCTCCAAGAGTGGGAAGAAATTAAAGC
AAGATAGGCTATTAAGTGCAGAGGGAGAGAAAATGCCTCCAACATGTGAGGAAGTAATGAG
AGAAATCATAGAATTTCTTCCGCTTCCTCGCTCACTGACTCGCTGCGCTCGGTCGTTCGGCTG
CGGCGAGCGGTATCAGCTCACTCAAAGGCGGTAATACGGTTATCCACAGAATCAGGGGATA
ACGCAGGAAAGAACATGTGAGCAAAAGGCCAGCAAAAGGCCAGGAACCGTAAAAAGGCCG
CGTTGCTGGCGTTTTTCCATAGGCTCCGCCCCCCTGACGAGCATCACAAAAATCGACGCTCA
AGTCAGAGGTGGCGAAACCCGACAGGACTATAAAGATACCAGGCGTTTCCCCCTGGAAGCT
CCCTCGTGCGCTCTCCTGTTCCGACCCTGCCGCTTACCGGATACCTGTCCGCCTTTCTCCCTTC
GGGAAGCGTGGCGCTTTCTCAATGCTCACGCTGTAGGTATCTCAGTTCGGTGTAGGTCGTTC
GCTCCAAGCTGGGCTGTGTGCACGAACCCCCCGTTCAGCCCGACCGCTGCGCCTTATCCGGT
AACTATCGTCTTGAGTCCAACCCGGTAAGACACGACTTATCGCCACTGGCAGCAGCCACTGG
TAACAGGATTAGCAGAGCGAGGTATGTAGGCGGTGCTACAGAGTTCTTGAAGTGGTGGCCT
AACTACGGCTACACTAGAAGGACAGTATTTGGTATCTGCGCTCTGCTGAAGCCAGTTACCTT
CGGAAAAAGAGTTGGTAGCTCTTGATCCGGCAAACAAACCACCGCTGGTAGCGGTGGTTTTT
TTGTTTGCAAGCAGCAGATTACGCGCAGAAAAAAAGGATCTCAAGAAGATCCTTTGATCTTT
TCTACGGGGTCTGACGCTCAGTGGAACGAAAACTCACGTTAAGGGATTTTGGTCATGAGATT
ATCAAAAAGGATCTTCACCTAGATCCTTTTAAATTAAAAATGAAGTTTTAAATCAATCTAAA
GTATATATGAGTAAACTTGGTCTGACAGTTACCAATGCTTAATCAGTGAGGCACCTATCTCA
GCGATCTGTCTATTTCGTTCATCCATAGTTGCCTGACTCCGGGGGGGGGGGGCGCTGAGGTC
TGCCTCGTGAAGAAGGTGTTGCTGACTCATACCAGGCCTGAATCGCCCCATCATCCAGCCAG
AAAGTGAGGGAGCCACGGTTGATGAGAGCTTTGTTGTAGGTGGACCAGTTGGTGATTTTGAA
CTTTTGCTTTGCCACGGAACGGTCTGCGTTGTCGGGAAGATGCGTGATCTGATCCTTCAACTC

AGCAAAAGTTCGATTTATTCAACAAAGCCGCCGTCCCGTCAAGTCAGCGTAATGCTCTGCCA
GTGTTACAACCAATTAACCAATTCTGATTAGAAAAACTCATCGAGCATCAAATGAAACTGCA
ATTTATTCATATCAGGATTATCAATACCATATTTTTGAAAAAGCCGTTTCTGTAATGAAGGAG
AAAACTCACCGAGGCAGTTCCATAGGATGGCAAGATCCTGGTATCGGTCTGCGATTCCGACT
CGTCCAACATCAATACAACCTATTAATTTCCCCTCGTCAAAAATAAGGTTATCAAGTGAGAA
ATCACCATGAGTGACGACTGAATCCGGTGAGAATGGCAAAAGCTTATGCATTTCTTTCCAGA
CTTGTTCAACAGGCCAGCCATTACGCTCGTCATCAAAATCACTCGCATCAACCAAACCGTTA
TTCATTCGTGATTGCGCCTGAGCGAGACGAAATACGCGATCGCTGTTAAAAGGACAATTACA
AACAGGAATCGAATGCAACCGGCGCAGGAACACTGCCAGCGCATCAACAATATTTTCACCT
GAATCAGGATATTCTTCTAATACCTGGAATGCTGTTTTCCCGGGGATCGCAGTGGTGAGTAA
CCATGCATCATCAGGAGTACGGATAAAATGCTTGATGGTCGGAAGAGGCATAAATTCCGTC
AGCCAGTTTAGTCTGACCATCTCATCTGTAACATCATTGGCAACGCTACCTTTGCCATGTTTC
AGAAACAACTCTGGCGCATCGGGCTTCCCATACAATCGATAGATTGTCGCACCTGATTGCCC
GACATTATCGCGAGCCCATTTATACCCATATAAATCAGCATCCATGTTGGAATTTAATCGCG
GCCTCGAGCAAGACGTTTCCCGTTGAATATGGCTCATAACACCCCTTGTATTACTGTTTATGT
AAGCAGACAGTTTTATTGTTCATGATGATATATTTTTATCTTGTGCAATGTAACATCAGAGAT
TTTGAGACACAACGTGGCTTTCCCCCCCCCCCCATTATTGAAGCATTTATCAGGGTTATTGTC
TCATGAGCGGATACATATTTGAATGTATTTAGAAAAATAAACAAATAGGGGTTCCGCGCACA
TTTCCCCGAAAAGTGCCACCTGACGTCTAAGAAACCATTATTATCATGACATTAACCTATAA
AAATAGGCGTATCACGAGGCCCTTTCGTC

A.2 Trastuzumab Light Chain Insert

Trastuzumab Light Chain – Stop Codon

GCCGCCACCATGAGTGTGCTCACTCAGGTCCTGGCGTTGCTGCTGCTGTGGCTTACAGGTGC
CAGATGTGCCGACATTCAGATGACCCAGTCTCCCAGCAGCCTGTCCGCCTCCGTCGGGGATA
GAGTGACCATTACTTGTAGAGCCAGCCAGGATGTGAACACCGCCGTGGCTTGGTATCAGCAG
AAGCCAGGGAAAGCACCCAAGCTGCTGATCTACTCTGCCAGTTTCCTGTATTCTGGCGTCCC
TAGCCGGTTTTCAGGAAGCAGATCCGGCACCGACTTCACTCTGACCATTAGCTCCCTGCAGC
CCGAGGATTTTGCTACATACTATTGCCAGCAGCACTATACCACACCCCCTACATTCGGCCAG
GGGACTAAAGTGGAAATTAAGCGTACGGTGGCTGCACCATCTGTCTTCATCTTCCCGCCATC
TGATGAGCAGTTGAAATCTGGAACTGCCTCTGTTGTGTGCCTGCTGAATAACTTCTATCCCAG
AGAGGCCAAAGTACAGTGGAAGGTGGATAACGCCCTCCAATCGGGTAACTCCCAGGAGAGT
GTCACAGAGCAGGACAGCAAGGACAGCACCTACAGCCTCAGCAGCACCCTGACGCTGAGCA
AAGCAGACTACGAGAAACACAAAGTCTACGCCTGCGAAGTCACCCATCAGGGCCTGAGCTC
GCCCGTCACAAAGAGCTTCAACAGGGGAGAGTGTTAATAG

A.3 Trastuzumab-4m5.3 Heavy Chain Insert

Trastuzumab Heavy Chain – Gly_4Ser Linker – 4m5.3 scFv – Stop Codon

GCCGCCACCATGAAATGGAGCTGGGTCTTTCTCTTCCTGATGGCAATGGTTACAGGGGTCAA
TTCAGAAGTGCAGCTGGTGGAATCCGGAGGTGGACTGGTGCAGCCTGGGGGAAGCCTGAGA
CTGAGTTGTGCCGCATCTGGGTTTAACATTAAGGACACCTACATCCACTGGGTGCGACAGGC
TCCAGGCAAAGGGCTGGAGTGGGTCGCAAGAATCTACCCTACCAACGGATACACACGGTAT
GCCGACTCCGTGAAGGGCAGATTCACAATCAGCGCAGATACTTCCAAAAACACCGCCTACCT
GCAGATGAACAGCCTGAGGGCCGAAGATACTGCTGTCTACTATTGCAGTCGCTGGGGGGGG
GATGGGTTTTACGCTATGGATTACTGGGGGCAGGGCACTCTGGTGACTGTCTCCTCCGCTAG
CACCAAGGGCCCATCGGTCTTCCCCCTGGCACCCTCCTCCAAGAGCACCTCTGGGGGCACAG
CGGCCCTGGGCTGCCTGGTCAAGGACTACTTCCCCGAACCGGTGACGGTGTCGTGGAACTCA
GGCGCCCTGACCAGCGGCGTGCACACCTTCCCGGCTGTCCTACAGTCCTCAGGACTCTACTC
CCTCAGCAGCGTGGTGACCGTGCCCTCCAGCAGCTTGGGCACCCAGACCTACATCTGCAACG
TGAATCACAAGCCCAGCAACACCAAGGTGGACAAGAAAGTTGAGCCCAAATCTTGTGACAA
AACTCACACATGCCCACCGTGCCCAGCACCTGAACTCCTGGGGGGACCGTCAGTCTTCCTCT
TCCCCCCAAAACCCAAGGACACCCTCATGATCTCCCGGACCCCTGAGGTCACATGCGTGGTG
GTGGACGTGAGCCACGAAGACCCTGAGGTCAAGTTCAACTGGTACGTGGACGGCGTGGAGG
TGCATAATGCCAAGACAAAGCCGCGGGAGGAGCAGTACAACAGCACGTACCGTGTGGTCAG
CGTCCTCACCGTCCTGCACCAGGACTGGCTGAATGGCAAGGAGTACAAGTGCAAGGTCTCCA
ACAAAGCCCTCCCAGCCCCCATCGAGAAAACCATCTCCAAAGCCAAAGGGCAGCCCCGAGA
ACCACAGGTGTACACCCTGCCCCCATCCCGGGATGAGCTGACCAAGAACCAGGTCAGCCTG
ACCTGCCTGGTCAAAGGCTTCTATCCCAGCGACATCGCCGTGGAGTGGGAGAGCAATGGGC
AGCCGGAGAACAACTACAAGACCACGCCTCCCGTGCTGGACTCCGACGGCTCCTTCTTCCTC
TACAGCAAGCTCACCGTGGACAAGAGCAGGTGGCAGCAGGGGAACGTCTTCTCATGCTCCG
TGATGCATGAGGCTCTGCACAACCACTACACGCAGAAGAGCCTCTCCCTGTCTCCGGGTAAA
GGAGGAGGAGGCTCTGGAGGAGGCGGGAGTGGAGGCGGGGGAAGCGACGTCGTTATGACT
CAAACACCACTATCACTTCCTGTTAGTCTAGGTGATCAAGCCTCCATCTCTTGCAGATCTAGT
CAGAGCCTCGTACACAGTAATGGAAACACCTATTTACGTTGGTACCTGCAGAAGCCAGGCCA
GTCTCCAAAGGTCCTGATCTACAAAGTTTCCAACCGAGTTTCTGGGGTCCCAGACAGGTTCA
GTGGCAGTGGATCAGGGACAGATTTCACACTCAAGATCAACAGAGTGGAGGCTGAGGATCT
GGGAGTTTATTTCTGCTCTCAAAGTACACATGTTCCGTGGACGTTCGGTGGAGGCACCAAGC
TTGAAATTAAGTCCTCTGCTGATGATGCTAAGAAGGATGCTGCTAAGAAGGATGATGCTAAG
AAAGATGATGCTAAGAAAGATGGTGGCGTCAAACTGGATGAGACTGGAGGAGGCTTGGTGC
AACCTGGGGGGGCCATGAAACTCTCCTGTGTTACCTCTGGATTCACTTTTGGTCACTACTGGA
TGAACTGGGTCCGCCAGTCTCCAGAGAAAGGACTGGAGTGGGTAGCACAATTTAGAAACAA
ACCTTATAATTATGAAACATATTATTCAGATTCTGTGAAAGGCAGATTCACCATCTCAAGAG
ATGATTCCAAAAGTAGTGTCTATCTGCAAATGAACAACTTAAGAGTTGAAGACACGGGTATC
TATTACTGTACGGGTGCTTCCTATGGTATGGAATACTTGGGTCAAGGAACCTCAGTCACCGT
CTCCTGATAA

A.4 Trastuzumab-4m5.3 Light Chain Insert

Trastuzumab Light Chain – Gly_4Ser – 4m5.3 – Stop Codon

GCCGCCACCATGAGTGTGCTCACTCAGGTCCTGGCGTTGCTGCTGCTGTGGCTTACAGGTGC
CAGATGTGCCGACATTCAGATGACCCAGTCTCCCAGCAGCCTGTCCGCCTCCGTCGGGGATA
GAGTGACCATTACTTGTAGAGCCAGCCAGGATGTGAACACCGCCGTGGCTTGGTATCAGCAG
AAGCCAGGGAAAGCACCCAAGCTGCTGATCTACTCTGCCAGTTTCCTGTATTCTGGCGTCCC
TAGCCGGTTTTCAGGAAGCAGATCCGGCACCGACTTCACTCTGACCATTAGCTCCCTGCAGC
CCGAGGATTTTGCTACATACTATTGCCAGCAGCACTATACCACACCCCCTACATTCGGCCAG
GGGACTAAAGTGGAAATTAAGCGTACGGTGGCTGCACCATCTGTCTTCATCTTCCCGCCATC
TGATGAGCAGTTGAAATCTGGAACTGCCTCTGTTGTGTGCCTGCTGAATAACTTCTATCCCAG
AGAGGCCAAAGTACAGTGGAAGGTGGATAACGCCCTCCAATCGGGTAACTCCCAGGAGAGT
GTCACAGAGCAGGACAGCAAGGACAGCACCTACAGCCTCAGCAGCACCCTGACGCTGAGCA
AAGCAGACTACGAGAAACACAAAGTCTACGCCTGCGAAGTCACCCATCAGGGCCTGAGCTC
GCCCGTCACAAAGAGCTTCAACAGGGGAGAGTGTGGAGGAGGAGGCTCTGGAGGAGGCGG
GAGTGGAGGCGGGGGAAGCGACGTCGTTATGACTCAAACACCACTATCACTTCCTGTTAGTC
TAGGTGATCAAGCCTCCATCTCTTGCAGATCTAGTCAGAGCCTCGTACACAGTAATGGAAAC
ACCTATTTACGTTGGTACCTGCAGAAGCCAGGCCAGTCTCCAAAGGTCCTGATCTACAAAGT
TTCCAACCGAGTTTCTGGGGTCCCAGACAGGTTCAGTGGCAGTGGATCAGGGACAGATTTCA
CACTCAAGATCAACAGAGTGGAGGCTGAGGATCTGGGAGTTTATTTCTGCTCTCAAAGTACA
CATGTTCCGTGGACGTTCGGTGGAGGCACCAAGCTTGAAATTAAGTCCTCTGCTGATGATGC
TAAGAAGGATGCTGCTAAGAAGGATGATGCTAAGAAAGATGATGCTAAGAAAGATGGTGGC
GTCAAACTGGATGAGACTGGAGGAGGCTTGGTGCAACCTGGGGGGGCCATGAAACTCTCCT
GTGTTACCTCTGGATTCACTTTTGGTCACTACTGGATGAACTGGGTCCGCCAGTCTCCAGAGA
AAGGACTGGAGTGGGTAGCACAATTTAGAAACAAACCTTATAATTATGAAACATATTATTCA
GATTCTGTGAAAGGCAGATTCACCATCTCAAGAGATGATTCCAAAAGTAGTGTCTATCTGCA
AATGAACAACTTAAGAGTTGAAGACACGGGTATCTATTACTGTACGGGTGCTTCCTATGGTA
TGGAATACTTGGGTCAAGGAACCTCAGTCACCGTCTCCTAATAG

Appendix B. Protocols

B.1 Cell Culture: Thaw Protocol

This protocol was obtained from Cary Opel (Wittrup Lab, http://cfopel.com/).

Action	Check
Pre-warm media.	
Thaw vial in 37°C bath for 1-2 minutes, careful not to let the cells thaw completely.	
When the cells are almost completely thawed, add 1 mL of growth media to the vial.	
Gently swirl and transfer to 15 mL falcon tube.	
Add 2 mL of growth media and swirl gently to allow osmotic equilibrium.	
Add 10 mL of growth media and mix gently.	
Centrifuge cells at 600 g for 5 min.	
Aspirate supernatant.	
Resuspend in 10 mL of growth media.	
Transfer to 10 cm dish.	
Check cells for confluence over the next 2 days.	

B.2 Cell Culture: Passaging Protocol

This protocol was modified from a protocol obtained from Cary Opel (Wittrup Lab, http://cfopel.com/).

Action	Check
Pre-warm appropriate media and trypsin (Trypsin EDTA 1X 0.25% Trypsin/2.21 mM EDTA).	
Remove old dish from incubator.	
Aspirate spent media.	
Rinse cells with 10 mL PBS (w/o Ca++ or Mg++) and aspirate.	
Add 2 mL of trypsin and incubate at room temperature or 37°C for 1 to 5 min depending on cell type.	
Tip dish and check to ensure all cells have been detached from the dish surface.	
Add 8 mL media to dish and thoroughly rinse cells from the surface.	
Transfer cell/trypsin suspension to 15 mL falcon tube.	
Count cells. Cell Count = $\frac{Dilution\ Factor * \#\ cells\ counted * 10{,}000}{\#\ squares\ counted} * Total\ Volume$ =	
Centrifuge cells at 600 g for 5 min.	
Add 9 mL media to a new dish.	
After centrifugation, aspirate supernatant.	
Resuspend pellet in x mL media (where x:1 is the desired split ratio).	
Pipette to break up cell clumps.	
Transfer 1 mL resuspended cells into new dish.	
Check cells for confluence over the next 2-3 days.	

B.3 Cell Culture: Freezing Protocol

This protocol was modified from a protocol obtained from Cary Opel (Wittrup Lab, http://cfopel.com/).

Action	Check
Prepare and filter freezing media (typically media supplemented with 5-10% DMSO).	
Pre-warm growth media.	
Remove 10 cm dish from incubator.	
Aspirate spent media.	
Rinse cells with 10 mL PBS (w/o Ca++ or Mg++) and aspirate.	
Add 2 mL of trypsin and incubate at room temperature or 37°C for 1 to 5 min depending on cell type.	
Tip flask and check to ensure all cells have been detached from the dish surface.	
Add 8 mL media to dish and thoroughly rinse cells from the surface.	
Transfer cell/trypsin suspension to 15 mL falcon tube.	
Count cells. Cell Count = $\frac{Dilution\ Factor * \#\ cells\ counted * 10{,}000}{\#\ squares\ counted} * Total\ Volume$ =	
Centrifuge cells at 600 g for 5 min.	
Resuspend pellet in 1 mL freezing media per 1e6 cells, at this point it is critical to move quickly as DMSO is toxic to cells at room temperature and above.	
Transfer 1 mL resuspended cells into cyro-vials.	
Transfer cells to Mr. Frosty and freeze at -80°C overnight.	
Transfer cells to liquid nitrogen.	

B.4 Flow Cytometric Clonogenic Assay

Action	Check
Make stock of PBS with 0.1% BSA. (Measure 0.1g of BSA, add 100mL of ddH_2O, then filter).	
Warm PBS/ 0.1% BSA stock.	
Add 20uL of DMSO to one vial of CellTrace Violet.	
Mix 8mL of media and 10.03uL of 2.5 g/L Doxorubicin Stock to make a 5.41μM stock.	
Trypsinize and count cells. Number of cells_____	
Resuspend to $1x10^6$ cells/mL in prewarmed PBS/0.1% BSA.	
Take an aliquot of 4mL of cell suspension and put in 50mL conical tube.	
Add 4uL of CellTrace Violet solution to the 4mL of cell suspension.	
Incubate with dye at 37°C for 10minutes (use timer!)	
Quench staining by adding 20mL of ice-cold media.	
Incubate on ice for 5min.	
Pellet cells.	
Wash the cells by resuspending in 4mL of fresh media. Wash 3x.	
Add 100uL of cells to wells A2-D3 of the plates. Set up as below. For A1 put 100uL of cells, unstained with CellTrace Violet.	

	Doxorubicin Concentration (mol/L)	Volume(mL) of Cells	Volume (uL) of Stock Added	Volume (mL) of Media
A3	5.00E-06	0.3	3700.0	0.0
B1	2.50E-06	0.3	1850.0	1850.0
B2	1.25E-06	0.3	925.0	2775.0
B3	6.25E-07	0.3	462.5	3237.5
C1	3.13E-07	0.3	231.3	3468.8
C2	1.56E-07	0.3	115.6	3584.4
C3	7.81E-08	0.3	57.8	3642.2
D1	3.91E-08	0.3	28.9	3671.1
D2	1.95E-08	0.3	14.5	3685.5
D3	9.77E-09	0.3	7.2	3692.8

After 24 h, wash away Doxorubicin and replace with fresh media.	
Trypsinize and prep for flow cytometry.	
Read on flow cytometer.	

B.5 Alexa 647 Labeling of T-DM1 or Trastuzumab

Desalting (to remove storage buffer for T-DM1) – If the antibody is already in PBS, this step can be skipped.

Action	Check
Desalt using two Zeba Spin Column (40K MWCO, 0.5mL) with 4x desalting.	
For 8 columns, remove the column's bottom closure and loosen cap.	
Place columns in a 1.7mL microcentrifuge tube.	
Centrifuge at 1500xg for 1 min.	
Discard flow-through. Put the column back into the tube.	
Add 300uL of PBS. Centrifuge at 1500xg for 1 min.	
Discard flow-through. Put the column back into the tube.	
Add 300uL of PBS. Centrifuge at 1500xg for 1 min.	
Discard flow-through. Put the column back into the tube.	
Add 300uL of PBS. Centrifuge at 1500xg for 2 mins.	
Blot the bottom of the column. Transfer column to **new** microcentrifuge tube.	
Add 110uL of sample to two columns.	
Add 15uL of PBS as stacker.	
Centrifuge at 1500xg for 2 mins. Save flowthrough.	
Add all of flowthrough to two new, prepped columns.	
Repeat twice.	
Measure final concentration on Nanodrop. Conc. : _____	
Add enough PBS to get to 500uL of 2 mg/mL.	

Alexa-647 Labeling Reaction (with kit)

The steps listed below describe the procedure used when labeling with the Alexa Fluor® 647 Protein Labeling Kit (Catalog number: A-20173).

Action	Check
Add 1mL of ddH_2O to vial of sodium bicarbonate (component B).	
Vortex until fully dissolved.	
Add 50uL of 1M biocarbonate to 500uL of desalted T-DM1.	
Allow a vial of reactive dye to warm up to room temperature.	
Transfer T-DM1 solution to the vial.	
Stir reaction mixture for 30 min - 1 hour at room temperature. Be sure to have column prepared to start purification immediately. Be cautious to not over-label the antibody.	

Column Purification of Labeled Antibody from Free Fluorophore

Action	Check
Prepare column.	
Prepare Elution buffer by add 9mL of ddH_2O to 1mL of elution buffer.	
Stir the purification resin and pipet into the column. Pack until 3cm from top of column.	
Allow excess buffer to drain through column bed.	
Add reaction mixture to column. Rinse reaction vial with 100uL of elution buffer and apply to column.	
Slowly add elution buffer. Continue adding elution buffer until labeled protein has been eluted (typically about 30 minutes).	
Collect all fractions. First colored band is labeled T-DM1.	

Alexa-647 Labeling Reaction (without kit)

Alternatively, the Alexa Fluor® 647 NHS Ester (Succinimidyl Ester) dye (Catalog number A-20006) may be purchased individually. The following procedure may be used in that case.

Action	Check
Add 0.081g of sodium bicarbonate to 964uL H_2O.	
Vortex until fully dissolved.	
Add 20uL of 1M biocarbonate to 200uL of desalted T-DM1.	
Add 1 uL of Alexa 647 (at 10 ug/uL) solution to vial.	

In this case, the labeled antibody can be purified from the free fluorophore using a size exclusion column on the FPLC. (Free fluorophore in the column can be damaging to the column or other proteins, so be sure to ask which columns it would be ok to use for this purpose. A thorough cleaning of the column may also be required.)

B.6 Bang's Lab Beads Fluorescence Signal Calibration

This protocol was developed based on the Quantum™ Simply Cellular® anti-Human IgG Product Manual (Bang's Laboratories, Inc. Catalog #816).

Action	Check
Manually shake bottles to ensure uniform suspension.	
Add one drop of micropsheres to a 1.5mL microcentrifuge tube. (Do blank & 1-4)	
Add 50 uL of PBS to each tube.	
Add 10 uL of AF647 Tras A114C (1.2 mg/mL from Chethana- Pfizer) to all tubes except blank.	
Incubate for 30 mins at room temperature.	
Add 1mL of PBS and centrifuge at 2500 x G for 5 minutes.	
Wash 2 times (centrifuge at 2500 x G for 5 minutes). Be especially careful not to aspirate off the microspheres!	
Resuspend in 500 uL of PBS.	
Put in tubes for flow cytometry.	
Run on Flow cytometer.	
Analyze data.	

B.7 K_D Measurement

Action	Check
Fix 10^6 cells according to the standard protocol using BD Fixation Buffer.	
Set up Falcon Tubes with TDox as described in spreadsheet. (Use B as stock to make stock A and C as stock to make B)	
Add 1500 cells to each tube.	
Incubate overnight at 37 °C.	
Pellet cells (300 x g, 5 mins, 4 °C)	
Wash twice with 1mL cold stain buffer (PBSA).	
Resuspend in 500 uL of cold stain buffer.	
Read on Flow Cytometer.	

Conc. (M)	Stock (mL)	Buffer (mL)	Total Volume		Which Stock
6.25E-13	12.5	37.5	50	mL	A
1.25E-12	25.0	25.0	50	mL	A
2.5E-12	50.0	0.0	50	mL	A
5E-12	25.0	25.0	50	mL	B
1E-11	50.0	0.0	50	mL	B
2E-11	0.6	9.4	10	mL	C
4E-11	1.3	8.8	10	mL	C
8E-11	2.5	7.5	10	mL	C
1.6E-10	5.0	5.0	10	mL	C
3.2E-10	10.0	0.0	10	mL	C

	A	B	C	
Create Stock at:	2.5E-12	1E-11	3.2E-10	M
Total Volume Needed:	87.5	15.0	7.8	mL
Total Volume to make:	90	15	10	mL
Amt stock to add:	703.13	468.75	0.40	uL

B.8 Net Internalization Assay

The internalization assay used by Schmidt et al.[9] was a reference for the design of the assay described here.

Action	Check
Plate 10^5 cells per well (7 wells for each cell line) in 24-well plate, with 0.5 mL media (total)	
Let adhere overnight	
Create **10nM** stock of Alexa-647 T-DM1 in each media: - RPMI (5.5mL with 6.88 uL of Alexa-647 T-DM1) - McCoy's (3mL with 3.75 uL of Alexa-647 T-DM1)	
At each time point (9 hrs, 6hrs, 3hrs, 1.5 hrs) - Remove plate from incubator. - Remove media. - Replace media with 0.5mL of 10nM stock of T-DM1 - Return to incubator.	
At end point, remove plates from incubator and wash all cells once with PBS.	
Trypsinize with 0.5mL of Trypsin/ EDTA. Let incubate at 37°C for 5 minutes.	
Resuspend in 500uL of stain buffer	
Add 10uL of Goat anti-Human IgG (H+L) Alexa 488 Ab	
Put on rotator in cold room for 30 mins.	
Pellet. Wash twice with 0.5mL of stain buffer.	
At some point, remove and trypsinize one of the untreated cell wells.	
Fix and treat as follows: - Pellet. Add 200uL of stain buffer to resuspend. - Pellet. Add 200uL of stain buffer to resuspend. - Pellet. - Add 100uL of BD Fixation Buffer. - Incubate at 4°C for 25 mins. - Pellet. - Add 0.5mL of 10nM stock of T-DM1 in media to each. - Incubate for 45 mins at 37°C. - Pellet. Wash twice with 0.5mL of stain buffer. - Read on flow cytometer.	

B.9 Non-Specific Uptake Assay

The non-specific uptake assay used by Schmidt et al.[9] was a reference for the design of the assay described here.

Action	Check
Plate 10^5 cells per well (6 wells for each cell line) in 24-well plate, with 0.5 mL media (total)	
Let adhere overnight	
Treat cells with 1000 nM Trastuzumab. Add 2.4 uL of Trastuzumab to 5 wells per cell line.	
At each time point (9 hrs, 6hrs, 3hrs, 1.5 hrs) - Remove plate from incubator. - Add 0.725 uL of T-DM1 (to make 10 nM) to each well. - Return to incubator.	
At end point, remove plates from incubator and wash all cells once with PBS.	
Trypsinize with 0.5 mL of Trypsin/ EDTA. Let incubate at 37 °C for 5 minutes.	
Pellet.	
Wash twice in 0.5 mL of cold stain buffer.	
Resuspend in 250uL of cold stain buffer.	
Keep on ice and read on Accuri.	
About 1.5 h before end of uptake period, treat as follows:	
Fix and treat as follows: - Pellet. Add 200uL of stain buffer to resuspend. - Pellet. Add 200uL of stain buffer to resuspend. - Pellet. - Add 100uL of BD Fixation Buffer. - Incubate at 4°C for 25 mins. - Pellet. - Add 0.5mL of 10nM stock of T-DM1 in media to each. - Incubate for 45 mins at 37°C. - Pellet. Wash twice with 0.5mL of stain buffer. - Read on flow cytometer.	

B.10 Degradation Assay

<table>
<tr><th>Action</th><th>Check</th></tr>
<tr><td>Plate 0.1x10^6 cells per well (2 6 well plates per cell line) with 3mL of media per well.</td><td></td></tr>
<tr><td>Let adhere overnight.</td><td></td></tr>
<tr><td></td><td></td></tr>
<tr><td>Add 4.5ug of Alexa-647 T-DM1 to each well. (for 10nM T-DM1)</td><td></td></tr>
<tr><td>Let incubate for ~30 mins.</td><td></td></tr>
<tr><td></td><td></td></tr>
<tr><td>Wash all wells with 4mL of PBS twice.</td><td></td></tr>
<tr><td>Replace with 4mL of fresh, warm media.</td><td></td></tr>
<tr><td>At each time point,
- Remove media and save.
- Wash with 4mL ice-cold PBS.
- Add 100uL of ice-cold cell lysis buffer (with Protease inhibitors added (using mini-pack)
- Scrape cells.
- Collect cells & buffer.
- Put on rotator in cold room for 30 mins.
- Pellet at 4°C, 12,000 rpm for 20 mins.
- Collect 75uL of supernatant and save.</td><td></td></tr>
<tr><td><table><tr><th>Sample #</th><th>Date Taken</th><th>Time</th></tr><tr><td>1</td><td></td><td></td></tr><tr><td>2</td><td></td><td></td></tr><tr><td>3</td><td></td><td></td></tr><tr><td>4</td><td></td><td></td></tr><tr><td>5</td><td></td><td></td></tr><tr><td>6</td><td></td><td></td></tr></table></td><td></td></tr>
<tr><td>Run gel at 250V for 15 mins with cell lysis samples and media</td><td></td></tr>
</table>

B.11 Flow Cytometry Assay to Determine Efflux Rate

<table>
<tr><th>Action</th><th>Check</th></tr>
<tr><td>Plate 0.1x10^6 cells per well (2 6 well plates per cell line) with exactly 3mL of media per well.</td><td></td></tr>
<tr><td>Let adhere overnight.</td><td></td></tr>
<tr><td></td><td></td></tr>
<tr><td>Add 4.5ug of Alexa-647 T-DM1 to each well. (for 10nM T-DM1)</td><td></td></tr>
<tr><td>Let incubate for ~30 mins.</td><td></td></tr>
<tr><td></td><td></td></tr>
<tr><td>Wash all wells with 4mL of PBS twice.</td><td></td></tr>
<tr><td>Replace with 4mL of fresh, warm media.</td><td></td></tr>
<tr><td>At each time point,
- Remove media and save.
- Wash with 4mL ice-cold PBS.
- Add 1mL Trypsin.
- Let sit for 1-2 minutes.
- Remove from plate. Centrifuge at 1000 rpm for 5 minutes.
- Resuspend in 500uL of FACS Buffer. Store on ice.
- Read on Accuri.</td><td></td></tr>
<tr><td><table><tr><th>Sample #</th><th>Date Taken</th><th>Time</th></tr><tr><td>1</td><td></td><td></td></tr><tr><td>2</td><td></td><td></td></tr><tr><td>3</td><td></td><td></td></tr><tr><td>4</td><td></td><td></td></tr><tr><td>5</td><td></td><td></td></tr><tr><td>6</td><td></td><td></td></tr><tr><td>7</td><td></td><td></td></tr><tr><td>8</td><td></td><td></td></tr></table></td><td></td></tr>
</table>

B.12 HEK293FS Transfection Protocol using PEI

This protocol was obtained from Cary Opel (Wittrup Lab, http://cfopel.com/).

<table>
<tr><th>Action</th><th>Check</th></tr>
<tr><td>Seed 3 x10^5 cells/mL 2 days prior to transfection.</td><td></td></tr>
<tr><td>Incubate at 37°C for 2 days.</td><td></td></tr>
<tr><td>Warm the following media: OPTI-PRO to RT, 1 mg/mL PEI to 37°C, Freestyle293 to 37°C.</td><td></td></tr>
<tr><td>Prepare DNA for each vessel:
<table><tr><th>Parameter</th><th>Condition</th><th>Check</th></tr><tr><td>OPTI-PRO (mL)</td><td>Up to 20 mL</td><td></td></tr><tr><td>DNA (x µg) (µL)</td><td>500 ug each of LC and Hc</td><td></td></tr></table></td><td></td></tr>
<tr><td>Prepare PEI/Media in a separate tube:
<table><tr><th>Solution</th><th>Condition</th><th>Check</th></tr><tr><td>OPTI-PRO (mL)</td><td>18</td><td></td></tr><tr><td>1 mg/mL PEI (µL)</td><td>2</td><td></td></tr></table></td><td></td></tr>
<tr><td>Incubate both solutions for 15 min at RT.</td><td></td></tr>
<tr><td>Add PEI to DNA while mixing gently:
<table><tr><th>Solution</th><th>Condition</th><th>Check</th></tr><tr><td>PEI Solution (mL)</td><td>20</td><td></td></tr><tr><td>DNA Solution (mL)</td><td>20</td><td></td></tr></table></td><td></td></tr>
<tr><td>Incubate for 15 min at RT.</td><td></td></tr>
<tr><td>Perform Cell Count, $\frac{Dilution\ Factor * \#\ squares\ counted * 10{,}000}{\#\ squares\ counted}$, ensure viability >90%.</td><td></td></tr>
<tr><td>Dilute cells 1e6 cells/mL of Freestyle 293 per vessel.</td><td></td></tr>
<tr><td>Perform transfection:
<table><tr><th>Solution</th><th>Condition</th><th>Check</th></tr><tr><td>Cells (mL)</td><td>1000</td><td></td></tr><tr><td>Slowly add DNA/PEI solution dropwise while mixing culture (mL)</td><td>40</td><td></td></tr></table></td><td></td></tr>
<tr><td>Incubate at 37°C for 6-8 days.</td><td></td></tr>
</table>

B.13 Protein A Purification Protocol

This protocol was modified from a protocol obtained from Cary Opel (Wittrup Lab, http://cfopel.com/).

Action	Check
Expected total protein should be less than 80% of column's binding capacity (20 mg/mL beads).	
Do not let the column fully drain or dry out during any step.	
Add 10X PBS to culture.	
Centrifuge culture at 13000 xg for 30 min at 4°C.	
0.22 µm filter supernatant.	
Pack column with 4 mL resin slurry (2 mL resin) and allow to settle. (Volume of resin can be scaled depending on size of column and expected quantity of protein.	
Rinse column with 20 mL PBS.	
Add supernatant to column and allow to drain, collecting flow-through.	
Wash column with 20 mL PBS.	
Add 1 mL of 1 M Tris pH 9 to a 50 mL centrifuge tube.	
Elute column with 10 mL 0.1 M Glycine HCl pH 3.5. If needed, collect 1 mL fractions.	
Regenerate column with 10 mL 0.1 M Glycine HCl pH 3.5. Columns can be regenerated 10 times.	
Store column by adding 10 mL PBS +0.02% Sodium Azide and letting drain, then adding an additional 5 mL and closing off the column. Refrigerate column upright.	
Concentrate and Buffer Exchange into PBS using Amicon Concentrators.	

B.14 In-Fusion Protocol

This protocol was obtained from Cary Opel (Wittrup Lab, http://cfopel.com/). See the In-Fusion® HD Cloning Kit User Manual (Clontech Laboratories, Inc.) for more detailed guidance.

<table>
<tr><th>Action</th><th>Check</th></tr>
<tr><td>Thaw reagents.</td><td></td></tr>
<tr><td>Add following reagents in order to thin-walled PCR tubes:

<table>
<tr><th>Parameter</th><th>Conditions</th><th>Check</th></tr>
<tr><td>Autoclaved H20 (µL)</td><td></td><td></td></tr>
<tr><td>Purified PCR fragment (µL)
<0.5 kb: 10-50 ng
0.5 to 10 kb: 50-100 ng
>10 kb: 50-200 ng</td><td></td><td></td></tr>
<tr><td>Linearized vector (µL)
<10 kb: 50-100 ng
>10 kb: 50-200 ng</td><td></td><td></td></tr>
<tr><td>5X In-Fusion HD Enzyme Premix (µL)</td><td>2</td><td></td></tr>
<tr><td>Total (µL)</td><td>10</td><td></td></tr>
</table></td><td></td></tr>
<tr><td>Gently mix reagents.</td><td></td></tr>
<tr><td>Incubate the reaction for 15 min at 50°C, then place on ice.</td><td></td></tr>
<tr><td>Immediately transform or store at -20°C.</td><td></td></tr>
</table>

B.15 E coli DNA Transformation Protocol

This protocol was obtained from Cary Opel (Wittrup Lab, http://cfopel.com/).

<table>
<tr><th>Action</th><th>Check</th></tr>
<tr><td>Pre-chill 1.5 mL centrifuge tubes on ice.</td><td></td></tr>
<tr><td>Preheat SOC medium and plates to RT.</td><td></td></tr>
<tr><td>Thaw cells on ice.</td><td></td></tr>
<tr><td>Add following reagents in order to pre-chilled tubes:

<table>
<tr><th>Item</th><th>Condition</th><th>Check</th></tr>
<tr><td>Cells (µL)</td><td>20</td><td></td></tr>
<tr><td>Plasmid (20 ng) (µL)</td><td>1</td><td></td></tr>
<tr><td>Incubate on ice (min)</td><td>15</td><td></td></tr>
<tr><td>Heat pulse tubes at 42°C (s)</td><td>45</td><td></td></tr>
<tr><td>Incubate on ice (min)</td><td>2</td><td></td></tr>
<tr><td>SOC Medium (µL)</td><td>480</td><td></td></tr>
<tr><td>Incubate at 37°C with agitation (hr)</td><td>1</td><td></td></tr>
<tr><td>Plate onto LB plates +x mg/L antibiotic (plates x µL)</td><td>1x10</td><td></td></tr>
</table></td><td></td></tr>
<tr><td>Incubate plates overnight at 37°C</td><td></td></tr>
<tr><td>Store plates at 4°C</td><td></td></tr>
</table>

<u>Recipe for SOC Media</u>

Weigh out the following materials. Add ddH_2O to reach 500 mL. Autoclave and aliquot for storage. Store in 4°C refrigerator or -20°C freezer.

10 g BactoTryptone
2.5 g BactoYeast Extract
0.292 g NaCl
0.093 g KCl
1.2 g $MgSO_4$
1.8 g D-glucose

B.16 Fixed Cell Microscopy

Action	Check
Sterilize cover slips by dipping in 70% ethanol. (7 total)	
Rinse with PBS.	
Put one cover slip in each well in six-well plate. - A: 1 plate with 3 wells (24 h) - B & C: 2 plates with 2 wells (5d and 6d)	
Plate 10^5 SK-BR-3 cells per well. (With 3 mL of media per well)	
Allow to adhere overnight.	
Treat Tras-Dox wells with 20 nM Tras-Dox (add 8.7 uL of P1).	
Mix 30 mL of media (McCoy's No Phenol Red) with 0.278 uL of Free Dox Stock (2.5 g/L). Replace media for 24 h Free Dox well.	
Let incubate for 24 h.	
Day 1: Fix cells on plate A.	
Day 2: Replace Tras-Dox in plates B & C. Replace media for untreated cells.	
Day 4: Replace Tras-Dox in plates B &C. Replace media for untreated cells.	
Day 5: Fix cells for plate B. On plate C, remove media, wash with PBS and replace with Free-Dox media.	
Day 6: Fix cells on plate C.	
Fixation Procedure:	
Rinse cells with PBS 3x.	
Fix cells: Cover with 1 mL of fixative.	
Let sit for 15 minutes at room temperature.	
Gently wash with PBS 2x for 2 minutes each.	
Put one drop of Vectashield (Mounting Media with DAPI) on glass slide.	
Place cover slip cell-side down on glass slide.	
Seal edges of cover slip with nail polish.	

B.17 Live Cell Microscopy

Action	Check
Plate 10^4 SK-BR-3 cells per well in 8-well chambered cover glass. (With 200 µL of media per well)	
Allow to adhere overnight.	
Treat Tras-Dox wells with 20 nM Tras-Dox (add 0.6 uL of P1).	
Mix 30 mL of media (McCoy's No Phenol Red) with 0.278 uL of Free Dox Stock (2.5 g/L). Replace media for 24 h Free Dox well.	
Let incubate for 24 h.	
Day 1: Treat for imaging cells on plate A.	
Day 2: Replace Tras-Dox in plates B & C. Replace media for untreated cells.	
Day 4: Replace Tras-Dox in plates B &C. Replace media for untreated cells.	
Day 5: Treat for imaging cells for plate B. On plate C, remove media, wash with PBS and replace with Free-Dox media.	
Day 6: Treat for imaging cells on plate C.	
Hoescht and Lysotracker Procedure:	
Make media with Hoescht and Lysotracker. Mix: - 8 mL media - 0.32 uL of 10 mg/mL Hoescht 33342 stock - 0.40 uL of Lysotracker Deep Red	
Add 200 uL to the wells of interest.	
Incubate for 30 mins at 37 °C.	
Wash with PBS gently, 3x.	
Replace with fresh media.	
Image on Delta Vision Microscope.	

Appendix C. Resume

KATIE MAASS

Email: kfmaass@gmail.com

Education

PhD Candidate, Chemical Engineering 2011 – present
Massachusetts Institute of Technology Cambridge, MA
Thesis: Quantitative Analysis of Cellular Processing of Antibody-Drug Conjugates
Minor: Biology and Biomedical Technologies
Expected Graduation: Dec. 2015

Bachelor of Science, Chemical Engineering, With Highest Honors 2007 – 2011
Minor: Business Foundations Austin, TX
University of Texas at Austin
Overall GPA: 3.99/4.00 Major GPA: 4.00/4.00

Research Experience

PhD Candidate and Hertz Fellow, Massachusetts Institute of Technology (Wittrup Lab) 2011 – present
- Established model and methods for parameter measurement of intracellular processing of antibody-drug conjugates (ADCs) Cambridge, MA
- Developed flow cytometric clonogenic assay to measure single-cell drug potency
- Collaborated with scientists at Pfizer (Groton, CT) and University at Buffalo (w/ Professor Dhaval Shah) to incorporate cellular level processing of ADCs into larger Pharmacokinetic/ Pharmacodynamic (PK/PD) model

Undergraduate Research Assistant, University of Texas at Austin (Peppas Lab) Aug. 2009 – Dec. 2010
- Directed individual research project using pH-sensitive polymer drug delivery system Austin, TX
- Evaluated loading and release capabilities after synthesizing and purifying polymer system
- Conducted research on the swelling behaviors of UV-initiated and thermally-initiated polymers of acrylic acid and acrylamide films

Research Intern, Materials Processing Center & Center for Materials Science and Engineering, Massachusetts Institute of Technology (Cima Lab) Summer 2009 Cambridge, MA
- Measured cell survival as a function of drug concentration and length of exposure to chemotherapeutic drug Cisplatin
- Learned how to culture cells, use sterile technique, and perform MTT assay
- Presented work in poster session open to MIT community

Work Experience

Merck Manufacturing Division, Engineering Intern Summer 2011
- Evaluated variability of bottles for oxygen sensitive drugs West Point, PA
- Determined precision and accuracy of in-house oxygen concentration measuring equipment

Merck Manufacturing Division, Engineering Intern Summer 2010
- Observed trends between anti-static agent potency and active pharmaceutical ingredient concentration, surface area, solubility, and identity Rahway, NJ
- Evaluated conductivity-increasing ability of compounds to screen for new anti-static agents
- Created conductivity measurement and anti-static agent knowledge management resources

SACHEM, Inc., Engineering Intern Summer 2008
- Ran small scale electrochemical cell to determine current efficiency Austin, TX
- Analyzed plant chilling system pipes, created drawings of the pipes, and estimated temperatures and flow rates to complete a material and energy balance on the system

Accomplishments

AAPS Biotechnology Graduate Student Symposium Award (2015)
AAPS Innovation in Biotechnology Award (2015)
MIT Graduate Women of Excellence Award (2015)
Fannie and John Hertz Foundation Fellowship Recipient (2011)
National Science Foundation Graduate Research Fellowship Recipient (2011)
Undergraduate Cockrell School of Engineering Student Leadership Award (2010)
Women in Engineering Program Excellence Award (2011), Champion Award (2010), Rising Star Award (2009)
Cockrell School of Engineering Scholarship (2007 – 2011)
Society of Women Engineers Baker Hughes Scholarship (2010 – 2011)
School of Engineering Scholarship (2007 – 2011)
Ruth M. Martin Endowed Presidential Scholarship (2007 – 2011)

Leadership Experience

Industrial Initiative Chair (2015): *MIT Biotechnology Group (MBG)*
Sponsorship Co-Chair (2013-2015): *MIT Cycling Club*
Elected Class Representative (2012 & 2013), *Graduate Student Advisory Board*, MIT Chemical Eng. Dept.
Participant, *Graduate Student Council for Course X*, MIT Chemical Eng. Dept. (2012)
Alto, *MIT Grad Student Choir* (2012 – 2015)
K-12 Outreach Committee Chair (Spring 2011), Team Active (2009-2011), Recruitment & Retention Committee Chair (Fall 2009): *Texas Tau Beta Pi Engineering Honor Society*
President (Spring 2011), Vice President (Fall 2010), Treasurer (2009-2010), Service Chair (Spring 2009), Pledge (Fall 2008): *Texas Omega Chi Epsilon Chemical Engineering Honor Society*
Region Conference Chair (2010-2011), Vice President of Executive Affairs (2009-10), Student Engineering Council Representative (2008-09): *Texas Society of Women Engineers*
Peer-Assistance Leader (PAL) 2008-2011: *Women in Engineering Program (WEP)*
Facilitator and Volunteer (2009-2011): *Engineering Leadership Team*
Student Cluster Leader (2009), Participant (2008): *Leadershape Texas*
Tutor (Fall 2010 and Fall 2009): *Student Engineers Educating Kids (SEEK)*

Skills

Laboratory: Flow Cytometry, Fluorescence Microscopy, Mammalian Cell Culture, Protein Analysis and Purification (SDS-PAGE Gels, Western Blots, Size-Exclusion Chromatography, Affinity Chromatography)

Software: MATLAB, ImageJ, FlowJo, GraphPad Prism, Microsoft Word, Excel, Powerpoint

Publications

Maass, K., Kulkarni, C., Betts, A., Wittrup, K.D. Determination of Cellular Processing Rates for a Trastuzumab-Maytansinoid Antibody-Drug Conjugate (ADC) Points to Key Parameters for ADC Design. Manuscript in preparation.

Singh, A., **Maass, K.**, Betts, A., Wittrup, K.D., Kulkarni, C., King, L., Shah, D. Evolution of Antibody-Drug Conjugate Tumor Disposition Model to Predict Preclinical Tumor Pharmacokinetics of Trastuzumab-Emtansine (T-DM1). Manuscript in preparation.

Maass, K.F, Kulkarni, C., Quadir, M.A., Hammond, P.T., Betts, A.M., Wittrup, K.D. (2015). A Flow Cytometric Clonogenic Assay Reveals Single-Cell Potency of Doxorubicin. Journal of Pharmaceutical Sciences. doi:10.1002/jps.24631

Caldorera-Moore, M., **Maass, K.**, Hegab, R., Fletcher, G., Peppas, N.A. (2015). Hybrid Responsive Hydrogel Carriers for Oral Delivery of Low Molecular Weight Therapeutic Agents. Journal of Drug Delivery Science and Technology. doi:10.1016/j.jddst.2015.07.023

Slaughter, B.V., Blanchard, A., **Maass, K.F.**, Peppas, N.A. (2015). Dynamic Swelling Behavior of Interpenetrating Polymer Networks in Response to Temperature and pH. Journal of Applied Polymer Science, 132(24).